UNIVERSITY OF VAASA

FACULTY OF TECHNOLOGY

ELECTRICAL ENGINEERING

Emma Söderäng

ANALYTICAL DYNAMIC THERMAL MODEL FOR SQUIRREL CAGE MOTORS USING SYSTEMMODELER

Master's thesis for the degree of Master of Science in Technology submitted for inspection

Vaasa 14.12.2016

Supervisor	Professor Timo Vekara
Instructor	D.Sc. (Tech.) Jouni Ikäheimo
Evaluator	Docent Jere Kolehmainen

PREFACE

This master thesis is written for ABB Motors and Generators. I would like to warmly thank all who have helped me during the writing process of my master thesis.

I would especially like to thank Jouni Ikäheimo for giving me the opportunity to write about this intresting subject and also for his valuable advices. I would also like to thank Timo Vekara for supervising and reviewing this thesis and also for his professional comments. Thank you also to Matti Fyhr for providing me with test results and guidance concerning the water cooled motor. Then I would also like to thank Jere Kolehmainen for evaluating my master thesis.

Finally I would like to thank my family and friends for all the support I have gotten while writing this thesis but also during my university studies.

Vaasa 14.12.2016

Emma Söderäng

TABLE OF CONTENTS

SYMBOLS AND ABBREVIATIONS

Greek symbols

α	Resistance temperature coefficient
α	Thermal diffusivity
β	Fluid coefficient of cubical expansion
δ	Air gap radial length
ε	Emissivity
μ	Dynamic viscosity
ρ	Density
σ	Stefan-Boltzmann constant
Ω_r	Angular velocity of the rotating rotor
Ω_s	Angular velocity of the air-gap flux

Other symbols

∇	Three-dimensional del operator
A	Area
A_{slot}	Interior slot surface
C	Heat capacity
c_p	Specific heat capacity
dT/dx	Temperature gradient
f	Frequency
F_g	Geometrical factor
g	Gravitational force of attraction
Gr	Grashof number
h	Heat transfer coefficient
h_{conv}	Convection heat transfer coefficient
$h_{equivalent}$	Equivalent heat transfer coefficient
h_{forced}	Forced convection heat transfer coefficient
h_{NC}	Natural convection heat transfer coefficient
h_{rad}	Radiation heat transfer coefficient

I	Electric current
k	Thermal conductivity
k_{air}	Thermal conductivity of air
k_{cuir}	Equivalent thermal conductivity
k_{ir}	Thermal conductivity in the radial direction of the core material
k_{shf}	Axial thermal conductivity of the shaft
L	Lenght
L_{ec}	Motor frame length
l_{ig}	Equivalent interface air gap length for the stator core to the frame
l_{sb}	Perimeter of the stator slot
L_{shf}	Shaft length
L_{TOT}	Stator core (and rotor core) length
m	Mass
Nu	Nusselt number
p	Pole number
P	Losses
P_{Add}	Additional losses
P_{Cur}	Rotor Joule losses
P_{Cus}	Stator Joule losses
P_{Fe}	Iron losses
p_{ir}	Reduction factor in percent
P_{mech}	Mechanical losses
P_{mech_factor}	Mechanical factor used with mechanical losses
Pr	Prandtl number
q	Rate of heat transfer
q''	Heat flux
R	Resistance
r	Radius
R_0	Natural convection thermal resistance between frame and ambient
$R_{0,r}$	Thermal resistance including natural convection and radiation
$r_{ag,m}$	Average of the stator and rotor radii
R_c	Conduction thermal resistance through the supports, mounting arrangement

R_{cond}	Conduction thermal resistance
R_{conv}	Convection thermal resistance
$R_{cu,ir}$	Conduction thermal resistance between stator copper and stator iron
R_{cy}	Cylinder thermal conduction resistance
R_{DC}	DC resistance
Re	Reynolds number
r_{ec}	Radius of the motor frame
R_{eca}	Thermal resistance between motor enclosure and ambient
Re_{crit}	Critical Reynolds number
$R_{ew,ec}$	Conduction thermal resistance between stator winding external connections and frame
$R_{ew,ia}$	Thermal resistance between stator winding external connections and inner air
R_f	Forced convection thermal resistance from the motor enclosure to ambient
$R_{ia,ec}$	Thermal resistance between internal air and end-caps
r_{iry}	Inner rotor yoke radius
r_{is}	Stator inner radius
r_{iy}	Inner stator yoke radius
r_m	Average value of the stator yoke radius
r_{or}	Outer rotor radius
r_{ory}	Outer rotor yoke radius
r_{oy}	Outer value of the stator yoke radius
R_r	Radial thermal resistance due to the rotor yoke and the axial resistance of the shaft part below the rotor core
R_r	Radiation thermal resistance from the motor enclosure to ambient
$R_{r,ag}$	Convection thermal resistance between rotor and air gap air
R_{rad}	Radiation thermal resistance
$R_{s,ag}$	Convection thermal resistance between stator teeth and air gap air
R_{shf}	Thermal resistance associated with shaft or with shaft and rotor
R_{sig}	Conduction resistance of the interface gap between the stator core and the motor frame
R_{st}	Radial conduction thermal resistance of the stator teeth
R_{sy1}	Radial conduction thermal resistance of the stator yoke, lower half part

R_{sy2}	Radial conduction thermal resistance of the stator yoke, upper half part
s	Slip
S_{cu}	Copper section in the stator slot
S_{slot}	Stator slot cross-sectional area
T	Temperature
T_{∞}	Temperature of a fluid at a distance from the surface
Ta	Taylor number
Ta_m	Modified Taylor number
t_{eq}	Equivalent thickness of the air and insulation in the stator slots
T_s	Surface temperature
T_{surr}	Temperature of surrounding surface
v	Velocity
V	Volume
v_p	Pheriperal speed of the rotor

Abbreviations

BSI1	Slot width, closer to the air gap
BSO1	Slot width, closer to the yoke
CFD	Computational Fluid Dynamics
DI1	Stator core inner diameter
DI2	Rotor core inner diameter
DO1	Stator core outer diameter
DOL	Direct On-Line
FC	Frequency Converter
FEA	Finite Element Analysis
HSN1	Winding height
HYOKE2	Yoke height of rotor
IC	International Cooling
IEC	International Electrotechnical Commission
IM	Induction Motor

KCU1	Slot filling factor
L_TOT	Lenght of stator core
LM1	Half length of coil
NTC	Negative Temperature Coefficient
PTC	Positive Temperature Coefficient
Q1	Number of stator slots
rpm	Revolutions per Minute
SM	SystemModeler
TEFC	Totally Enclosed Fan-Cooled, a motor type
VSD	Variable Speed Drive

VAASAN YLIOPISTO
Teknillinen tiedekunta
Tekijä: Emma Söderäng
Diplomityön nimi: Oikosulkumoottorien analyyttinen dynaaminen malli SystemModeler-ohjelmalla
Valvoja: Professori Timo Vekara
Ohjaaja: TkT Jouni Ikäheimo
Tarkastaja: Dosentti Jere Kolehmainen
Tutkinto: Diplomi-insinööri
Oppiaine: Sähkötekniikka
Opintojen aloitusvuosi: 2011
Diplomityön valmistumisvuosi: 2016 **Sivumäärä:** 134

TIIVISTELMÄ

Sähkömoottorin termisen käyttäytymisen tarkka laskeminen on kasvavan kiinnostuksen kohteena. Huolellisella suunnittelulla voidaan merkittävästi parantaa moottorin termistä käyttäytymistä ja kokonaissuorituskykyä. Lisäksi moottorin kuormituksen tärkein rajoittava tekijä on lämpötila.

Tässä diplomityössä tutkitaan kolmivaiheisia ajoittaiskäyttöisiä oikosulkumoottoreita. Nämä oikosulkukoneet voivat toimia alle ja yli nimellisvääntömomentin ja tämän vuoksi koneiden terminen malli eroaa jatkuvan tilan lämpenemämallista. Dynaamisessa lämpenemämallissa lämpö varastoituu moottorin eri osiin, kun taas jatkuvan tilan lämpenemämallissa moottorin lämpökapasiteetti voidaan jättää huomiotta. Jatkuvan tilan lämpenemämallissa simuloidaan ainoastaan termistä tasapainotilaa.

SystemModeler-ohjelmalla on mahdollista kehittää työkaluja erilaisille laskelmille. Tässä diplomityössä keskitytään lämpölaskelmiin ja tarkoituksena on selvittää, miten SystemModeler-ohjelmaa voitaisiin käyttää kehitettäessä lämpenemämalleja ajoittaiskäyttöisille oikosulkumoottoreille. Tavoitteena on kehittää helppokäyttöinen ja riittävän tarkka analyyttinen terminen malli. Moottorin tarvittavien parametrien on oltava helposti saatavilla ja moottorin perustiedot sekä käyttöjakson tiedot täytetään työkaluun. Lämpenemämalleissa suurena haasteena on se, että monia termisiä ilmiöitä on käytännössä mahdotonta laskea sekä se, että erilaiset korrelaatiot ovat välttämättömiä.

Kehitetyn työkalun avulla on mahdollista ennustaa ajoittaiskäyttöisen oikosulkumoottorin lämpeneminen. Koska kaikille moottorityypeille oli mahdollista saada jatkuvan tilan testituloksia, terminen malli voidaan kalibroida jatkuvassa tilassa ennen kuin simuloidaan dynaamista käyttäytymistä. SystemModeler-ohjelmalla kehitettyjen työkalujen etuina ovat luotujen koodien rakenteiden helppo saatavuus ja helppo muunneltavuus sekä mahdollisuus ajaa luotu malli verkon yli itsenäisenä työkaluna.

AVAINSANAT: SystemModeler, dynaaminen terminen analyysi, analyyttinen terminen malli, oikosulkumoottori

UNIVERSITY OF VAASA
Faculty of technology
Author: Emma Söderäng
Topic of the Thesis: Analytical dynamic thermal model for squirrel cage motors using SystemModeler
Supervisor: Professor Timo Vekara
Instructor: D.Sc. (Tech.) Jouni Ikäheimo
Evaluator: Docent Jere Kolehmainen
Degree: Master of Science in Technology
Major of Subject: Electrical Engineering
Year of Entering the University: 2011
Year of Completing the Thesis: 2016 **Pages:** 134

ABSTRACT

Importance of accurately predicting the thermal behavior of electric motors is of growing interest. This is due to the fact that careful design of a motor in terms of thermal behavior may significantly improve the overall performance of a motor. In addition, the temperature is the main limiting factor for motor loading.

This thesis focuses on transient thermal behavior for three phase squirrel cage motors of intermittent duty types. Motors of these duty types may operate below and above rated torque and hence their dynamic thermal model is different from a steady-state thermal model. In a dynamic thermal model heat is stored in the different parts of the motor while the stored heat can be neglected for stationary thermal modelling, where it is enough only to simulate for thermal equilibrium.

SystemModeler offers an opportunity to develop different tools for various types of calculations, but in this thesis the focus is on thermal analysis. The purpose of this thesis is to investigate how SystemModeler could be used when developing thermal models for squirrel cage motors of intermittent duty types. The target is to develop an analytical thermal model which is easy to use while being sufficiently accurate. The needed motor parameters should also be easily available. The basic information about the motor and information about operational as well as standstill time are filled into the tool. The main challenge with thermal models is the fact that many thermal phenomena are practically impossible to calculate and different correlations are needed.

With help of the tool it is possible to predict how a motor of intermittent duty type would be heated during operation. Since all motor types had test results for thermal equilibrium it was possible to calibrate the thermal model for steady state before simulating transient conditions. The main advantages with tools developed in SystemModeler are that the structures of the created codes are readily accessible and easily modifiable. In addition the created model can be run over the network as an independent tool.

KEYWORDS: SystemModeler, transient thermal analysis, analytical thermal model, squirrel cage motor

VASA UNIVERSITET
Tekniska fakulteten
Författare: Emma Söderäng
Ämnet för avhandlingen: Analytisk dynamisk termisk modell av induktionsmotorer i SystemModeler
Handledare: Professor Timo Vekara
Instruktör: TkD Jouni Ikäheimo
Utvärderare: Docent Jere Kolehmainen
Examen: Master of Science in Technology
Huvudämne: Electrical Engineering
Inskrivningsårs: 2011
Examensår: 2016 **Antal sidor:** 134

ABSTRAKT

Betydelsen av att noggrannt kunna förutsäga en motors termiska beteende är av ett växande intresse. Detta beror på det faktum att noggrann design av en motor kan förbättra motorns beteende och prestanda väsentligt. Dessutom är temperaturen den huvudsakliga begränsande faktorn för hur mycket en motor kan bli belastad.

Denna avhandling fokuserar på dynamiskt termiskt beteende för trefas induktionsmotorer med rotorbur av olika driftstarter. Motorer av olika driftstarter kan arbeta under och över nominellt vridmoment och därmed skiljer sig deras dynamiska termiska modell från en termisk modell i kontinuerligt läge. I en dynamisk termisk modell lagras värme i de olika delarna av motorn medan motorns värmekapacitet inte behöver tas i beaktande för statiska modeller, där det räcker att simulera termisk jämvikt.

SystemModeler erbjuder en möjlighet att utveckla olika verktyg för olika typer av beräkningar. I detta diplomarbete ligger fokus på termiska beräkningar. Syftet med detta diplomarbete är att undersöka hur SystemModeler skulle kunna användas vid utvecklingen av dynamiska termiska modeller för induktionsmotorer av olika driftstarter. Målet är att utveckla en analytisk termisk modell som är lätt att använda samtidigt som den är tillräckligt noggrann. Motorparametrarna som behövs bör vara lättillgängliga. Grundläggande information om motorn och information om driftstarten fylls i verktyget. Den största utmaningen med termiska modeller är det faktum att många termiska fenomen är praktiskt taget omöjliga att beräkna och därför behövs olika korrelationer.

Med hjälp av det uvecklade verktyget är det möjligt att förutsäga hur en motor av periodisk driftstart skulle värmas under drift. Eftersom alla motortyper hade testresultat för termisk jämvikt är det möjligt att kalibrera den termiska modellen för kontinuerligt läge innan man simulerar transienta förhållanden. Fördelarna med verktyg som utvecklats i SystemModeler är att kodernas strukturer är lättillängliga samt lätta att modifiera. Dessutom kan modellen köras över nätverket som ett självständigt verktyg.

NYCKELORD: SystemModeler, transient termisk analys, analytisk termisk modell, induktionsmotor

1 INTRODUCTION

This master thesis is written for ABB Motors and Generators. The purpose is to develope an analytical thermal model which could be utilized in order to estimate the thermal behavior of squirrel cage motors of intermittent duty types in a fast but sufficient accurate way. Sometimes it is necessary to estimate how different loading conditions affect a squirrel cage motor in order to avoid overheating. Fast estimations could be made with an analytical thermal model. It is important that the thermal model is simple to use, thus it is essential that all needed parameters are easily available. The analytical thermal model is developed in Wolfram SystemModeler (SM). (Wolfram SystemModeler 2016) The advantages, with tools developed with SystemModeler, are that the end user can easily comprehend and if required, also modify the structures of the models. Models may also be published and can thus even be run over the network and in this way the end user does not need a SystemModeler license.

When an electrical motor converts electrical energy into mechanical energy, some of the energy is lost and emitted as heat. The heat needs to be removed from the motor to the ambient. This process contains many complex phenomena. Proper thermal analysis is of highest importance in order to improve the machine design or to determine the loadability. However, there are many challenges when estimating the thermal behaviour; it is for example now practically too cumbersome to calculate all heat transfer phenomena by pure mathematics and several different empirical dependencies have to be used. In addition, the loss estimation may also be challenging. The challenge with estimating motor losses is bypassed in this thesis by using the calculation tool Adept for the loss calculation.

Temperature is usually considered as the main limiting factor for how much a squirrel cage motor can be loaded. If its thermal limits are exceeded it results in several undesired circumstances. The insulation materials are exposed to an accelerated oxidation process. Bearing lubricants may decay and the viscosity may increase. In addition, there are also other factors to be considered, such as mechanical stresses and changes in geometry due to thermal expansion of the different parts. (Kylander 1995: 11) At a certain

critical temperature of the stator windings, the insulation material burns and causes a breakdown. Therefore, it is of highest importance that the temperature limit of the insulation material is never exceeded. However, already at temperatures below the temperature limit, the motor performance is impaired with increasing winding temperature.

1.1 Purpose and limitations of the thesis

This master thesis focuses on how Wolfram SystemModeler can be utilized when analyzing the thermal behavior of three phase squirrel cage induction motors of intermittent duty types. Emphasis lies on the most common industrial motor type: totally enclosed fan-cooled (TEFC) squirrel cage induction motors but water cooled squirrel cage induction motors are also shortly studied. The analyzed motors are connected directly to the network, which means that they are direct on-line (DOL) motors and the rotational speed is not varying as for frequency converter (FC) operated motors.

The difference in motors of intermittent duty types compared with the continuous duty type S1 is that the thermal equilibrium is not reached. Thermal equilibrium occurs when the heat is generated in the motor and dissipated to the ambient at the same rates and as a consequence the motor part temperatures are stabilized. The majority of squirrel cage motors are of duty type S1 and often heat transfer is only studied for steady-state. Motors of intermittent duty types may operate at nominal torque, below nominal torque and above nominal torque. In addition, there is also often standstill time. It is hence important to know how the different motor losses vary with the load for different frame sizes as well as how the heat removal is affected by different loads.

Many applications such as automotive electric power-train, aircraft motors and generators and electromagnetic launchers, require short-time load and overload variations. Consequently, thermal transient analysis is of greatest importance in order to get the most out of the electrical machines and to characterize the thermal dynamic behavior. (Buyukdegirmenci 2013: 801)

1.2 Structure of the thesis

In Chapter 2, basic information about squirrel cage motors is presented; there is a section about the different loss components and then information about insulation, duty class types, temperature measurement methods and cooling methods. Chapter 3 focuses on heat transfer mechanisms for a motor and how thermal resistances can be used when analyzing the thermal behavior. Chapter 4 contains the theory behind the developed analytical model and equations for all used components. This chapter is described in detail in order to facilitate if the developed thermal model is modified. In Chapter 5 the thermal model is used and three different TEFC motors and one water cooled motor with simulation results are presented. In Chapter 6, the conclusions are presented and some future investigation suggestions are proposed. Chapter 7 summarizes this thesis.

2 SQUIRREL CAGE MOTOR

The most common motor for industrial applications today is the squirrel cage induction motor. The squirrel cage motor is an asynchronous motor which means that it needs a slip in order to create torque. The angular velocity of the rotating rotor is Ω_r and the air gap flux has an angular velocity of Ω_s. The difference between the velocities is called the slip and it is often given as a per unit value, hence: (Pyrhönen 2014: 342)

$$s = \frac{\Omega_s - \Omega_r}{\Omega_s}. \tag{1}$$

The active parts of a squirrel cage motor consist of a magnetic circuit, with a stationary stator and a rotating rotor, between them is an air gap. The stator winding is located in slots in the stator iron core. Alternating current from an external supply is fed into the stator winding, this induces current in the rotor circuit and due to this the rotor starts to rotate. The speed of the rotating magnetic flux depends on the frequency *f* of the power source and on the pole number *p* of the motor

$$\Omega_s = \frac{120f}{p}, \tag{2}$$

where the unit of the speed is rpm. Squirrel cage motors have rotor bars which are short-circuited by rotor end-rings. (Bansal 2006: 139–140)

2.1 Losses in squirrel cage motors

When modeling the thermal behavior of a squirrel cage motor, it is important to determine the losses and their locations. The calculation tool Adept is able to calculate the motor losses accurately and therefore Adept is utilized when determining the losses for different motor types. The losses calculated with Adept are filled into the developed tool.

When the distribution of losses for different parts of a motor and the heat removal power are accurately determined, it is possible to calculate the heat distribution of the motor. The heat distribution is completely different for transient states than for stationary states. For example, when the motor is overloaded for a short time the excess heat is stored in the heat capacity of the machine. (Pyrhönen 2014: 523)

The losses of a squirrel cage motor may be divided into these categories:

- Joule losses
    - In stator conductors P_{Cus}
    - In rotor conductors P_{Cur}
- Iron losses in the magnetic circuit P_{Fe}
- Additional losses P_{Add}
- Mechanical losses P_{Mech}. (Pyrhönen 2014: 524)

Figure 1 shows the typical loss distribution of 4 pole squirrel cage induction motors for output powers up to 90 kW.

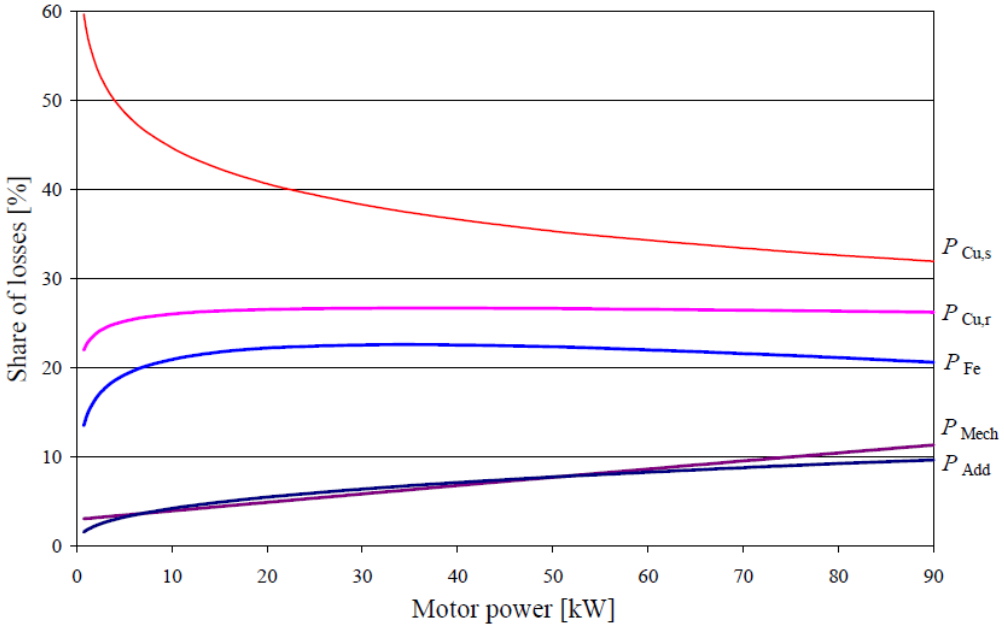

Figure 1. The typical loss distribution as a function of output power of 4 pole TEFC squirrel cage induction motors. (Puranen 2006: 126)

For dynamic thermal models for motors with different operational conditions, it is important to know how the losses change with the load; the losses can also be divided into no-load losses and load losses:

No-load losses

- Iron losses in the core
- Windage and friction losses

Load losses

- Stator Joule losses
- Rotor losses
- Stray load losses (ABB 2014: 61).

2.1.1 Joule losses

The Joule losses consist of the stator and rotor Joule losses. For a 3-phase motor the stator and rotor Joule losses are

$$P_{\mathrm{Cus}} = 3R_{\mathrm{s}}I_s^2 \tag{3}$$

and

$$P_{\mathrm{Cur}} = 3R_{\mathrm{r}}I_{\mathrm{r}}^2, \tag{4}$$

where R is the resistance per phase and I is the current per phase. (Kylander 1995: 22)

The Joule losses change as a function of the temperature, the resistance increases directly proportional to the temperature

$$R = R_{\mathrm{DC}}(1 + \alpha\Delta T), \tag{5}$$

where R_{DC} is the DC resistance, α the resistance temperature coefficient and T the temperature. (Puranen 2006: 113) The temperature coefficient for copper is $3.9 \cdot 10^{-3}$ 1/K and for aluminium $4.0 \cdot 10^{-3}$ 1/K. (Mäkelä 2010: 177)

2.1.2 Iron losses

Iron losses derive from alternating magnetic flux in the different parts of the motor. Iron core losses can be divided into eddy current losses and hysteresis losses. Hysteresis losses are directly proportional to the frequency while the eddy current losses are proportional to the square of the frequency. Hysteresis losses depend on the material hysteresis loop. Eddy currents in solids easliy become remarkable and therefore magnetic cores are made of thin sheets instead of solid objects. (Pyrhönen 2014: 194–200)

2.1.3 Additional losses

Additional losses are also called stray-load losses. Additional losses are the losses left after subtracting the Joule losses, iron losses and mechanical losses from the total losses. The additional losses derive from several different phenomena, some of them are very difficult to calculate or model accurately. (Pyrhönen 2014: 526)

A significant part of the additional losses are iron and eddy current losses caused by the leakage fluxes, which are flux components that do not contribute to the electro-mechanical energy conversion. (Puranen 2006: 62, 114)

2.1.4 Mechanical losses

Mechanical losses consist of friction and windage losses. These losses derive from bearing friction and air resistance. The design of cooling fan is important for these losses, because the fan has to be big enough to handle sufficient heat removal but still not too big, so the losses as well as noise level increase too much. (ABB 2014: 61) The mechanical losses depend on the rotational speed of the motor and fan, hence motor pole number as well as operational frequency affect.

2.2 Insulation classes

The insulation of the winding has different maximum temperature limits depending on the insulation material. The most commonly used insulation system for industrial motors is class F insulation with temperature rise class B. ABB uses class F insulation which gives the maximum hotspot winding temperature a value of 155 °C and the maximum winding temperature measured with the resistance measurement method a value of 145 °C.

Class F insulation system has maximum ambient temperature 40 °C, maximum permissible temperature rise 105 K and a hotspot temperature margin of +10 K. Class B temperature rise has a maximum permissible temperature rise of 80 K and the other limits the same as class F, this gives ABB products a safety margin of 25 °C. The safety margin can be used when for example overloading the motor for short time periods or with a higher ambient temperature. The margin can also extend the insulation lifetime since the insulation lifetime is highly dependent on the temperature. Figure 2 illustrates the different insulation classes and their temperature limits. (ABB 2014: 44)

It is possible to estimate the lifetime of insulations with statistical methods, the lifetime shortens exponentially with the temperature rise of the machine over a broad temperature range. The lifetime of the insulation is shortened by as much as 50 % with a 10 K temperature rise. The lifetime of the bearings may be shortened similarly. However, the electric machines may tolerate temporary high-temperatures, depending on the duration and peak value. (Pyrhönen 2014: 524)

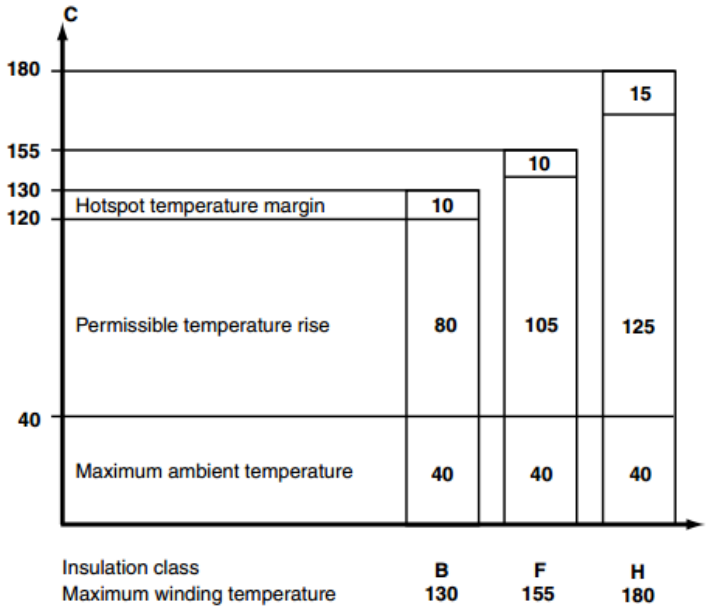

Figure 2. The different insulation classes. (ABB 2014: 44)

2.3 Duty class types

The standards IEC 60034-1 and VDE 0530 Part 1 define different duty types named S1–S10. S1 is continuous running duty and rated operation values given in catalogues are based on S1. In S1 thermal equilibrium is reached. For the duty types S2–S8, the duty cycles are too short for thermal equilibrium to be reached. The duty types S8–S10 include speed variations which are not considered in this thesis. Many of the intermittent duty types have lower temperature rise and therefore the output can usually be higher than the rated output for S1 continuous duty. (ABB 2014: 56, 60)

The different duty types defined in the standards IEC 60034-1 and VDE 0530 Part 1 are shortly described as follows:

- S1 Continuous running duty
- S2 Short-time duty
- S3 Intermittent duty
- S4 Intermittent duty with starting
- S5 Intermittent duty with starting and electrical braking
- S6 Continuous operation periodic duty
- S7 Continuous operation periodic duty with electrical braking
- S8 Continuous-operation periodic duty with related load speed changes
- S9 Duty with non-periodic load and speed variations
- S10 Duty with discrete constant loads and speeds. (ABB 2014: 56–59)

2.4 Temperature measurement methods

When performing tests for every motor type, temperatures are measured from the frame, stator winding and D-end bearing for every squirrel cage motor. Sometimes the rotor temperature is also documented in the test report. There are three different ways to measure the temperatures: resistance, thermistor and thermocouples. The IEC 60034-1 standard defines the different temperature measurement methods.

With the resistance method the average stator winding temperature can be measured. The winding resistance is measured for the cold and hot winding. The resistance difference gives an average value for the stator temperature rise. The resistance method is based on the resistance temperature dependency. When measuring the temperature by the resistance method the maximum error is estimated to be 3 %. The error caused by the resistance method is mainly due to the often unknown purity of copper. However, commercial copper wires have a minimum of 97 % of the conductivity of copper. (Kylander 1995: 19)

Measurement using thermistor is the most sensitive temperature measurement method. The response is strongly nonlinear. The function of thermistors is based on the temperature dependency of semiconductors. The temperature dependency may be positive or

negative; NTC (Negative Temperature Coefficient) or PTC (Positive Temperature Coefficient). (University of Helsinki 2007)

Measurement using thermocouples are widely used temperature measurement method due to simplicity and their low price, they also have a wide temperature range. Their function is based on the Seebeck effect. The Seebeck effect is that at the junction of two different types of conductors a thermoelectric voltage is induced. The two conductors have to be of different materials and the induced thermoelectric voltage depends on the used materials. (University of Helsinki 2007)

2.5 Cooling of squirrel cage motors

IEC 60034-6 standard defines the different cooling methods for electrical machines. The cooling classification is designated with numbers and letters. ABB has these different cooling options for the low voltage motors:

- IC 410: totally enclosed motor without a fan
- IC 411: totally enclosed standard motors, frame-surface cooled with a fan
- IC 416: totally enclosed motors with an auxiliary fan motor
- IC 418: totally enclosed motors, frame-surface cooled without a fan
- IC 31W: inlet and outlet pipe or duct circulated: water cooled motors.

ABB's totally enclosed standard motors are IC 411 motors. (ABB 2014: 29) The fan is mounted on the shaft and hence it rotates with the same angular speed as the shaft and motor. Consequently, the convection heat removal rate of the motor is affected by the motor rotational speed; for higher speed the heat removal is more efficient and for lower speed the heat removal is at a slower rate.

3 HEAT TRANSFER GENERALLY AND APPLIED TO MOTORS

Heat transfer, which is thermal energy in transit, occurs when a temperature difference exists between media or in a medium. There are different types of heat transfer processes and they are called: conduction, convection and thermal radiation. Conduction is heat transfer that occurs across a stationary medium, a solid or a fluid. Convection, on the other hand, refers to heat transfer that occurs between a surface and a moving fluid when a temperature difference exists between them. Thermal radiation does not require a medium in order for heat transfer to occur. Radiation is energy emitted by any surface or matter that is at a nonzero temperature and the emitted energy is in form of electromagnetic waves. (Bergman 2011: 2)

Heat removal from a squirrel cage motor may happen in three different ways; by conduction, convection or radiation. A medium can only involve two ways of heat transfer simultaneously even though there are three different heat transfer mechanisms. A still fluid has heat transfer by conduction and possibly radiation. A flowing fluid has heat transfer by convection and radiation. Conduction in a fluid may be regarded as a special case of convection, when there are no fluid motion. Heat transfer through a fluid may hence be by conduction or convection, not both. In vacuum, radiation is the only heat transfer mechanism since convection and conduction require a medium. (Cengel 2003: 30)

3.1 Conduction

Conduction is heat transfer in a solid, liquid or gas due to a temperature difference, a temperature gradient. The thickness, geometry and material of a medium, as well as the temperature difference across the medium determines the heat rate. Fourier's law determines the heat flux and may be called the conduction rate equation. (Bergman 2011: 68, Cengel 2003: 18)

We may use for heat rate

$$q_{\mathrm{x}} = -kA\frac{\mathrm{d}T}{\mathrm{d}x} \tag{6}$$

or for the heat flux

$$q_{\mathrm{x}}^{"} = \frac{q_{\mathrm{x}}}{A} = -k\frac{\mathrm{d}T}{\mathrm{d}x}, \tag{7}$$

where k is the thermal conductivity of the material, A is the heat transfer area and dT/dx is the temperature gradient. The direction of heat transfer is always a normal to the heat transfer area A. The temperature gradient dT/dx consists of the temperature difference ΔT and the thickness Δx. The minus sign derives from the fact that heat is always transferred from a higher temperature to a lower temperature. (Bergman 2011: 69, Cengel 2003: 18)

Heat flux is a vector quantity, which leads to a more general form of Equation 7 as

$$\boldsymbol{q}" = -k\nabla T = -k\left(\boldsymbol{i}\frac{\partial T}{\partial x} + \boldsymbol{j}\frac{\partial T}{\partial y} + \boldsymbol{k}\frac{\partial T}{\partial z}\right), \tag{8}$$

where ∇ is the three-dimensional del operator and $T(x,y,z)$ is the scalar temperature field. (Bergman 2011: 69)

The thermal conductivity k of a material determines the capability of the material to transfer heat; a high value means that the material is a good heat conductor while a low value means that the material is a poor heat conductor. The thermal conductivity is temperature dependent, for some materials the variations are negligible while for other materials the variations are significant and have to be considered. For example, the thermal conductivity of copper increases dramatically at 20 K where it reaches a value of 20 000 W/m°C, copper then becomes a superconductor. However, the temperature range that a motor experiences is relatively narrow and temperature variations do not need to be considered. Conductivity analysis would also become far more complex if the temperature dependency of k would be considered, therefore it is treated as constants

in calculations. Table 1 presents the thermal conductivites for some common materials used in electric motors at room temperature (293 K). (Cengel 2003: 22, Pyrhönen 2014: 536)

Table 1. Thermal conductivities for some common materials used in electric motors at room temperature (293 K). (Pyrhönen 2014: 536)

Material	**Thermal conductivity *k* (W/K m)**
Air, stagnant	0.025
Aluminium, pure	231
Aluminium, electrotechnical	209
Copper, electrotechnical	394
Insulation, typical insulation system	0.2
Iron, pure	74.7
Iron, cast	40–46
Steel, carbon steel 0.5 %	45
Steel, electrical sheet, in the direction of lamination	22–40
Steel, electrical sheet, normal to lamination	0.6

In transient heat conduction analysis, the thermal diffusivity is an important material property. The thermal diffusivity, α, is a measure for how fast heat diffuses through a material. The thermal diffusivity is the ratio of the heat conducted through a material to the heat stored per unit volume. A large thermal diffusivity means that the heat propagates fast through the material into the medium and hence only a small amount of heat is absorbed by the material. The thermal diffusivity α can be calculated as

$$\alpha = \frac{k}{\rho c_{\mathrm{p}}}, \tag{9}$$

where c_{p} is the specific heat capacity of the material and ρ is the density of the material. The unit for thermal diffusivity is m^2/s. (Cengel 2003: 23)

3.2 Convection

Convection is energy transfer between a surface and a fluid or gas moving over the surface. Convection includes two ways of energy transfer; the combined effects of conduction and fluid motion. The heat transfer between the solid surface and the fluid is by conduction if the bulk fluid is not moving, and the faster the fluid is moving the greater the convection heat transfer. The heat transfer is hence faster for moving fluids but it is also more complicated to determinate the heat transfer rates for moving fluids. When analyzing the convection energy transfer, it is of great importance to understand the concept of boundary layers. There are velocity, thermal and concetration boundary layers and they are connected to the friction coefficient, convection heat transfer coefficient and convection mass transfer coefficient. (Bergman 2011: 378, Cengel 2003: 25)

If the fluid is forced to flow over a surface by for example a pump, fan or the wind then the convection is called forced convection. On the other hand, if the fluid is moving due to buoyancy forces that arise because of the density differences caused by variations in temperature, then the convection is called natural or free convection. For a solid surface in an environment without any external impacts on the fluid motion, there may be two ways of heat transfer, natural convection and conduction. For example, consider a hot block, if the temperature difference between the block and the surrounding air is big enough the warm air near the block surface will rise since it is lighter than the cooler air above, which will fall, this is natural convection. If the temperature difference between

the block and the air is not big enough to overcome the resistance of the air to start moving, then the heat transfer will be by pure conduction. (Cengel 2003: 26)

The rate of convection heat transfer is expressed by Newton's law of cooling as follows:

$$q = hA(T_s - T_\infty), \tag{10}$$

where h is the convection heat transfer coefficient in W/m^2·K, A is the heat transfer surface area, T_s is the surface temperature and T_∞ is the temperature of the fluid at a distance from the surface. Close to the surface the fluid temperature is basically the same as the surface temperature. The convection heat transfer coefficient h depends on several variables, such as the the properties of the fluid (dyanmic viscosity μ, thermal conductivity k, density ρ and specific heat capacity c_p), the nature of the fluid motion (turbulent or laminar flow), the surface geometry and roughness and the bulk fluid velocity. (Cengel 2003: 26, 334)

Since the convection calculation process is quite complicated, there are some dimensionless parameters in order to facilitate the process. There are different correlations that are suitable for different surface shapes, for example cylinders and flat plates but also for more complex structures such as channels of different shapes. The dimensionless parameters suitable for the prediction of convection in motors are: Reynolds (*Re*), Grashof (*Gr*), Prandtl (*Pr*) and Nusselt (*Nu*) numbers. However, there are numerours dimensionless parameters available. (Staton 2005: 623)

The typical forms of the correlations are Equation 11 for natural convection and Equation 12 for forced convection:

$$Nu = a(GrPr)^b, \tag{11}$$

$$Nu = a(Re)^b(Pr)^c, \tag{12}$$

where a, b, and c are constants which mostly depend on geometric properties. The dimensionless numbers are defined as in Table 2.

Table 2. Reynolds, Grashof, Prandtl and Nusselt numbers defined.

Dimensionless parameter	Description
$Re = \frac{\rho v L}{\mu}$	Reynolds number; is a measure of how turbulent the flow is.
$Gr = \frac{\beta g \Delta T \rho^2 L^3}{\mu^2}$	Grashof number; is a measure of the amount of the natural convection in the fluid flow
$Pr = \frac{c_p \mu}{k}$	Prandtl number; describes static properties of the fluid
$Nu = \frac{hL}{k}$	Nusselt number; is a measure of the heat-transfer coefficient for fluid flows

Here

h	heat-transfer coefficient (W/m^2·K)
μ	fluid dynamic viscosity (kg/s·m)
ρ	fluid density (kg/m^3)
k	fluid thermal conductivity (W/m·K)
c_p	fluid specific heat capacity (kJ/kg·K)
v	fluid velocity (m/s)
ΔT	temperature difference between the surface and the fluid (°C or K)
L	characteristic length of the surface (m)
β	fluid coefficient of cubical expansion 1/(273+T_{FLUID}) (1/K)
g	gravitational force of attraction (m/s^2). (Staton 2005: 623, Jääskeläinen 2009: 10)

The function of the Nusselt number is to describe the effectiveness of convection heat transfer compared with conduction heat transfer. When a flow becomes turbulent, the Reynolds number value is called the critical Reynolds number Re_{crit}. For a tube the Re_{crit} is 2300 and for a flat surface $5 \cdot 10^5$. A low Pr (<1) indicates that the heat transfer of thermal diffusivity is large compared with heat transfer rate obtained with the fluid speed. When Pr is 1, the thermal and velocity boundary layers are equal. (Pyrhönen 2014: 542–543)

Natural convection depends mainly on the temperature difference between the component and the fluid flowing over it as well as on the fluid properties. Forced convection, on the other hand, depends mainly on the fluid velocity and the fluid properties. However, it also depends on the temperature to some extent since fluid properties are temperature dependent. Natural convection is usually easier to predict since the local fluid velocity is not needed. (Staton 2005: 623) Table 3 presents some typical values for the convection heat transfer coefficient. (Cengel 2003: 26)

Table 3. Typical values for different types of convection.(Cengel 2003: 26)

Type of convection	***h*, W/(m^2°C)**
Free convection of gases	2–25
Free convection of liquids	10–1000
Forced convection of gases	25–250
Forced convection of liquids	50–20000
Boiling and condensation	2500–100000

Convection is the main heat removal process for machines. The flows inside the machine are often turbulent, hence increasing the heat transfer inside the machine. (Jäaskeläinen 2009: 2) For electrical motors, convection heat transfer occurs especially in these three regions:

- Between the frame and the ambient air
- Between the end windings and the end-region air and end-caps, and
- Between the stator, air-gap and rotor. (Puranen 2006: 107)

The calculation of convection heat transfer from the frame to the ambient is usually difficult due to the cooling fins in the frame. Cooling fins are extended surfaces that increase the convection heat transfer from the frame. The convection heat transfer coefficient is often determined by tests. The calculation of the convection heat transfer from the end windings to the end-region air is also demanding and an accurate calculation is practically impossible. This is because of the complex geometry of the end windings

and therefore the heat transfer should be estimated with experimental tests. The convection heat transfer calculation from the rotor to the stator with the air gap between is also practically impossible. Fluid disturbances in the air gap due to the slotting of the stator and rotor is the challenge when performing calculations. (Puranen 2006: 107) However, many different approximations for calculating these convective heat transfer coefficients have been researched and possible ways to estimate the different coefficients are presented in Chapter 4.

3.3 Radiation

Radiation heat transfer is the least significant when it comes to heat transfer mechanisms for electric machines. Radiation has a significant role when the temperature difference between a surface and the surrounding is big. For motors with forced cooling the frame temperature usually reamins quite low and hence radiation has a neglectable role. For self-cooled motors, the frame reaches higher temperatures and the radiation has to be considered. (Puranen 2006: 106) For a TEFC IM with a shaft-mounted fan, the radiation from the frame to ambient have to be considered if the fan rotates at a low speed. (Boglietti 2009a: 879)

Net rate of radiation heat transfer for a surface with temperature T_s, completely enclosed by a significantly larger surrounding surface with temperature T_{surr} is calculated with

$$\dot{Q_{rad}} = \varepsilon\sigma A_s(T_s^4 - T_{surr}^4), \tag{13}$$

where ε is the emissivity of the surface, A_s is the surface area and σ is Stefan-Boltzmann constant ($5.67 \cdot 10^{-8} \frac{W}{m^2K^4}$). (Cengel 2003: 28–29)

Table 4 contains the emissivities of some common materials used in electrical machines.

Table 4. Approximate emissivities of some materials used in typical electrical machines. (Pyrhönen 2014: 541)

Material	**Emissivity ε**
Polished aluminium	0.04
Polished copper	0.025
Mild steel	0.2–0.3
Cast iron	0.3
Stainless steel	0.5–0.6
Black paint	0.9–0.95
Aluminium paint	0.5

The emissivity ε can have values from 0 to 1, a ”transparent” material has 0 and a black body has 1. Inside the machine condcution and convection dominate and hence radiation can be neglected, this is due to the low emissivities of typical machine materials such as copper and steel and in addition the surface areas are small. (Puranen 2006: 109)

3.4 Thermal resistances

When performing an analytical thermal analysis, a thermal network is needed. The thermal model is composed of thermal resistances, thermal capacitances and heat sources. The thermal resistances are calculated as in Table 5.

Table 5. Thermal resistances for the different types of heat transfer.

Thermal resistance (K/W)	**Type of heat transfer**
$R_{\mathrm{cond}} = \frac{l}{kA}$	Conduction
$R_{\mathrm{conv}} = \frac{1}{h_{\mathrm{conv}} A_{\mathrm{s}}}$	Convection
$R_{\mathrm{rad}} = \frac{1}{h_{\mathrm{rad}} A_{\mathrm{s}}}$	Radiation

Here

A is the cross-sectional area (m^2)
A_s is the surface area (m^2)
l is the length (m)
k is the thermal conductivity (W/mK)
h_{conv} is the convection heat transfer coefficient (W/m^2K)
h_{rad} is the radiation heat transfer coefficient (W/m^2K).

The radiation h_{rad} heat transfer coefficient can be calculated as

$$h_{\mathrm{rad}} = \frac{\dot{Q}_{\mathrm{rad}}}{A_{\mathrm{s}}(T_{\mathrm{s}} - T_{\mathrm{surr}})} = \varepsilon\sigma(T_{\mathrm{s}}^2 + T_{\mathrm{surr}}^2)(T_{\mathrm{s}} + T_{\mathrm{surr}}). \quad (14)$$

When calculating radiation, it is important to remember to keep the temperatures in Kelvin. With help of h_{rad} it is possible to express radiation in an analogous way to convection. When a surface is surrounded by air, convection and radiation happen simuntaneously and their thermal resistances are parallel to each other in a thermal network. However, if $T_{\mathrm{surr}} \approx T_{\infty}$, an equivalent heat transfer coefficient may be calculated and then h_{conv} is replaced by $h_{\mathrm{equivalent}}$ in the convection resistance, consequently one thermal resistance is enough for both radiation and convection in the network. $h_{\mathrm{equivalent}}$ is calculated as (Cengel 2003: 129–130)

$$h_{\mathrm{equivalent}} = h_{\mathrm{conv}} + h_{\mathrm{rad}}. \quad (15)$$

4 ANALYTICAL THERMAL MODELS FOR SQUIRREL CAGE MOTORS

When thermally analyzing an electric motor, there are both analytical and numerical methods. With the numerical methods, including the finite-element analysis (FEA) and the computational fluid dynamics (CFD), it is possible to accurately model any geometry. With CFD it is possible to simulate complex thermal flows such as the end winding area and obtain heat transfer coefficients. Simulation programs using numerical methods are however very time demanding in terms of model setup as well as computational time. In the design stage of a motor, numerical methods are very beneficial due to the accuracy. On the other hand, if the purpose is fast calculations with sufficient accuracy, analytical methods are mostly used, especially for online applications. (Boglietti 2016: 2714)

In this thesis, an analytical thermal model is developed in Wolfram SystemModeler. With the program SystemModeler it is possible to publish online tools. The target is to develop a simple thermal model with sufficiently accurate results. With a thermal equivalent circuit the internal temperature distribution can be determined. Thermal quantities have analogous electrical quantities and hence the heat flow is analogous to the electric current flow. (Pyrhönen 2014: 548–549) When constructing a thermal network, the motor is first divided into separate geometrical sections. The sections are then connected to neighboring sections through thermal resistances. Since this thesis works with transient heat transfer, thermal capacitances are added to all the sections that consist of solid material. The components where the losses are generated are described with internal heat generation. (Puranen 2006: 109)

Accordingly, the thermal models consist of these components:

- **Thermal resistors**, which conduct the heat flow. The thermal resistance *R* with the SI unit K/W is filled into the component. The value of *R* is determined by the geometric data and materials of the motor. No heat is stored in thermal resistors.
- **Nodes**, which are regions with constant temperature between other components. The SI unit of a node temperature is K.
- **Thermal capacitors**, which store heat energy. A heat capacitor is determined by the geometric data and materials of the motor. The SI unit is Ws/K.
- **Loss sources of different types**, some losses are temperature dependent and some losses are highly dependent on the load. Loss sources in a thermal circuit are similar to current sources in electric circuits. The unit in SI system is W.

The construction of a typical TEFC squirrel cage induction motor is shown in Figure 3. A squirrel cage motor may be divided into the different parts described with numbers in the figure.

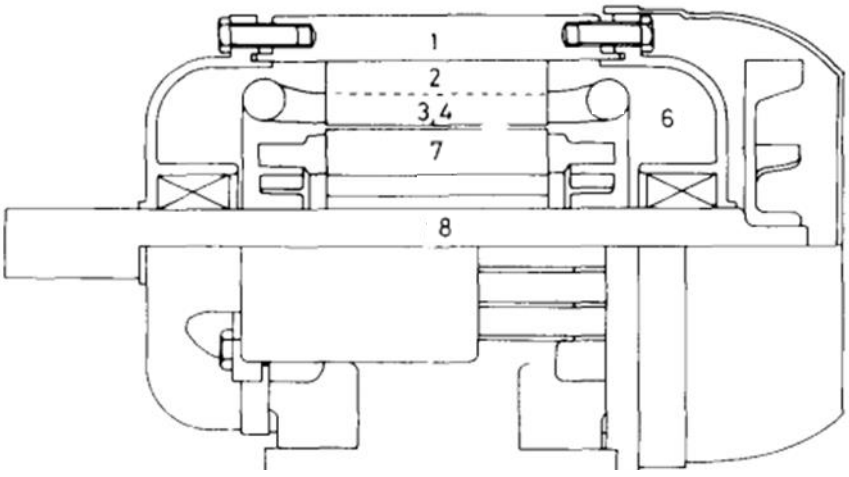

1. Frame
2. Stator yoke
3. Stator teeth
4. Stator winding
5. Air gap
6. End-cap air
7. Rotor (bars, rings and iron)
8. Shaft

Figure 3. The construction of a typical TEFC squirrel cage induction motor. Modified. (Mellor 1991: 206)

The majority of the electrical machines used for industrial applications run continuously in duty cycles where a steady-state temperature is reached, due to this fact the heat transfer is often studied in steady state. Studies performed for steady-state heat transfer

can neglect the heat capacitances in the model. However, a model without heat capacitances cannot estimate thermal behavior accurately enough for motors with loading variations in transient state. High temporary over loadings leads to high losses and high temperature gradients. (Puranen 2006: 102) If performing a simulation for a transient model with constant losses, the results are the same as for a stationary model; however it takes some time for the temperatures to reach thermal equilibrium. When simulating a thermal model without heat capacitors, the thermal equilibrium temperatures are reached immediately.

Today, there are numerous thermal models for electric motors available and many of them have been tested; some more accurately and some only for a few motors. Several developed models are complex networks, which is not a problem when performing computer simulations. However, the problem is often to determine all model parameters in a relatively easy way with sufficient accuracy. Many researchers have also tried to simplify the accurate complex models. The heat transfer in a squirrel cage motor takes several paths but it has been proven that many of these paths can be neglected in the model and still quite accurate results are achieved. (Boglietti 2003: 945)

4.1 Thermal model in steady state

First, a simple thermal model for stationary analysis is developed in SystemModeler in order to verify that the model with all thermal resistances is accurate enough. All motor types have test reports where the stationary thermal behavior is documented for a rated operating point; therefore the first thermal model is developed with the test reports as confirmation and calibration of the model.

A thermal model used for the design stage of a motor should be very accurate and complex but for fast estimations of temperatures for already existing motors a simplified model can be used. A complex and accurate thermal network model for steady-state analysis may look like the model in Figure 4 which was used by Kylander (1995).

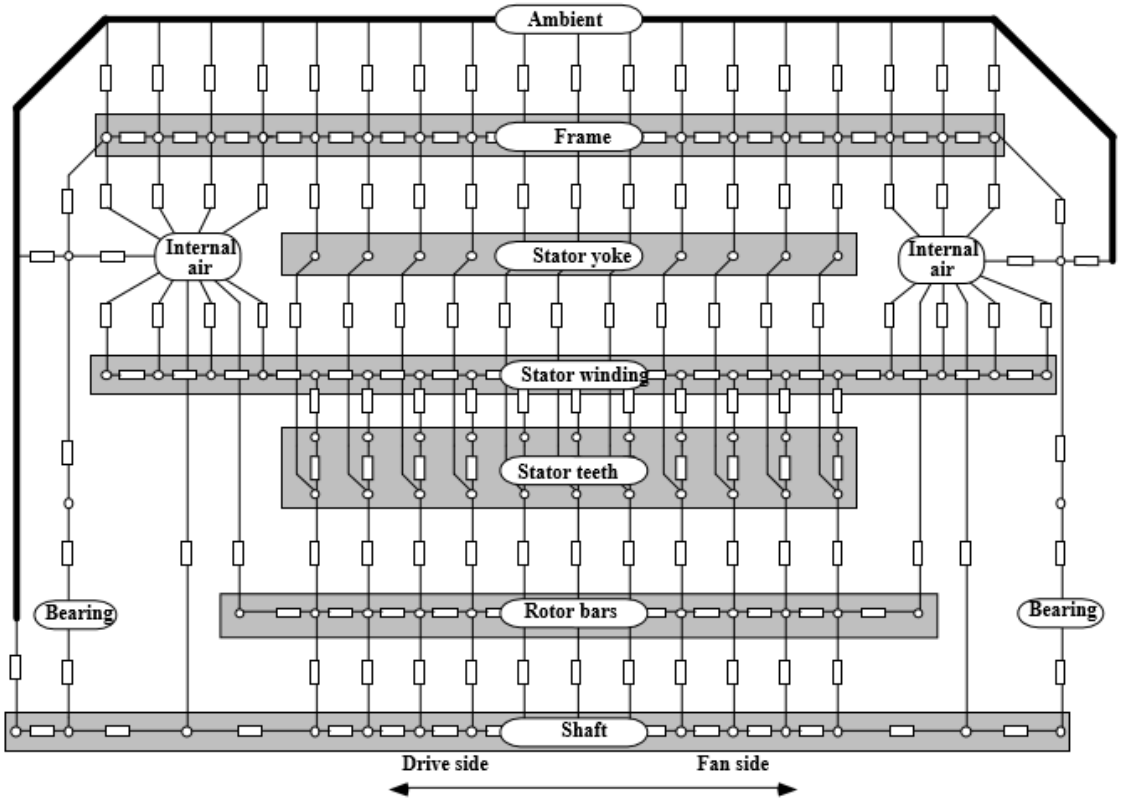

Figure 4. A complex thermal network with 170 thermal resistances, the network is primarly intended for the design process of an induction motor. (Kylander 1995: 47)

A simplified model for thermal analysis of an induction motor was developed by Boglietti (2003). The model started from a much more complex but very accurate model developed by Mellor and Turner in 1991. The simplified model is presented in Figure 5.

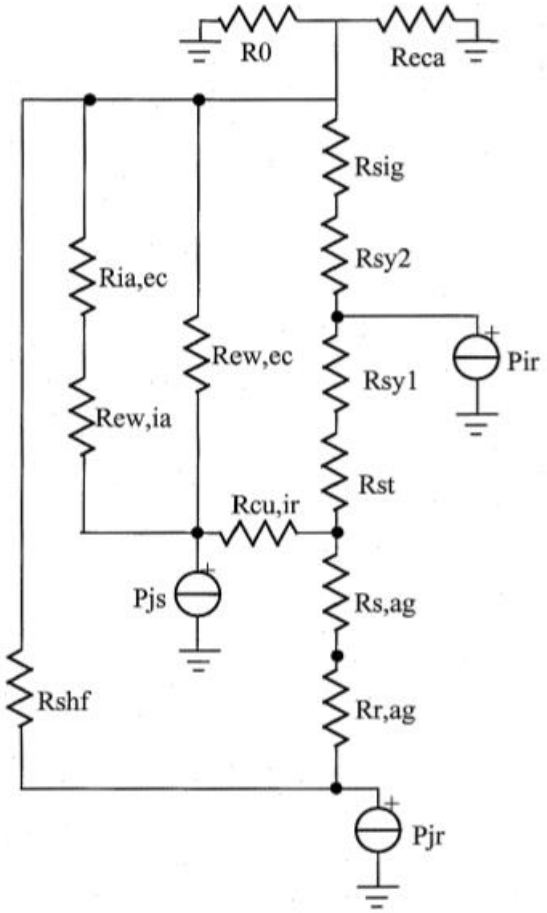

Figure 5. A simple stationary thermal model for induction motors developed from a complex thermal model. (Boglietti 2003: 946)

The model takes into account the conduction heat flux in the axial direction only in the shaft. The other conduction thermal resistances are computed using the equations of the hollow cylinder. The inner heat sources are assumed to be uniformly distributed and every cylinder is assumed to be thermally symmetrical in the radial direction. In addition, a motor symmetry is assumed around the shaft and the asymmetrical temperature distribution due to a possible fan in one end is neglected. For motors with variable speed, the convective thermal resistances are assumed to not be constant. The simplified equations used for hollow cylinders has a percentage error better than 2.5 % compared to the more complex equations used by Mellor and Turner in 1991. The error is hence lower than the uncertainty when calculating convection resistances. (Boglietti 2003: 945–946)

Thermal conduction resistance of a hollow cylinder is

$$R_{\mathrm{cy}} = \frac{1}{2\pi Lk} \ln\left(\frac{r_2}{r_1}\right), \tag{16}$$

where r_2 is the outer radius, r_1 is the inner radius, L is the length and k is the thermal conductivity. (Cengel 2003: 147)

The stationary model used in this thesis is similar to the one in Figure 5 but the additional and mechanical losses are also added and the thermal resistance R_{shf} is divided into R_{r} and R_{shf}. The resistance $R_{\mathrm{ew,ec}}$ is removed since the total thermal resistances between the end winding and enclosure have another approach in the developed model compared to the model developed in 2003 by Boglietti. The stationary thermal model used in this thesis is shown in Figure 6. The thermal resistances used in the model developed by Boglietti in 2003 and the model used in this thesis are shortly described in Table 6. The thermal capacitances are here not yet included.

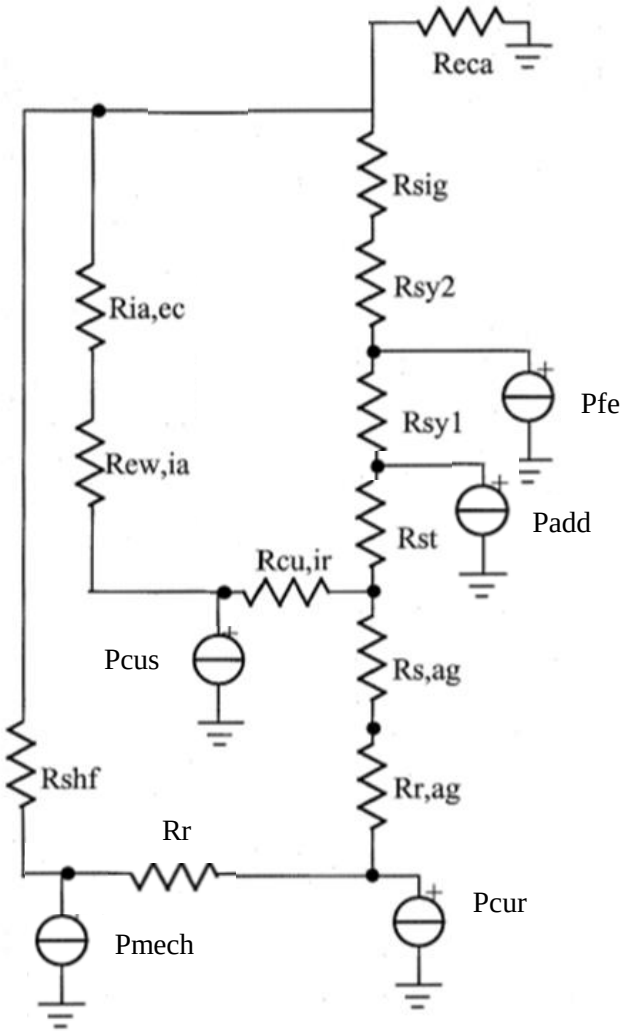

Figure 6. The model developed for this thesis, with the model developed by Boglietti (2003) as base.

Table 6. Thermal resistances and their two different descriptions.

Thermal resistance	Description (Boglietti 2003)	Modified description (used in this thesis)
R_{eca}	Convection thermal resistance between frame and ambient including forced convection	Equivalent thermal resistance between frame and ambient including: forced convection, natural convection and radiation
R_0	Natural convection thermal resistance between frame and ambient	-
$R_{ia,ec}$	Convection thermal resistance between internal air and end-caps	Equivalent thermal resistance between internal air and end-caps
R_{sy1}	Radial conduction thermal resistance of the stator yoke, lower half part	The same as in (Boglietti 2003)
R_{sy2}	Radial conduction thermal resistance of the stator yoke, upper half part	The same as in (Boglietti 2003)
R_{st}	Radial conduction thermal resistance of the stator teeth	The same as in (Boglietti 2003)
$R_{cu,ir}$	Conduction thermal resistance between stator copper and stator iron	The same as in (Boglietti 2003)
$R_{ew,ec}$	Conduction thermal resistance between stator winding external connections and frame	-
$R_{ew,ia}$	Convection thermal resistance between stator winding external connections and inner air	Equivalent thermal resistance between stator winding external connections and inner air
$R_{s,ag}$	Convection thermal resistance between stator teeth and air gap air	The same as in (Boglietti 2003)
$R_{r,ag}$	Convection thermal resistance between rotor and air gap air	The same as in (Boglietti 2003)
R_{sig}	Conduction resistance of the interface gap between the stator core and the motor frame	The same as in (Boglietti 2003)
R_{shf}	Radial rotor yoke thermal resistance, axial shaft thermal resistance	Axial conduction thermal resistance of the shaft part outside the rotor core
R_r	-	The radial thermal resistance due to the rotor yoke and the axial resistance of the shaft part below the rotor core

The losses are the stator Joule losses P_{Cus}, the rotor Joule losses P_{Cur}, the iron losses $P_{Fe,}$ the mechanical losses P_{mech} and the additional losses P_{add}.

Even if there were detailded information about the geometrical and material properties of a motor, it is not enough to accurately predict the thermal behavior of the motor. This is due to the fact that there are numerous complex thermal phenomena in electric motors that cannot be solved by pure mathematics. Often empirical data are used in analytical models in order to calibrate the model and to improve the accuracy. (Boglietti 2008: 1158)

4.2 Thermal model in transient state

When calculating transient thermal behavior, the thermal capacitances are required in the thermal model since excess heat is stored when the motor is running at overload. The dynamic thermal model looks like the stationary one, only heat capacitors are added to parts made of solid material.

For transient models, the conductive heat transfer is practically the same as for stationary models. However, the convective heat transfer is on the other hand not the same for stationary and transient models. The fluid velocity is often varying in transient simulations. The heat transfer coefficient of the end windings is a constant for steady state simulations but when simulating transient heating conditions, the convective heat transfer coefficient will depend on the temperature-dependent fluid properties as well as other factors which affect the flow. In an environment with air and forced convection, the magnitude of the convective heat transfer coefficient is usually between 30 and 300 W/m^2K. Due to the wide heat transfer coefficient range, non-negligible errors may arise if the coefficient is assumed to be constant. (Hettegger 2010: 581) However, if the rotor rotational speeds are assumed to be close to nominal speed for overloads and underloads and zero for standstill, only two different scenarios may be considered. For frequency converter operated motors with a varying rotational speed, the convection heat transfer coefficients cannot be assumed to be constant.

With the dynamic model it is possible to simulate standstill periods. In a standstill period, the loss inputs are zero and the rotor rotational speed is also zero. This affects all convection heat transfer coefficients and hence the convection thermal resistances. The dynamic model tries to evaluate standstill convection heat transfer coefficients which are lower than the coefficients for nominal speed.

There are IMs operating on variable-load constant-frequency duty cycles. Constant frequency also means constant speed. There are also IMs operating on variable-load variable-frequency duty cycles. The IMs operating with variable speed are significantly more challenging to model with a dynamic thermal model. There are two main differences, variable speed causes a shaft-mounted fan to rotate in the same speed as the motor and at low rotating speeds the heat transfer from the frame is significantly reduced. The second aspect is the change of iron losses, while iron losses are affected by different operating frequencies and hence the internal loss distributions as well as temperatures are affected. In addition, there are current harmonics in windings generating additional heating. (Valenzuela 2004: 692) The developed dynamic model takes into account only two different cases:

1. Squirrel cage induction motor with shaft mounted fan rotating at constant speed or at zero speed
2. Water cooled squirrel cage induction motor with constant water flow also when the motor is stationary

A dynamic thermal model for FC-operated motors is left for future investigation.

Thermal model for water cooled motor in transient state

Since water has a higher thermal conductivity than air, it also has higher heat transfer coefficients associated with it. As a consequence, water cooling is more effective than air cooling. On the other hand, water cooling has potential problems such as leakage, corrosion, extra weight and condensation and therefore it is often used only for applications where a high power density is required and air cooling is not sufficient. (Cengel 2003: 833)

ABB has a range of water cooled motors in IEC frame sizes 280–450. Water ducts in the frame transfers away the generated heat in an highly efficient way. The high cooling efficieny is also maintained at low rotational speeds. Typical applications where water cooling is advatageous are thruster and propulsion motors, wind turbine generators, water and waste water pumps, tunnel-boring machines, extruders, printing presses and paper machines. (ABB 2016a) Figure 7 shows a water cooled motor. There are radial water cooling ducts instead of the axial fins for a typical standard squirrel cage motor.

Figure 7. A water cooled motor with integrated radial water cooling ducts in the frame. (ABB 2016a)

The cooling effect of the water increases with decreasing input water temperature. It is recommended that the maximum inlet water temperature is 40 °C for frame sizes 355–450 and 30 °C for frame sizes 280–315. The water temperature rises while flowing through the cooling jackets and the outlet water has then a temperature 7–15 °C higher than the inlet water. (ABB 2011: 5)

A thermal model for water cooled squirrel cage motors is similar to the thermal model for standard squirrel cage motors. The equivalent thermal resistance from the motor frame to the ambient is the difference; it is much smaller for water cooled motors.

4.3 Evaluation of thermal resistances

Many researchers have tried to develope approximations for calculating the different thermal resistances, thus there are numerous different equations for the different resistances. Many parameters can be easily calculated with sufficient accuracy but there are however some parameters that are challenging to estimate.

Critical parameters in this thermal model are:

- Equivalent thermal resistance between external frame and ambient
- Equivalent thermal conductivity between stator winding and lamination
- Equivalent thermal resistance between end winding and end-caps, and
- Interface gap between stator lamination and external frame.

Different empirical dependencies for more demanding parameters have though been found. However, some of these critical parameters would need measured values or values obtained from numerical simulation methods, but since it is not possible to perform tests or numerical simulations for every single motor in a simple thermal model, other ways are implemented.

When calculating the different thermal resistances, many parameters and constants are needed. Some of them are presented in Figure 8 and Table 7 and the rest are presented in the concerned sections.

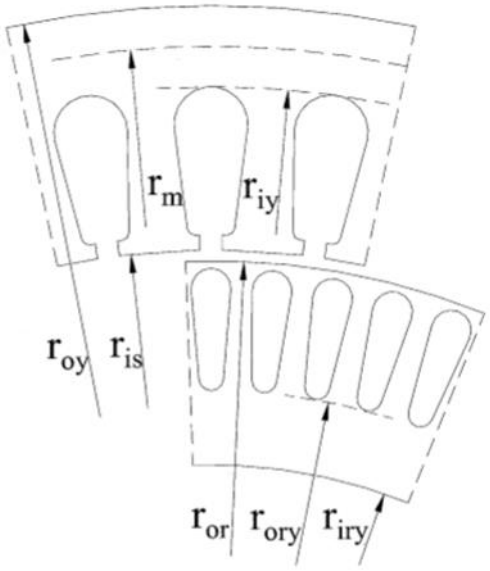

The radial dimensions are:

r_{oy}	outer value of the stator yoke radius
r_m	average value of the stator yoke radius
r_{iy}	value of the inner stator yoke radius
r_{is}	stator inner radius
r_{or}	outer rotor radius
r_{ory}	outer rotor yoke radius
r_{iry}	inner rotor yoke radius.

Figure 8. The main radial dimensions in a squirrel cage motor. (Boglietti 2003: 948)

Table 7. Heat transfer properties of some common materials used in electric motors at room temperature (293 K). (Pyrhönen 2014: 536)

Material	**Thermal conductivity k(W/K m)**	**Specific heat capacity c_p (kJ/kg K)**	**Density ρ (kg/m^3)**	**Resistivity (Ω m·10^{-8})**
Air, stagnant	0.025	1	1.20	
Aluminium, pure	231	0.899	2700	2.7
Aluminium, electrotechnical	209	0.896	2700	2.8
Copper, electrotechnical	394	0.385	8960	1.75
Insulation, typical insulation system	0.2			
Iron, pure	74.7	0.452	7897	9.6
Iron, cast	40–46	0.5	7300	10
Steel, carbon steel 0.5 %	45	0.465	7800	14–18
Steel, electrical sheet, in the direction of lamination	22–40		7700	25–50
Steel, electrical sheet, normal to lamination	0.6			

Dynamic viscosity of air at room temperature (20 °C) is $1.81 \cdot 10^{-5}$ Pa·s. (Boglietti 2003: 952)

The calculations of the thermal resistances are next presented.

4.3.1 One half of the radial conduction thermal resistances of the stator yoke, inner part (R_{sy1})

This conduction thermal resistance, R_{sy1}, can be estimated with good precision when the dimensions are known

$$R_{\mathrm{sy1}} = \frac{1}{2\pi k_{\mathrm{ir}} L_{\mathrm{TOT}}} \ln\left(\frac{r_{\mathrm{m}}}{r_{\mathrm{iy}}}\right), \tag{17}$$

where k_{ir} is the thermal conductivity in the radial direction of the stator core material and L_{TOT} is the stator core (and rotor core) length. (Boglietti 2003: 948) The value of k_{ir} is set to 35 W/(m·K) in the developed thermal model.

4.3.2 One half of the radial conduction thermal resistance of the stator yoke, outer part (R_{sy2})

This conduction thermal resistance, R_{sy2}, can be estimated with good precision when the dimensions are known

$$R_{\mathrm{sy2}} = \frac{1}{2\pi k_{\mathrm{ir}} L_{\mathrm{TOT}}} \ln\left(\frac{r_{\mathrm{oy}}}{r_{\mathrm{m}}}\right), \tag{18}$$

where k_{ir} is the thermal conductivity in the radial direction of the stator core material. (Boglietti 2003: 948)

4.3.3 Convection thermal resistances between the rotor, air gap and stator ($R_{\mathrm{s,ag}}$ and $R_{\mathrm{r,ag}}$)

The air gap is the most significant cooling channel for the machine, the flow inside the air gap removes heat generated in the rotor while it also removes friction losses and a part of the stator losses. (Jääskeläinen 2009: 2) The air gap thermal resistances need two different values, one value for when the motor is at standstill and one value for when the motor is rotating.

The convection coefficient related to the air gap depends on the length of the air gap, rotation speed of the rotor, the length of the rotor and the kinematic viscosity of the streaming fluid. When determining the heat transfer coefficient in the annulus, the Tay-

lor equation can be used. The Taylor number Ta describes the ratio of viscous forces to the centrifugal forces (Pyrhönen 2014: 545–546)

$$Ta = \frac{\rho^2 \Omega^2 r_{\mathrm{ag,m}} \delta^3}{\mu^2}, \tag{19}$$

where ρ is the mass density of the fluid, Ω is the angular velocity of the rotor, $r_{\mathrm{ag,m}}$ the average of the stator and rotor radii of the air gap, δ the radial length of the air gap, μ the dynamic viscosity of the fluid. A modified Taylor number, Ta_{m}, takes into account the radial air gap length and the rotor radius

$$Ta_{\mathrm{m}} = \frac{Ta}{F_{\mathrm{g}}}, \tag{20}$$

where F_{g} is the geometrical factor which is defined by equation

$$F_{\mathrm{g}} = \frac{\pi^4 \left[\frac{2r_{\mathrm{ag,m}} - 2.304\delta}{2r_{\mathrm{ag,m}} - \delta}\right]}{1697 \left[0.0056 + 0.0571 \left(\frac{2r_{\mathrm{ag,m}} - 2.304\delta}{2r_{\mathrm{ag,m}} - \delta}\right)^2\right] \left[1 - \frac{\delta}{2r_{\mathrm{ag,m}}}\right]^2}. \tag{21}$$

The radial length of the air gap is practically so small compared to the rotor radius that F_{g} is close to one and therefore $Ta_{\mathrm{m}} \approx Ta$. The Nusselt number is according to Becker and Kaye (1962):

- $Nu = 2$ for $Ta_{\mathrm{m}} < 1700$ (laminar flow)
- $Nu = 0.128 Ta_{\mathrm{m}}^{0.367}$ for $1700 < Ta_{\mathrm{m}} < 10^4$
- $Nu = 0.409 Ta_{\mathrm{m}}^{0.241}$ for $10^4 < Ta_{\mathrm{m}} < 10^7$.

The Nusselt number can then be used to calculate the heat transfer coefficient for one air gap surface which is from the rotor to the air gap or from the stator to the air gap when the thermal conductivity of air is k_{air} (Pyrhönen 2014: 546)

$$h = \frac{Nuk_{\text{air}}}{\delta}. \tag{22}$$

For a stationary motor, the Nusselt number is 2 which corresponds to the fact that heat transfer across the air gap is by conduction only. The Nusselt number may also be 2 for rotating motors if the air flow in the air gap is laminar, which is the case for many small and medium sized motors. (Mellor 1991: 207–208)

When *h* is calculated the thermal resistance is

$$R = \frac{1}{hA_{\text{s}}}, \tag{23}$$

where

$$A_{\text{s}} = 2\pi r_{\text{or}} L_{\text{TOT}}, \tag{24}$$

from the rotor to the air gap and

$$A_{\text{s}} = 2\pi r_{\text{is}} L_{\text{TOT}}, \tag{25}$$

from the stator to the air gap. (Boglietti 2003: 948)

There are some complications associated with the air gap heat transfer. For example, the heat transfer is affected by the surface roughness; a rough rotor has a heat transfer coefficient 40–70 % higher than a smooth rotor according to studies. This is because the roughness of the surfaces enlarges the cooling area and increases turbulence. In addition, the air gap length is temperature dependent due to thermal expansion of the rotor and stator. (Pyrhönen 2014: 546, Kylander 1995: 52) However, these aspects are not taken into consideration in this thesis.

4.3.4 Radial conduction thermal resistance of the stator teeth (R_{st})

This thermal resistance, R_{st}, can be estimated with quite a good precision, it takes into account the thermal flux from the stator teeth to the stator yoke. The stator teeth thermal resistance is calculated as for a cylinder.

$$R_{\mathrm{st}} = \frac{1}{2\pi k_{\mathrm{ir}} L_{\mathrm{TOT}} p_{\mathrm{ir}}} \ln\left(\frac{r_{\mathrm{iy}}}{r_{\mathrm{is}}}\right), \tag{26}$$

where p_{ir} is a reduction factor in percent and k_{ir} is the thermal conduction of the stator iron. p_{ir} is the teeth iron volume divided by the total teeth and slots volume. (Boglietti 2003: 948)

An approximation for p_{ir} is calculatad as

$$p_{\mathrm{ir}} = 1 - \frac{\mathrm{Q1} \cdot S_{\mathrm{slot}}}{\pi r_{\mathrm{iy}}^2 - \pi r_{\mathrm{is}}^2}, \tag{27}$$

where Q1 is the number of stator slots from Adept and S_{slot} is the stator slot cross-sectional area.

4.3.5 Axial conduction thermal resistance of the shaft (R_{shf})

This thermal resistance, R_{shf}, takes into account the axial thermal resistance of the shaft part outside the rotor core

$$R_{\mathrm{shf}} = \frac{1}{2}\left(\frac{0.5(L_{\mathrm{shf}} - L_{\mathrm{TOT}})}{k_{\mathrm{shf}} \pi r_{\mathrm{iry}}^2}\right), \tag{28}$$

where the shaft radius and the inner rotor yoke radius are considered to be the same. (Boglietti 2003: 949) L_{shf} is the shaft length and can be taken from the dimension prints, which are available online in the ABB Library. k_{shf} is the axial thermal conductivity for the shaft, whose value is set to 50 W/(m·K) in the developed model.

4.3.6 Radial thermal resistance due to the rotor yoke and the axial thermal resistance of the shaft part below the rotor core (R_r)

This thermal resistance, R_r, takes into account:

- The radial thermal resistance due to the rotor yoke
- The axial thermal resistance of the shaft part below the rotor core

This thermal resistance associated with the rotor and shaft can be calculated as

$$R_r = \frac{1}{2\pi k_{ir} L_{TOT}} \ln\left(\frac{r_{ory}}{r_{iry}}\right) + \frac{1}{4}\left(\frac{0.5 L_{TOT}}{k_{shf} \pi r_{iry}^2}\right), \tag{29}$$

where the shaft radius and the inner rotor yoke radius are considered to be the same. (Boglietti 2003: 949)

4.3.7 Thermal resistances between the stator winding external connection and inner air and frame

The convection heat transfer coefficient in the winding ends is the most complicated to calculate; this is because the flow field is too demanding to model. The convective heat transfer coefficient in the end winding space depends on the angular velocity of the rotor and on the geometry of the end region. The type of winding as well as the cooling method also affects the convection heat transfer coefficient of the winding ends. With numerical simulation such as CFD is it possible to get accurate values of the heat transfer coefficients in the end winding space. It is also possible to measure these thermal resistance associated with the end-space with a low frequency test. Analytically it is still impossible to get accurate values of the convective heat transfer coefficients in the end winding space. (Hettegger 2012: 2299, Puranen 2009: 121, Pyrhönen 2014: 546)

Due to the fact that it is practically impossible to estimate these thermal resistances, they are also a source to calculation errors in the developed model. Especially since these thermal resistances affect the simulated stator winding temperature significantly.

However, it is not possible to perform a CFD analysis or measure these thermal resistances for every single motor and therefore empirical dependencies have to be used.

A simplified thermal network as that in Figure 9 can be used to describe heat transfer between the end windings and the motor frame. In the figure, R_{NC} is the natural convection heat transfer which is the natural convection between the end windings and the inner air and the natural convection between the inner air and the motor frame in series. R_{RAD} is the radiation thermal resistance between the end windings and the motor frame. $R_{IA\text{-}MF}$ and $R_{EW\text{-}IA}$ are the forced convetion thermal resistances between the end-windings, inner air and motor frame. For a motor at standstill, the thermal resistance path for forced convection has to be considered as infinite. (Boglietti 2007: 1218)

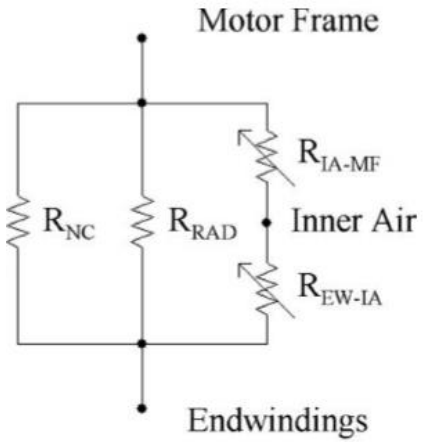

Figure 9. A simplified thermal network describing the heat transfer from the end windings to the motor frame. (Boglietti 2007: 1218)

$R_{IA\text{-}MF}$ and $R_{EW\text{-}IA}$ depend on the inner air movements. In fact, the end winding cooling effects in motors are highly dependent on the inner air speed. However, the inner air speed is not easy to estimate and therefore the pheriperal speed of the rotor is usually used. Squirrel cage motors have short-circuit rings with several wafters and fins and as a consequence air whirls are generated inside the motor end-caps. These air whirls increase the forced convection heat transfer between the end windings and end-caps. The end-space in squirrel cage motors may have different appearances which naturally leads to differences in air flow and hence heat transfer. Figure 10 presents three different examples of how the end-space may look in motors. (Boglietti 2007: 1214–1216)

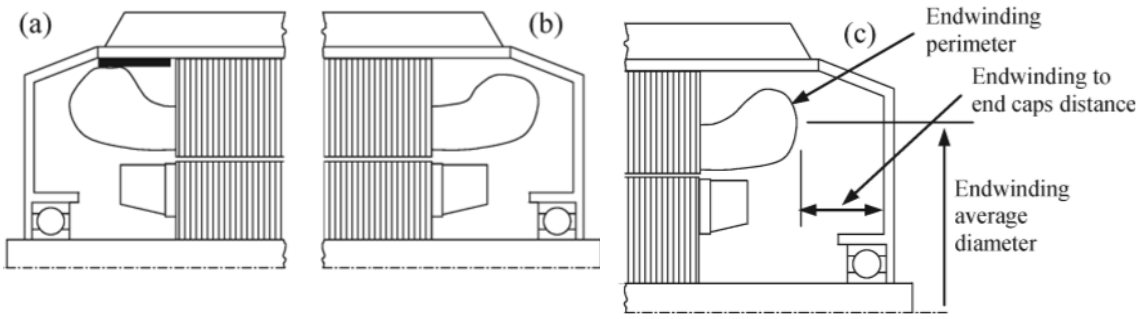

Figure 10. Different types of end-space regions.The black plate in (a) is an insulation plate. (Boglietti 2007: 1216)

The end-space is sometimes different in the drive end and non-drive end of the motor. As shown in Figure 10 (a), the end winding may be in contact with the enclosure through a thin insulation plate, this forms a conduction heat transfer path. The end winding may be inside the end-cap space as i Figure 10 (b). In Figure 10 (c) the end winding is not inside the end-cap space and there are more free space. (Boglietti 2007: 1216) In the developed thermal model, the natural convection, radiation and forced convection are all described with two thermal resistances in series. This is due to the fact that an equivalent heat transfer coefficient which represents forced convection, natural convection and radiation is used because of the empirical dependencies found in literature. The theory mentioned in Section 3.4 can be applied to the different thermal resistances presented in Figure 9; it is possible to add their different heat transfer coefficients and then to have only two different equivalent thermal resistances; one between the end windings and the inner air and the other between the inner air and the motor frame. In case of standstill, the forced convection heat transfer coefficient is zero.

The thermal resistances in Figure 9 can be regarded as an equivalent thermal resistance between the end windings and the motor frame, $R_{\mathrm{EW,MF}}$, which can be calculated with

$$R_{\mathrm{EW,MF}} = \frac{1}{\frac{1}{R_{\mathrm{NC}}} + \frac{1}{R_{\mathrm{RAD}}} + \frac{1}{R_{\mathrm{IA-MF}} + R_{\mathrm{EW-IA}}}}. \tag{30}$$

The heat transfer coefficients would look like

$$h_{\text{forced}} = \frac{1}{(R_{\text{IA-MF}} + R_{\text{EW-IA}})A_{\text{es}}} \tag{31}$$

$$h_{\text{NC}} = \frac{1}{R_{\text{NC}}A_{\text{es}}} \tag{32}$$

and

$$h_{\text{RAD}} = \frac{1}{R_{\text{RAD}}A_{\text{es}}}, \tag{33}$$

where A_{es} is the total end windings and end-caps surface areas. The equivalent convection heat transfer coefficient would be calculated as

$$h_{\text{equivalent}} = h_{\text{forced}} + h_{\text{NC}} + h_{\text{RAD}}. \tag{34}$$

If substituting the expressions for the different heat transfer coefficients into Equation 30, the equivalent heat transfer coefficient is

$$h_{\text{equivalent}} = \frac{1}{R_{\text{EW,MF}}A_{\text{es}}} \tag{35}$$

and the total thermal resistance between end windings and enclosure is

$$R_{\text{EW,MF}} = \frac{1}{h_{\text{equivalent}}A_{\text{es}}}, \tag{36}$$

which can be split into two resistances in series:

$$R_{\text{ew,ia}} = \frac{1}{A_{\text{ew}}h_{\text{ew}}} \tag{37}$$

and

$$R_{\mathrm{ia,ec}} = \frac{1}{A_{\mathrm{ec}} h_{\mathrm{ec}}}, \tag{38}$$

where A_{ew} is the surface area of the end windings and A_{ec} is the surface area of the end caps, $h_{\mathrm{equivalent}}$ has the same value as h_{ew} and h_{ec}. A_{ew} and A_{ec} can be approximated as

$$A_{\mathrm{ew}} = \frac{\pi}{2}\left((LM1 - L_{\mathrm{TOT}})2\pi r_{\mathrm{is}} + (LM1 - L_{\mathrm{TOT}})2\pi r_{\mathrm{iy}}\right) \tag{39}$$

and

$$A_{\mathrm{ec}} = 2\pi r_{\mathrm{ec}}^2, \tag{40}$$

where LM1 is half length of coil which is taken from Adept and r_{ec} is the radius of the motor frame which is approximately the IEC frame size of the motor. $\frac{\pi}{2}$ is a correction coefficient due to the fact that the endwinding surface is not smooth, because of the wires. The computation of A_{ec} should be more accurate but due to the difficulties it would cause, Equation 40 is considered reasonable at this point. These surface areas are the surfaces of the two end winding and two inner end-cap surfaces. It should be observed that these approximation are not that accurate but they give roughly estimated values in a simple way. (Boglietti 2003: 949, Boglietti 2007: 1220)

In order to calculate the thermal resistances $R_{\mathrm{ew,ia}}$ and $R_{\mathrm{ia,ec}}$, a value for the equivalent heat transfer coefficient is needed. Due to the importance of inner speed in endwinding cooling, many researchers have tried to find dependencies for the end windings heat transfer coefficients as functions of the rotor pheriperal speed. Boglietti (2007) found the correlations presented in Figure 11 and Boglietti (2009b) found the correlations presented in Figure 12. The results are in line with results published earlier by different researchers, these results are presented in Figure 13. (Boglietti 2007: 1214, 1221)

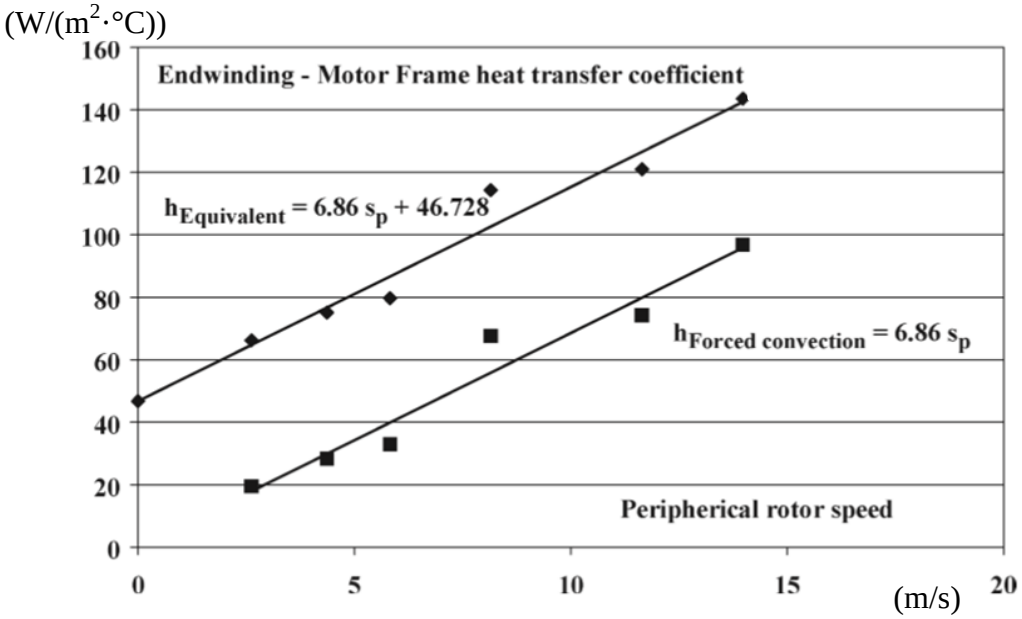

Figure 11. Heat transfer coefficients as a function of the peripheral rotor speed for a MA132 prototype. (Boglietti 2007: 1221)

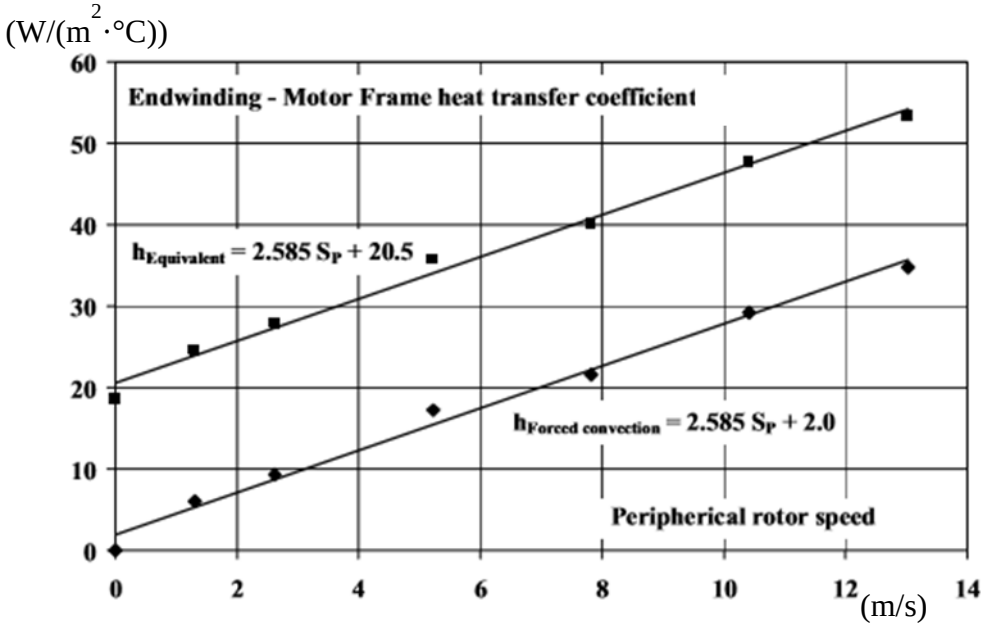

Figure 12. Heat transfer coefficients as a function of the peripheral rotor speed for a standard TEFC squirrel cage induction motor with rated output 2.2 kW. (Boglietti 2009b: 2)

In Figure 11, it can be seen that the forced convection coefficient equals zero when the rotor is not rotating, this is due to the fact that the forced convection thermal path is nonactive for zero rotational speed of the rotor. This verifies the measured results. (Boglietti 2007: 1221) Figures 11 and 12 also show that there are differences in the end winding heat transfer coefficients. For a more general thermal model, which is supposed to calculate the thermal behaviour for a wide range of motors, these end winding heat transfer coefficients should be more accurately investigated for different end-space geometries and frame sizes.

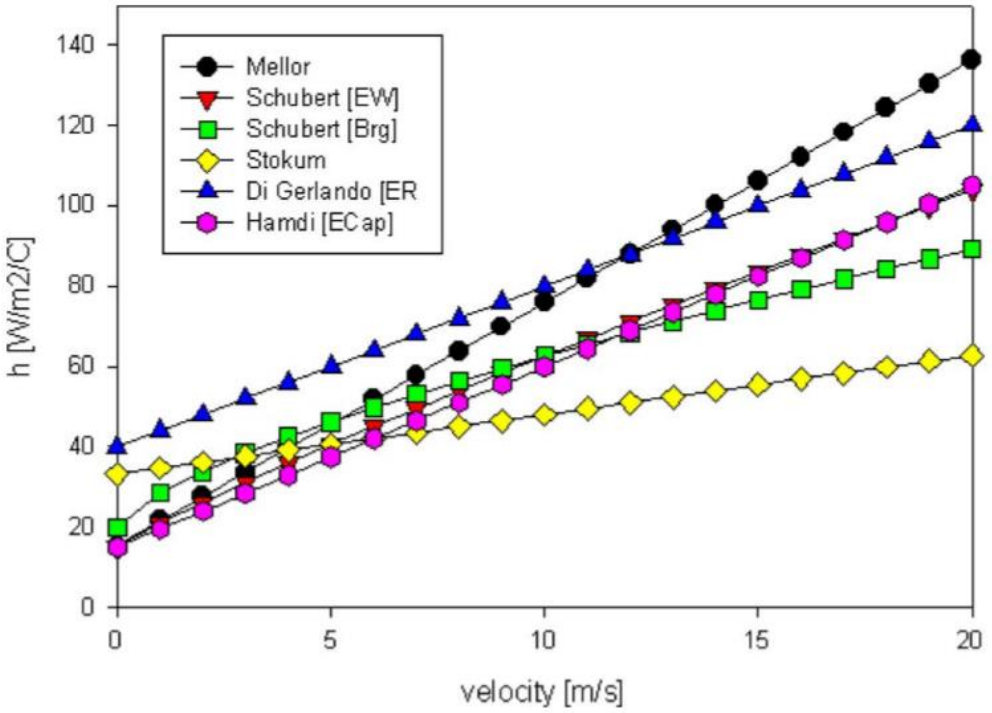

Figure 13. Correlations in the end regions for TEFC induction motors published by several different researchers. (Boglietti 2007: 1214)

The published correlations for the equivalent (radiation, natural convection and forced convection) heat transfer coefficients in the end-space region for TEFC IMs presented in Figure 13 all show the same linear behavior. However, they show some deviations from each other. Some of these correlations have been measured several years ago, when the insulation thermal conductivity was lower than today and in addition the rotors may have been wound rotors without fins and wafters which increase the heat

transfer. Some of these research papers in Figure 13 do not mention the testing methodology. (Boglietti 2007: 1215) For all measured equivalent heat transfer coefficients versus rotor pheriperal speed in Figures 11, 12 and 13, the dependency is linear, at least in the considered speed range. In measurements, it has been proven that the inner ventilation is more effective if there are more free space in the end-space region. Due to this, the equivalent heat transfer coefficient should be adjusted according to the end-space region geometry. (Boglietti 2007: 1221)

As a compromise between measured values of the end winding heat transfer coefficients, the convection heat coefficient for forced convection was suggested to be calculated according to Equation 41 by Bogletti (2007)

$$h = 6.22 v_{\mathrm{p}}. \tag{41}$$

In the developed thermal model, radiation, natural convection and forced convection combined are considered in the end-space region. They can be calculated with Equation 42, which is also a compromise between measured values and the equation was suggested by Boglietti (2007) as

$$h = 41.4 + 6.22 v_{\mathrm{p}}, \tag{42}$$

where v_{p} is the pheriperal speed of the rotor. For a stationary motor, h is then 41.4 W/(m^{2}K) which derives from natural convection and radiation. However, these equations are compromises of many measured values and for some motors it may be inaccurate as can be seen in Figure 12, where the investigated motor had a quite different dependecy for h. For example, the amount of inner air, the dimensions of the end windings, the rotor fins and tips and formation of the end shields all affect the value of h. (Boglietti 2007: 1221) For large motors, the rotor pheriperal speed may rise above 40 m/s or even 50 m/s and for rotor pheriperal speed values of that range, h would rise to a quite high value which may be regarded as too high. In the model, two modified equations for h are used when v_{p} rises above 30 m/s, they are

$$h = 41.4 + 5.22v_{\mathrm{p}}, \tag{43}$$

when $30 < v_{\mathrm{p}} < 40$ and

$$h = 41.4 + 4v_{\mathrm{p}}, \tag{44}$$

when $v_{\mathrm{p}} \geq 40$.

The rotor pheriperal speed is calculated as follows:

$$v_{\mathrm{p}} = r_{\mathrm{or}}\Omega, \tag{45}$$

where

$$\Omega = \frac{\mathrm{rpm} \cdot 2\pi}{60}. \tag{46}$$

4.3.8 Conduction thermal resistance between stator winding and iron ($R_{\mathrm{cu,ir}}$)

The thermal resistance between the stator winding and iron, $R_{\mathrm{cu,ir}}$, is a critical parameter since a large amount of heat is generated in the stator windings and hence a large amount of heat passes through this thermal resistance. In the axial direction of the stator winding it can be assumed that only the copper will conduct heat, but in the radial direction an equivalent thermal conductivity should be determined. The winding consists of the conductors surrounded by insulation material, possibly a resin to fill up excess space in the slots, a slot liner between the slot and the stator iron and in addition there may also be undesired air bubbles. The conductor has very good heat-conducting properties while the insulation has poor heat-conducting properties. For the radial direction, the thermal conductivity of copper is omitted. Between the slot liner and the stator iron there are a lot of air gaps due to the rough surface, however these air gaps are not considered in the model used in this thesis. (Puranen 2006: 118-120, Pyrhönen 2014: 550)

Since the majority of industrial motors have random wound windings, it is impossible to model each individual conductor. In addition, it is not even necessary to do that in order to estimate the temperature distribution. The most important is to model the buildup of the temperature from the wall of the slot to the centre of the slot. This is possible by using an equivalent thermal conductivity for the insulation and impregnation materials. The equivalent thermal conductivity depends on many complex factors, such as the insulation technique and quality of the impregnation. There may be air bubbles in the slot and they will decrease the equivalent thermal conductivity since air has approximately a thermal conductivity ten times lower than typical insulators. (Boglietti 2008: 1153, Puranen 2006: 119)

Different correlations for estimating the equivalent thermal conductivity have been found, one correlation for the equivalent thermal conductivity is

$$k_{\mathrm{cuir}} = 0.2425[(1 - KCU1)S_{\mathrm{slot}}L_{\mathrm{TOT}}]^{-0.4269}, \tag{47}$$

where *K*CU1 is the slot filling factor. The correlation has been found when investigating motors from two different manufacturers, the different manufacturers most likely have different impregnation processes and therefore the correlation should be reliable. (Boglietti 2008: 1153) In order for this dependency to work, the volume inside the square brackets is in cm^3. According to this dependency, the equivalent thermal conductivity k_{cuir} lies usually in the range 0.03–0.15 W/(m·K). However, as a comparison example, another correlation, presented by Staton in 2005 suggested equivalent thermal conductivity values in the range 0.06–0.09 W/(m·K) for industrial TEFC induction motors, depending on the stator slot filling factor.

When the equivalent thermal conductivity k_{cuir} is known, the thermal resistance is easily calculated with

$$R_{\mathrm{cu,ir}} = \frac{t_{\mathrm{eq}}}{k_{\mathrm{cu,ir}}A_{\mathrm{slot}}Q1}, \tag{48}$$

where t_{eq} is the equivalent thickness of the air and insulation in the stator slots, k_{cuir} is the equivalent conductivity coefficient of the air and insulation material in the stator slots. A_{slot} is the interior slot surface. The equivalent thickness of the air and insulation t_{eq} and the interior slot surface A_{slot} can be calculated with

$$t_{\mathrm{eq}} = \frac{S_{\mathrm{slot}} - S_{\mathrm{cu}}}{l_{\mathrm{sb}}} \tag{49}$$

and

$$A_{\mathrm{slot}} = l_{\mathrm{sb}} L_{\mathrm{TOT}}, \tag{50}$$

where S_{slot} is the stator slot cross-sectional area, S_{cu} is the copper section in the stator slot and l_{sb} is the perimeter of the stator slot. (Boglietti 2003: 950)

The cross-sectional area of the stator slot is approximated in a simple way by values found in Adept as

$$S_{\mathrm{slot}} = \mathrm{BSO1} \cdot \mathrm{HSN1} \tag{51}$$

and the stator slot perimeter is also approximated in a simplified way as

$$l_{\mathrm{sb}} = \mathrm{BSO1} + 2 \cdot \mathrm{HSN1} + \mathrm{BSI1}, \tag{52}$$

where BSO1 is the slot width closer to the yoke, HSN1 is the winding height and BSI1 is the slot width closer to the air gap. Figure 14 presents a few of the slot types that are possible in Adept.

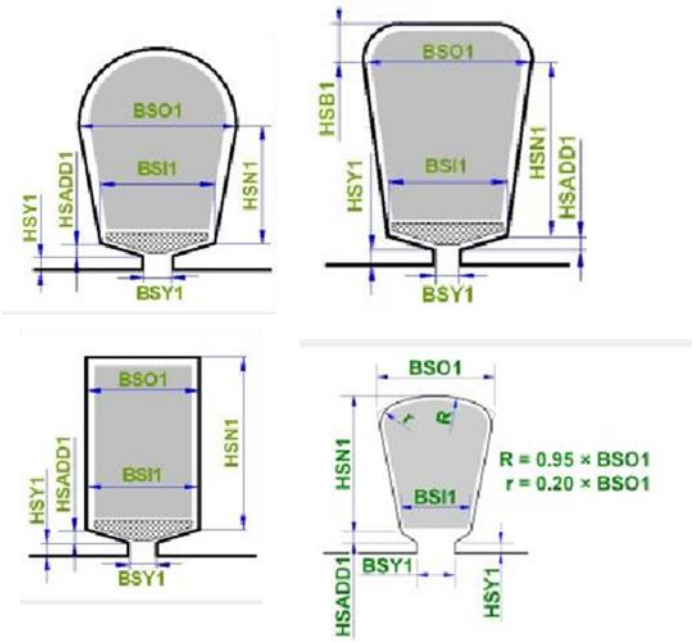

Figure 14. Some of the different stator slot types that are available in Adept. (Adept)

As can be seen from Figure 14, the area approximation is not accurate for all slot types. The perimeter approximation is not either accurate for all stator slot types.

4.3.9 Interface gap conduction resistance between stator core and motor frame (R_{sig})

This thermal resistance, R_{sig}, can be estimated with

$$R_{\text{sig}} = \frac{l_{\text{ig}}}{2k_{\text{air}}\pi r_{\text{oy}}L_{\text{TOT}}}, \tag{53}$$

where l_{ig} is the equivalent interface air gap length for the stator core to the frame. (Boglietti 2003: 950) The interface gap is a critical parameter and it depends on many factors such as the material hardness, smoothness of the surfaces, interface pressure and air pressure. This interface gap is of great importance since a large amount of the losses cross this path. It is not possible to calculate the interface gap value since it also depends on core-frame inserting process as well as the core assembly. For industrial induction motors, values between 0.01–0.08 mm have been measured and therefore it is recommended to vary l_{ig} between its expected upper and lower limit in order to determine its importance and then it is also necessary to calibrate l_{ig} with help of test results

in stationary mode. (Boglietti 2009a: 879–880) Due to temperature variations in the motor and thermal expansion, the interface gap will vary as a function of the temperature. This fact is however not considered in the model. (Puranen 2006: 120)

Table 8 presents interface gaps measured between the frame and the lamination. The interface gap has a surprisingly large effect on the stator winding and rotor temperature results. Its effects on the temperatures of some motors are investigated a little bit more precisely in Section 5.4.5 with a sensitivity analysis.

Table 8. Interface gaps found between the frame and lamination. (Staton 2005: 622)

Motor	**Interface gap (mm)**
4 kW TEFC IM	0.042
7.5 kW TEFC IM	0.076
15 kW TEFC IM	0.077
30 kW TEFC IM	0.016
55 kW TEFC IM	0.037
142 mm cast aluminum housing BPM	0.01
Range of 335–500 mm cast iron IMs	0.015
130 mm diameter aluminum IM	0.02
Average of the data above	0.037

The data in Table 8 has been determined by measuring the temperatures on both sides of the gap while passing a known amount of losses through the gap. If the frame is made of aluminium, it should result in a reduced interface gap due to the fact that aluminium is soft compared to cast iron, but this reduced interface gap is not realized at higher temperatures because of the difference in thermal expansion rates. Therefore, the interface gap increases with temperature and hence the advantage of aluminium softness is often eliminated. (Staton 2005: 621)

4.3.10 Thermal resistances between the frame and ambient

For the total thermal resistance between the frame and ambient, there are numerous different approximation ways available in the literature. When using the thermal model developed in this thesis, it is assumed that test reports are available for all motor types for a specific steady-state operating point and therefore a relatively simple approach may be considered.

Since all losses generated in the motor pass from the frame to the ambient, the total resistance from the frame to the ambient can be determined by dividing the motor frame temperature rise by the total amount of losses generated according to (Puranen 2006: 120)

$$R_{\mathrm{eca}} = \frac{\Delta T_{\mathrm{frame}}}{P_{\mathrm{tot}}}. \tag{54}$$

The temperature rise of the frame, $\Delta T_{\mathrm{frame}}$, can be taken directly from the test report, however, often it needs to be slightly adjusted in order for the simulated frame temperature to match the measured frame temperature. The process is hence as follows: the frame temperature can be seen from the test report, and then R_{eca} can be adjusted until the simulated frame temperature matches the measured one. As mentioned, this is for the specific tested operating point and if for example the speed changes, new test results would be required in order for this to work properly. If the fan speed increases, R_{eca} would decrease and vice versa, but for a specific air velocity and hence motor speed, the value of R_{eca} is constant. If the motor is stationary and the speed equals zero, this thermal resistance is largely affected and empirical dependencies need to be considered. The theory behind this total resistance is shortly reviewed.

The heat transfer from the motor frame to the ambient may be described with four thermal resistances as in Figure 15.

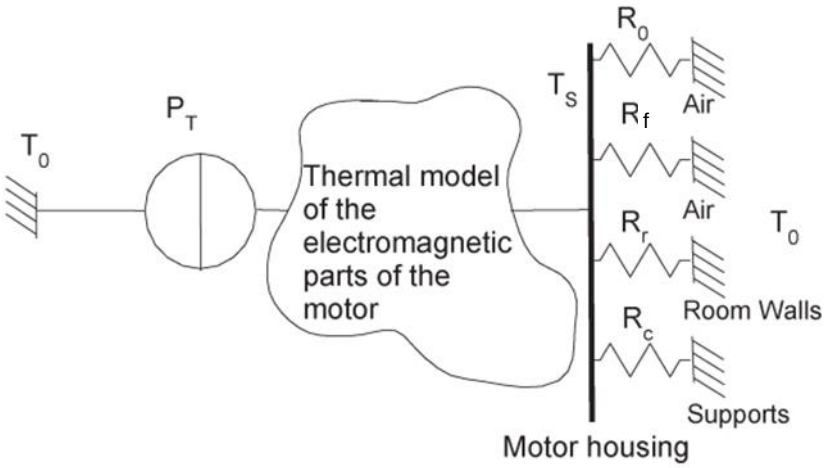

Figure 15. A thermal model describing the thermal resistances between the motor frame and the ambient (modified). (Boglietti 2006: 688)

R_0 is due to natural convection, R_f is due to forced convection, R_r is due to the radiation and R_c is the conduction heat transfer through the supports. R_c depends hence on the mounting arrangement and will be ignored in this thesis. R_r can be neglected when the motor is cooled with a fan, however, if the fan rotates at a very low speed, then the role of R_r can be significant. (Boglietti 2006: 688) For TEFC motors, the convective heat transfer coefficient for the heat removal from the frame to the surroundings depends largely on the air velocity from the fan. (Pyrhönen 2014: 545)

For operating points without test results, there are many different correlations for the forced convection thermal resistance, for smooth motor frames and also for finned frames. The different correlations use dimensionless numbers in order to estimate the convection heat transfer coefficient *h*. For different correlations, the inlet air velocity on the motor frame from the fan is needed. The speed of cooling air is difficult to estimate correctly and in addition the air speed distribution over the frame is not constant. This is due to air leakage and the fact that some of the fin channels are blocked by for example bolts or terminal boxes. Relationships have however been found for the air velocity. Nevertheless, when empirical dependencies with dimensionless numbers and air velocity were used in the developed thermal model, it was clear that the frame to ambient thermal resistance needed to be compensated in order for the frame temperature to

match tested results. Therefore, it was determined that the thermal resistance between frame and ambient can be calibrated with the simple Equation 54 instead of using different more complex dependencies and still be required to calibrate.

However, if the convection heat transfer coefficient h is known, the thermal resistance is

$$R = \frac{1}{hA_s}, \tag{55}$$

where A_s is the surface area of the frame. The convection heat transfer coefficient h may be between 20 and 40 W/m^2·K for natural convection while the value can exceed 80 W/m^2·K for forced convection. (Hachicha 2011: 3) Due to the finned surface, the surface area is bigger than for a plain cylinder. For a plain cylinder A_s is calculated according to

$$A_s = 2\pi r_{ec} L_{ec} + 2\pi r_{ec}^2, \tag{56}$$

where L_{ec} is the motor frame length which can be taken from for example dimension prints. However, the area for a plain cylinder is far too small for many finned motor frames and therefore two correction factors are used depending on frame size. The motor frame surface area is then for IEC frame sizes below 160

$$A_s = \frac{(2\pi r_{ec} L_{ec})}{0.6} + 2\pi r_{ec}^2 \tag{57}$$

and for IEC frame sizes above and equal to 160

$$A_s = \frac{(2\pi r_{ec} L_{ec})}{0.4} + 2\pi r_{ec}^2. \tag{58}$$

The correction factors 0.6 and 0.4 derive from surface area calculation for finned frames but for many motors the correction factors should be even smaller resulting in even bigger areas. In order to not overestimate the surface areas, these values are chosen at this

point. For water cooled motors, without finned frames, the motor surface area is calculated as for a plain cylinder.

For the dynamic model and a standstill scenario, the relationship below for natural convection and radiation can be used to estimate the thermal resistance for the frame when the rotational speed equals zero for TEFC IMs. For TEFC motors which usually have finned frames, the thermal resistances R_0 and R_r, can be estimated by using a correlation between the equivalent resistance $R_{0,r}$ and the motor frame surface area. Tests were carried out on TEFC induction machines in the power range 1.5–1000 kW and the dependency presented in Figure 16 was discovered. (Boglietti 2008: 1152)

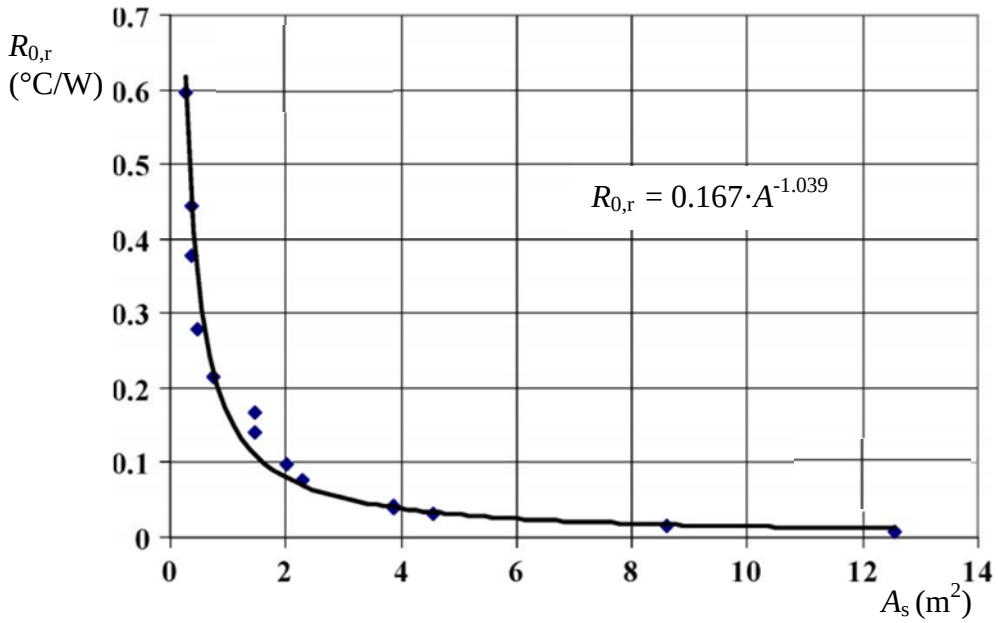

Figure 16. The combined natural convection and radiation equivalent resistance $R_{0,r}$ as a function of the motor frame surface area for TEFC induction motors 1.5–1000 kW. (Boglietti 2008: 1153)

The area A_s used in the correlation is for a finned surface area. The area used in the developed thermal model is the area for a smooth cylinder with a correction factor for the stator frame.

For water cooled motors, the water is assumed to be running through the water channels also when the motor is at standstill and therefore the thermal resistance for water cooled motors is always due to forced convection of water and hence natural convection and radiation can be neglected.

4.4 Evaluation of thermal capacities

When performing a transient thermal analysis, the thermal capacities have to be included in the model. The thermal capacity determines the ability to store heat energy. How much heat a thermal capacitor can store depends on the specific heat capacity c_p of the material and the mass of the capacitor. With the density and volume of the material it is possible to calculate the heat capacity according to Equation 59. If the mass is known, it is possible to use the mass of a part instead of the volume and density. The heat capacity of a part is calculated with

$$C = \rho V c_\mathrm{p} = m c_\mathrm{p}. \tag{59}$$

Since Adept gives the masses of the motor active parts, the mass will be used for the active parts in these thermal models. For the other significant parts, which are the frame with end-shields and the shaft, the masses can be taken for example from part drawings.

The specific heat capacities needed are presented in Table 9.

Table 9. Specific heat capacites needed for the heat capacitors in SystemModeler. (Adept, Pyrhönen 2014: 536)

Material	**Specific heat capacity c_p (J/kg·K)**
Stator and rotor cores	460
Shaft	475
Stator copper winding	380
Frame, cast iron	500
Frame, aluminium	900
Rotor bars and rings, aluminium	900
Insulation	1.045
Water	4190

4.4.1 Heat capacity of stator winding

The copper mass can easily be taken from Adept. The heat capacity of the stator winding is then

$$C_{\text{winding}} = m_{\text{winding}} \cdot c_{\text{copper}}. \tag{60}$$

The insulation heat capacity can be evaluated according to

$$C_{\text{ins}} = S_{\text{slot}} L_{\text{TOT}} Q1(1 - KCU1)\rho_{\text{ins}} c_{\text{ins}} \tag{61}$$

(Boglietti 2016: 2716) The density value used for the insulation is 70 kg/m^3.

4.4.2 Heat capacity of stator iron parts

The mass of the stator iron can be taken from Adept. The heat capacity of the stator iron is then

$$C_{\text{st iron}} = m_{\text{st iron}} \cdot c_{\text{st iron}}. \tag{62}$$

4.4.3 Heat capacity of rotor iron

The mass of the rotor iron can be taken from Adept. The heat capacity of the rotor iron is then

$$C_{\text{rt iron}} = m_{\text{rt iron}} \cdot c_{\text{rt iron}}. \tag{63}$$

4.4.4 Heat capacity of rotor bars and rings

The masses of the bars and rings can be taken from Adept. The heat capacity of the squirrel cage is then

$$C_{\text{sq cage}} = (m_{\text{bars}} + m_{\text{rings}}) \cdot c_{\text{sq cage}}. \tag{64}$$

4.4.5 Heat capacity of frame

The mass of the frame can be taken from the frame drawing and the masses of the end-shields can be taken from the end-shield drawings. The heat capacity of a cast iron stator frame with end-shields is then

$$C_{\text{frame}} = (m_{\text{frame}} + 2 \cdot m_{\text{endshield}}) \cdot c_{\text{castiron}}. \tag{65}$$

The frame may also be made of aluminium and in that case the aluminium mass is multiplicated by the specific heat capacity of aluminium instead. In the SM model it is possible to choose cast iron frame or aluminium frame and then the simulation program chooses the right specific heat capacity.

For water cooled motors, the heat capacity of the water is added to this heat capacity in the model. It may be important to consider the amount of water for transient simulations

since water has a high specific heat capacity and therefore a significant amount of heat may be stored in the cooling water if the amount of water is big.

4.4.6 Heat capacity of shaft

The mass of the shaft may be taken from the shaft drawing. The heat capacity of the shaft is then

$$C_{\text{shaft}} = m_{\text{shaft}} \cdot c_{\text{shaft}}. \tag{66}$$

4.5 Evaluation of heat sources

The heat sources are the different motor losses. It is important to know how the different losses vary with the load and temperature in order to do a dynamic thermal model. The losses can be accurately calculated with Adept.

Another important thing regarding the losses is the loss allocation. It is important to estimate how the different losses are splitting up in the motor thermal network. Stator copper losses can be injected to the stator winding node. The additional losses can be apportioned to the stator teeth and stator yoke interface. The iron losses are injected to the middle of the stator yoke. The rotor losses are injected to the rotor. (Benamrouche et al. 2006: 264) Mechanical losses consist of friction and windage losses, the windage losses are mainly due to the fan and they do not contribute to the heating of the machine. This is because the dissipated energy is used to accelerate the cooling air. The friction losses are located in the bearings and in the bearing sealings and hence they contribute to the heating. (Kylander 1995: 23, Pechanek 2015: 560)

For motors with higher output power, the mechanical losses are a significant part of the total losses and they cannot be neglected. For motors with rated output power around 80 kW the amount of mechanical losses usually are around 10 % of the total losses and thereafter the mechanical loss share is increasing further. Due to this fact, a part of the

mechanical losses have to be injected to the shaft node even though it is challenging to know how big part of the mechanical losses that are generated in the bearings.

The rotor temperature is not calculated properly with the above loss allocation. Since all rotor losses are injected to the same node in the developed thermal network, the temperature gradient will be too high. In order to get a better temperature value the rotor should be modelled more accurately. The rotor temperature is however not so important for induction motors but for permanent magnet synchronous motors it is critical due the magnets in the rotor. (Dajaku 2006: 1–2)

With help of Adept and its tool Optimizer it is also easy to see how the different loss types are changing with the load. Some motors were calculated with Optimizer in order to visualize the loss variations. Figure 17 shows the loss variations as a function of the load for the motor M3BP 200 MLA 4 with output power 30 kW and operating frequency 50 Hz. Similar behaviors were seen for other frame sizes. It can be noticed that the variations in rotor and stator Joule losses cannot be neglected. For standstill scenarios, all loss components are equal to zero.

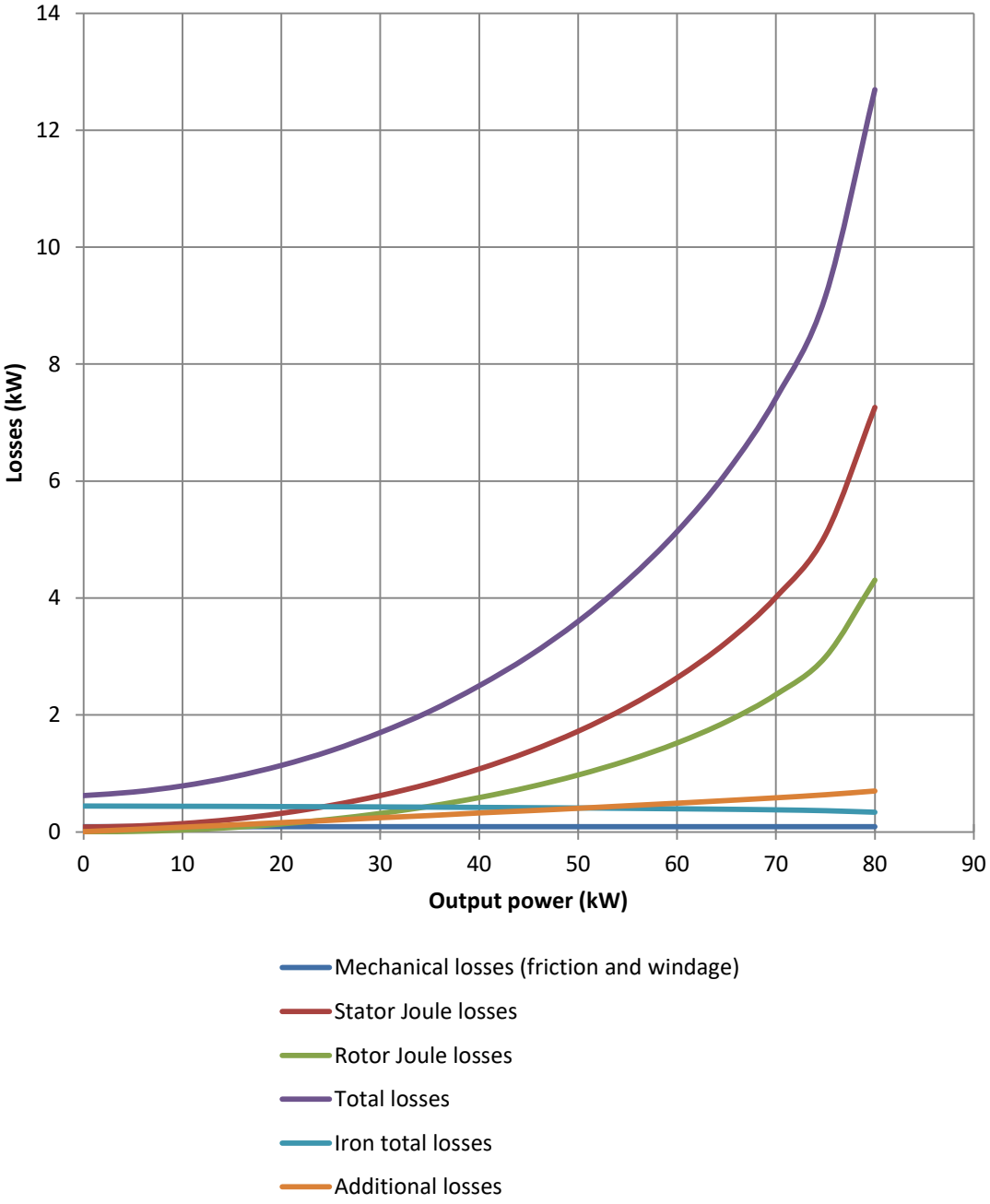

Figure 17. Loss components with the changing load for the motor M3BP 200 MLA 4, 30 kW, 50 Hz.

4.5.1 Evaluation of stator Joule losses (P_{Cus})

The stator Joule losses, P_{Cus}, grow almost exponentially with the output power, as shown in Figure 17. For the stator Joule losses, a linear resistive temperature coefficient for copper is used in order to simulate the increasing stator copper losses with

temperature. The value for the resistive temperature coefficient is $3.9 \cdot 10^{-3}$ 1/K. (Mäkelä 2010: 177)

For the stationary model, the stator Joule losses can be described with a Fixed Heat Flow-component but for the dynamic model they are described with a CombiTimeTable togheter with a Prescribed Heat Flow-component. The user checks from Adept the stator Joule loss values for different underloads and overloads and fills into the CombiTimeTable called LossTable.

4.5.2 Evaluation of rotor Joule losses (P_{Cur})

The rotor Joule losses, P_{Cur}, grow almost exponentially with the output power, as shown in Figure 17. For the rotor Joule losses, a linear resistive temperature coefficient for aluminium is used in order to simulate the increasing rotor Joule losses with temperature. The value for the resistive temperature coefficient is $4.0 \cdot 10^{-3}$ 1/K. (Mäkelä 2010: 177)

For the stationary model, the rotor Joule losses can be described with a Fixed Heat Flow-component but for the dynamic model they are described with a CombiTimeTable togheter with a Prescribed Heat Flow-component. The user checks from Adept the rotor Joule loss values for different underloads and overloads and fills into the CombiTimeTable called LossTable.

4.5.3 Evaluation of iron losses (P_{Fe})

For the stationary model, the iron losses P_{Fe} can be described with a Fixed Heat Flow-component but for the dynamic model they are described with a CombiTimeTable togheter with a Prescribed Heat Flow-component. The user checks from Adept the iron loss values for different underloads and overloads and fills into the CombiTimeTable called LossTable.

4.5.4 Evaluation of additional losses (P_{add})

For the stationary model, the additional losses P_{add} can be described with a Fixed Heat Flow-component but for the dynamic model they are described with a CombiTimeTable togheter with a Prescribed Heat Flow-component. The user checks from Adept the additional loss values for different underloads and overloads and fills into the CombiTimeTable called LossTable.

4.5.5 Evaluation of mechanical losses (P_{mech})

Since the mechanical losses, P_{mech}, are a significant part of the total losses for bigger frame sizes, a part of them should be involved in the thermal model. With help of a mechanical loss factor, P_{mech_factor}, in the thermal model it is possible to account for a part of the mechanical losses. The default value of the mechanical loss factor is 0.5 which means that half of the mechanical losses calculated by Adept are contributing to the heating of the machine. This value can though be adjusted, for smaller frame sizes the mechanical factor does not make any significant difference since the amount of mechanical losses is so small, but for larger motors the effect may be considerable.

For the stationary model, the mechanical losses P_{mech} can be described with a Fixed Heat Flow-component but for the transient model they are described with a CombiTimeTable togheter with a Prescribed Heat Flow-component. The user checks from Adept the mechanical loss values for different underloads and overloads and fills into the CombiTimeTable called LossTable.

For water cooled motors, which do not have cooling fans, all of the mechanical losses should be considered and hence P_{mech_factor} should be 1 which is automatically set in the developed thermal model when the user chooses water cooling as cooling method.

4.6 Thermal model calibration

If a specific motor or a specific type of motors would be thermally analyzed, it would be possible to create a very accurate analytical thermal model by measuring or numerically simulating all critical parameters for the certain motors. However, the thermal model developed in this thesis is supposed to perform a reasonably accurate thermal analysis for a wide range of squirrel cage motors and therefore it is always necessary to calibrate the model for an operating point with test results before analyzing transient states without test results.

The two critical parameters that are calibrated for every motor are the equivalent interface gap between the stator core and the motor frame, l_{ig} and the total thermal resistance between the motor frame and the ambient, R_{eca}. The thermal resistance between the frame and ambient is calibrated by filling the frame temperature rise from the test report into the model. However, often the frame temperature rise from the test report needs to be adjusted in order for the simulated frame temperature to match the measured frame temperature. By adjusting l_{ig}, the winding temperature is affected while the frame temperature practically remains unaffected. l_{ig} can hence be adjusted in order to get a consistent value for the stator winding temperature. For motors with higher output power it is also necessary to take a closer look at the mechanical losses and it may be necessary to adjust the P_{mech_factor}.

However, sometimes calibration of l_{ig} and R_{eca} is not enough for a motor to achieve steady-state temperatures found in test reports. If this happens, it is most likely due to the end winding heat transfer coefficient. Since the heat transfer coefficient h_{ew} has rotor pheriperal speed dependencies varying approximately between $20+3\cdot v_p$ and $45+8\cdot v_p$ the difference in the possible value of h_{ew} may be large, especially for higher rotational speeds. Then there may be one more uncertain parameter, the equivalent thermal conductivity, k_{cuir}. When different empirical dependencies for k_{cuir} were compared, it was observed that there are variations in the value and their effects on the temperature results may be significant even though the difference was only for example 0.05 W/(m·K).

5 SIMULATIONS IN SYSTEMMODELER

SystemModeler is a complete physical tool for modeling and simulation. The standard Modelica model language is fully supported by SystemModeler. In this chapter, some basic information about Modelica and SystemModeler is presented. Then the developed analytical dynamic thermal model is presented and simulation results for four squirrel cage motors are shown. In the last section of this chapter a sensitivity analysis is performed for the four squirrel cage motors simulated earlier.

5.1 Modelica language

The Modelica language is developed by the Modelica Association, which is a non-profit organization seated in Linköping, Sweden. Modelica is an object-oriented language and it is freely available for encouraging research and industrial development. With Modelica it is possible to model multi-domain large, complex and heterogenous systems. Differential, algebraic and discrete functions are used to mathematically describe models in Modelica. Equations can be typed directly into Modelica and Modelica will automatically decide which variable needs to be solved. (Modelica Association 2014: 1) The Modelica language supports the reuse and exchange of components and models since that is of greatest importance for handling complexity efficiently. Therefore, models of standard components are usually available in the constantly growing Modelica Standard Library. In general, when building a new component, an existing one can be modified in order to fulfill the new requirements. (Otter 2001: 1–2)

5.2 Simulation software SystemModeler

SystemModeler consists of a Model Center which is for the modeling and a Simulation Center for the simulations. As mentioned above, SystemModeler contains the Modelica Standard Library. In this thesis, the Thermal standard package which contains the heat

transfer–package is mostly used. Other main packages such as Blocks, Constants, Math and SIunits are also used in order to compose the thermal models.

It is possible to see how every component is designed by choosing ‘View Documentation’ when right-clicking the component.

When building a model, there are two graphical views (icon and diagram) and then the text view. The simplest way to assemble the model is by drag-and-drop of components from the Modelica Standard Library even though it is also possible to write in the text view. The components are easily connected to each other with the ‘Connection Line Tool’. When all components are connected it is time to give values to all parameters. Before the simulation is started, the class is validated by clicking the ‘Validate Class’ button on the toolbar. The validation will detect and report errors and the errors are now shown is the ‘Messages’ view.

When a model is ready the ‘Simulation Center’ can be started. Before simulating, the simulation settings are determined. In the ‘Simulation Center’ it is possible to plot different variables. In this thesis, the most interesting variables are the temperatures for different parts of the motor. The parameters can be modified in ‘Simulation Center’ and the model can then be simulated again with the new parameter settings. There are five different solvers in the ‘Simulation Center’:

- DASSL, a variable step size and variable order solver. It uses a backward differentiation formula method.
- CVODES, a variable step size and variable order solver. It also uses a backward differentiation formula method and in addition it supports forward sensitivity analysis.
- Explicit Euler, fixed step size solver.
- Heun’s method, fixed step size solver.
- Runge Kutta (RK4), fixed step size solver. (Wolfram Research, Inc. 2012: 114)

When a model is complete, it is possible to use the publisher tool which generates documentation for Modelica classes. The documentation can be viewed in any web browser and it does not require SystemModeler. In order to get a graphical representation of the

published class in a web browser, Microsoft Silverlight plugin is required. It is also possible to update an already published class. (Wolfram Research Inc. 2012: 27–31)

5.3 Thermal models

All components used in the thermal model exist in the Modelica Standard Library. In order to facilitate for the end-user in SystemModeler, the parameters which the user gives in SystemModeler are minimized and when it is possible, the parameters are taken directly from Adept. In the thermal models presented in this chapter, the names of data presented in Table 10 are used.

Table 10. Names of data used in SystemModeler with corresponding descriptions.

Name in SystemModeler	Unit in SM	Value or equation	Description
P_{Cus}	W	User fills	Stator Joule losses
P_{Cur}	W	User fills	Rotor Joule losses
P_{Fe}	W	User fills	Iron losses
P_{mech}	W	User fills	Mechanical losses
P_{add}	W	User fills	Additional losses
T_{amb}	°C	User fills	Ambient temperature
T_{motor}	°C	User fills	Temperature of motor parts when starting.
DO1	mm	User fills	Stator core outer diameter, DO1 in Adept
DI1	mm	User fills	Stator core inner diameter, DI1 in Adept
DI2	mm	User fills	Rotor core inner diameter, DI2 in Adept
HYOKE2	mm	User fills	Yoke height of rotor, HYOKE2 in Adept
L_TOT	mm	User fills	Lenght of stator core (and rotor core), L_TOT1 and L_TOT2 in Adept
delta	mm	User fills	Air-gap length. Delta in Adept
L_{ec}	mm	User fills	Length of motor frame
L_{shf}	mm	User fills	Length of shaft
LM1	mm	User fills	Half length of coil, LM1 in Adept
l_{ig}	mm	User fills	Equivalent interface air-gap length for the stator core to the frame, can be assumed to be 0.01–0.08 mm. Check lower and upper limits.

Table continues

Table 10 continues

r_{ec}	mm	User fills	Radius of the motor frame. From frame size.
Q1	number	User fills	Number of slots in stator, Q1 in Adept
rpm	rpm	User fills	Motor nominal speed
BSO1	mm	User fills	Stator slot width, closer to the yoke. BSO1 in Adept
HSN1	mm	User fills	Winding height, HSN1 in Adept
BSI1	mm	User fills	Stator slot width, closer to the air-gap. BSI1 in Adept
KCU1		User fills	Stator slot filling factor, KCU1 in Adept
m_{st_iron}	kg	User fills	Mass of stator iron, from Adept
m_{rt_iron}	kg	User fills	Mass of rotor iron, from Adept
m_{st_copper}	kg	User fills	Mass of stator copper, from Adept
m_{rt_al}	kg	User fills	Mass of rotor bars and rings, from Adept
m_{ec}	kg	User fills	Mass of motor frame
m_{sh}	kg	User fills	Mass of the shaft
m_{water}	kg	User fills	Mass of the cooling water for water cooled motors
T_{rise_frame}	K	User fills	Temperature rise of the frame, initial value can be taken from the test report
P_{mech_factor}		User fills	Heating contribution of the mechanical losses
FrameMaterial		User fills	1 for cast iron 2 for aluminium

Table continues

Table 10 continues

Cooling		User fills	1 for shaft-mounted fan and 2 for water cooled motor
r_m	m	$(r_{oy}-r_{iy})/2+r_{iy}$	Average value of the stator yoke radius
r_{iy}	m	$r_{is}+HSN1$	Value of the inner stator yoke radius
r_{oy}	m	$DO1/2$	Outer value of the stator yoke radius
r_{is}	m	$DI1/2$	Stator inner radius
r_{or}	m	$r_{is}-delta$	Outer rotor radius
r_{ory}	m	$r_{iry}+HYOKE2$	Outer rotor yoke radius
r_{iry}	m	$DI2/2$	Inner rotor yoke radius
r_{agm}	m	$r_{or}+delta/2$	The average of the air-gap radius
h_{ag}	W/(m^2 ·K)	$Nu \cdot k_{air}/delta$	Convection heat coefficient for the air-gap
A	m^2	if $r_{ec} < 0.16$ and *Cooling* == 1 then $2 \cdot \pi \cdot r_{ec} \cdot L_{ec}/0.6 + 2 \cdot \pi \cdot r_{ec}^2$ elseif $r_{ec} >= 0.16$ and *Cooling* == 1 then $2 \cdot \pi \cdot r_{ec} \cdot L_{ec}/0.4 + 2 \cdot \pi \cdot r_{ec}^2$ else $2 \cdot \pi \cdot r_{ec} \cdot L_{ec} + 2 \cdot \pi \cdot r_{ec}^2$	Surface area of motor frame
p_{ir}		$1-Q1 \cdot S_{slot}/(\pi \cdot r_{iy}^2-\pi \cdot r_{is}^2)$	Reduction factor in percent, teeth iron volume divided by the total teeth and slots volume
Ta		$rho\_air^2 \cdot (rpm1 \cdot 2 \cdot \pi/60)^2 \cdot r_{agm} \cdot delta^3/my^2$	Taylor number for the air gap

Table continues

Table 10 continues

Nu		if Ta<1700 then 2 elseif Ta<10e4 then $0.128 \cdot Ta^{0.367}$ elseif Ta<10e7 then $0.409 \cdot Ta^{0.241}$ else 2	Nusselt number for the air gap
l_{sb}	m	$BSO1+2 \cdot HSN1+BSI1$	Stator slot perimeter
A_{slot}	m^2	$l_{sb} \cdot L\_TOT$	Interior slot surface area
S_{slot}	m^2	$BSO1 \cdot HSN1$	Slot cross-sectional area
t_{eq}	m	$(S_{slot}-S_{slot} \cdot KCU1)/l_{sb}$	Equivalent thickness of the air and insulation in the stator slots
k_{cuir}	W/(m·K)	$0.2425 \cdot ((1-KCU1) \cdot S_{slot} \cdot L\_TOT \cdot 10^6)^{(-0.4269)}$	Average thermal conductivity of a winding
A_{ew}	m^2	$\pi/2 \cdot ((LM1-L\_TOT) \cdot 2 \cdot \pi \cdot r_{is}+(LM1-L\_TOT) \cdot 2 \cdot \pi \cdot r_{iy})$	Surface area of the end windings
A_{ec}	m^2	$2 \cdot \pi \cdot r_{ec}^2$	Surface area of the end caps
h_{ew}	W/(m^2·K)	if v_p < 30 then $41.4+6.22 \cdot v_p$ elseif v_p<40 then $41.4+5.22 \cdot v_p$ else $41.4+4 \cdot v_p$	Equivalent heat transfer coefficient for the end windings
v_p	m/s	$r_{or} \cdot (rpm1 \cdot 2 \cdot \pi/60)$	Rotor peripheral speed
$P_{mech\_factor1}$		if $Cooling$ == 2 then 1 else $Pmech\_factor$	

Table continues

Table 10 continues

FrameHeatCapacity	J/K	if *FrameMaterial* == 1 then $m_{ec} \cdot cp_{iron\_cast}$ else $m_{ec} \cdot cp_{rt\_bars}$	Heat capacity of the frame
FrameHeatCapacityWater	J/K	if *Cooling* == 1 then 0 else $m_{water} \cdot cp_{\_water}$	Heat capacity of cooling water

The developed dynamic thermal model is presented in Figure 18. A stationary model would look like the dynamic model but the thermal capacitors would not be necessary. It is possible to simulate the steady-state temperatures also with the dynamic model if the losses have constant values and the simulation time is set sufficiently long so thermal equilibrium is reached. Therefore, the dynamic model is used also for steady-state temperature simulations here.

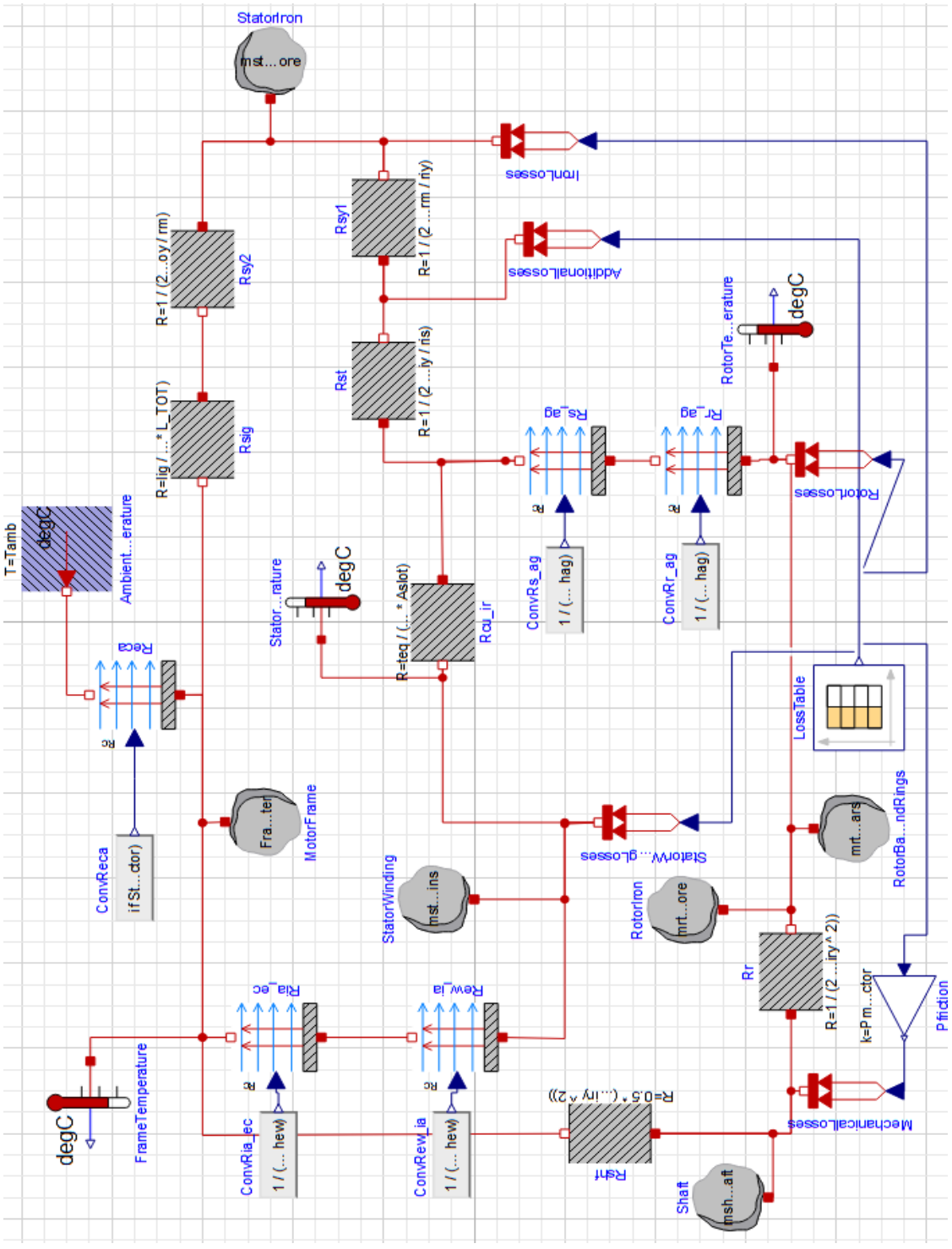

Figure 18. The developed dynamic thermal model in SystemModeler.

5.4 Simulations

Several different squirrel cage motor types were simulated with the model. Next simulations for three different standard TEFC squirrel cage IMs and one water cooled squirrel cage IM are presented in order to illustrate how the model performs. The temperature rises for different motor parts at rated load are also presented, the values are tested values from the ABB test reports, and the test reports are available online from the ABB Library for the standard TEFC squirrel cage IMs.

The temperature level of the stator winding insulation is the most critical temperature since the insulation temperature must not exceed the limit value given by the manufacturer, which is for ABB motors with class F insulation, 145 °C for average temperatures measured with the resistance method. Since the stator winding temperature is the crucial temperature of the motors, an accuracy requirement of 10 % difference from the test report results for steady-state is set.

For 15 simulated TEFC motors it was almost always possible to adjust l_{ig} and the frame thermal resistance R_{eca} and get winding and frame temperatures being basically exactly or close to the temperatures in test reports. However, there was one motor for which the winding temperature accuracy requirement was not met. When only l_{ig} was adjusted to its lower limit the winding was 15 % too hot compared to test results and when l_{ig} was adjusted to its lower limit and R_{eca} was calibrated in accordance with test results the winding was still 13 % too hot. Then there was one motor which did not meet the requirement when only l_{ig} was adjusted but when l_{ig} and R_{eca} were both adjusted in accordance with test report then the requirement was met. However, if noticing that steady-state simulation results do not match the test report results, it can be assumed that the transient simulation results are not in line with reality either. If the steady-state results are too hot the transient results are probably also too hot and vice versa. As explained in Section 4.6, it is most likely due to h_{ew} or k_{cuir} if the stator winding temperature in SM deviates by more than 10 % from tested values after calibration of l_{ig} and R_{eca}. Table 11 presents the values for three standard TEFC motors and one water cooled motor simulated with the developed model.

Table 11. Values for three standard motors and one water cooled motor simulated with the dynamic thermal model developed in SM.

Name in SystemModeler	**M3BP 71 ME 6**	**M3BP 180 MLB 4**	**M3BP 355 SMB 2**	**M3LP 500 LC 4**
P_{Cus}	53.9	589	2208	5870
P_{Cur}	19.1	300	2084	4510
P_{Fe}	5.19	339	2705	8240
P_{mech}	1.9	40	3000	4960
P_{add}	2.52	330	2710	4750
T_{amb}	25	25	25	25.9
DO1	110	283	600	860
DI1	70	190.2	330	525
DI2	20	60	130	180
HYOKE2	15.9	28.7	37.7	107.4
L_{TOT}	55	270	430	780
delta	0.25	0.6	2.8	3.5
L_{ec}	230	600	1270	1650
L_{shf}	264	684	1409	2050
LM1	120	497	1160	1480
l_{ig}	0.01–0.08	0.01–0.08	0.01–0.08	0.01–0.08
r_{ec}	71	180	355	500
Q1	36	36	60	96
rpm	887	1481	2980	1794
BSO1	4.5	11.5	12.8	12.6
HSN1	9.7	17.5	42	72

Table continues

Table 11 continues

BSI1	3.1	9	8.9	8
KCU1	0.676	0.66	0.635	0.61
m_{st_iron}	1.69	58.9	536	1683
m_{rt_iron}	1.12	41.4	185	801
m_{st_copper}	0.58	14.1	158	465
m_{rt_al}	0.18	5.61	24.2	95
m_{ec}	6.8	91.6	500	1767
m_{sh}	0.9	12.5	98	364
T_{rise_frame}	22	30	31.4	8.2
P_{mech_factor}	0.5	0.5	0.5	1
FrameMaterial	1	1	1	1
Cooling	1	1	1	2

For the water cooled motor, T_{amb} is the water inlet temperature and T_{rise_frame} is the temperature rise of the cooling water; the difference between water outlet and water inlet temperatures.

5.4.1 IEC frame size 71

Information about this motor is presented in Table 12. First two different simulations for rated output steady state with test results are carried out in order to see how the model performs for this motor. Then an intermittent duty cycle is simulated.

Table 12. Information about M3BP 71 ME 6. (ABB 2015a)

M3BP 71 ME 6	**Rated values**
Nominal voltage (V)	400
Rated power (kW)	0.18
Connection	Y
Speed (rpm)	887
Frequency (Hz)	50
Nominal current (A)	0.57
Efficiency (100 %)(%)	63.9
Power factor	0.74
Duty	S1

The tested steady-state thermal behavior of this motor is presented in Table 13.

Table 13. Tested temperature rises for 71 ME 6 motor. (ABB 2015a)

M3BP 71 ME 6	**Temperature rise (K) at rated load with ambient temperature 25°C**	**Measurement method**	**Temperature in the motor part (°C)**
Stator winding	35	Resistance	60
Frame	22	Thermometer	47
Bearing D-end	23	Thermometer	48
Rotor	43	Thermocouples	68

When simulating this motor for steady-state, the results presented in Table 14 are obtained. The simulation was started from ambient temperature. Figure 19 visualizes the comparison of stator winding and frame temperatures for test report and simulated with SM.

Table 14. Tested values compared to simulated values for M3BP 71 ME 6.

M3BP 71 ME 6	**Test report temperature (°C)**	**SystemModeler temperature (°C) calibrated l_{ig} (=0.02mm)**	**SystemModeler temperature (°C) calibrated l_{ig} (=0.043mm) and R_{eca}**
Stator winding average	60	60	60
Frame	47	50.0	47.1
Bearing D-end	48	-	-
Rotor	68	72.8	72.3

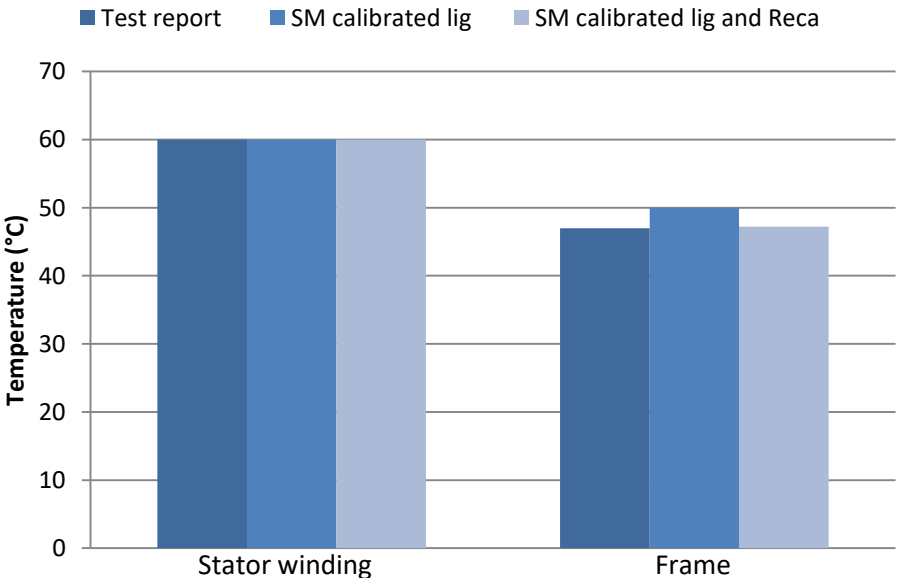

Figure 19. The stator winding and frame temperatures from test report and simulations compared for steady state.

When only l_{ig} was adjusted and R_{eca} was calculated by giving the frame temperature rise from the test report, the stator winding obtained a temperature equal to the tested stator winding temperature. The frame temperature was slightly high. When R_{eca} was adjusted in order for the simulated frame temperature to match the tested frame temperature, consistent temperatures for both the stator winding and frame could be obtained.

When this motor was calibrated for steady state a S3 40 % duty cycle was simulated. In this duty cycle the motor was running at 125 % load for 4 minutes and then kept at standstill for 6 minutes. This cycle was then repeated.

For 125 % overload (225 W) Adept gave the loss values presented in Table 15.

Table 15. Losses for 125 % overload (225W) for M3BP 71 ME 6. Losses are calculated by Adept.

Loss component	Loss value (W)
P_{Cus}	97.9
P_{Cur}	38.2
P_{Fe}	4.8
P_{mech}	1.9
P_{add}	3.6

When simulating this S3 40 % duty cycle in SM, the settings for the CombiTimeTable looks like in Figures 20, 21 and 22. It is important to fill the changed loss components directly into the CombiTimeTable (LossTable) since the loss values in the 'Parameters' view are also used to calculate the motor frame resistance R_{eca} and therefore their values are the loss values for the tested operating point.

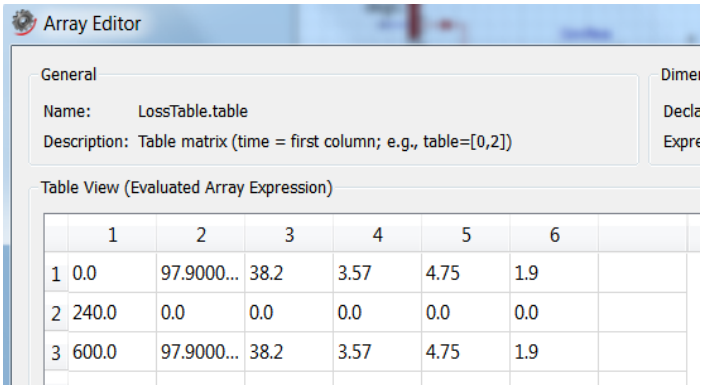

Figure 20. Information about the S3 40 % duty cycle at 125 % load in the CombiTimeTable.

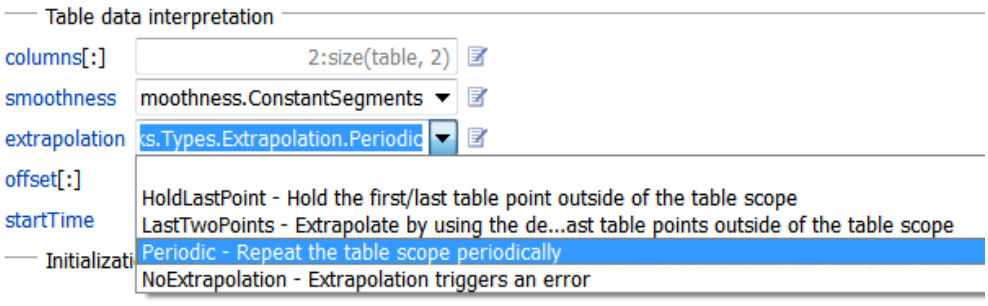

Figure 21. The setting for extrapolation is set to Periodic.

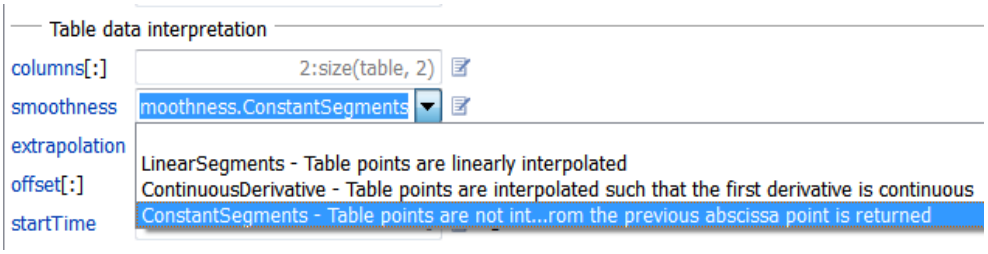

Figure 22. The losses are constant segments.

The simulation results when simulating a S3 40 % duty cycle at 125 % load are presented in Figure 23.

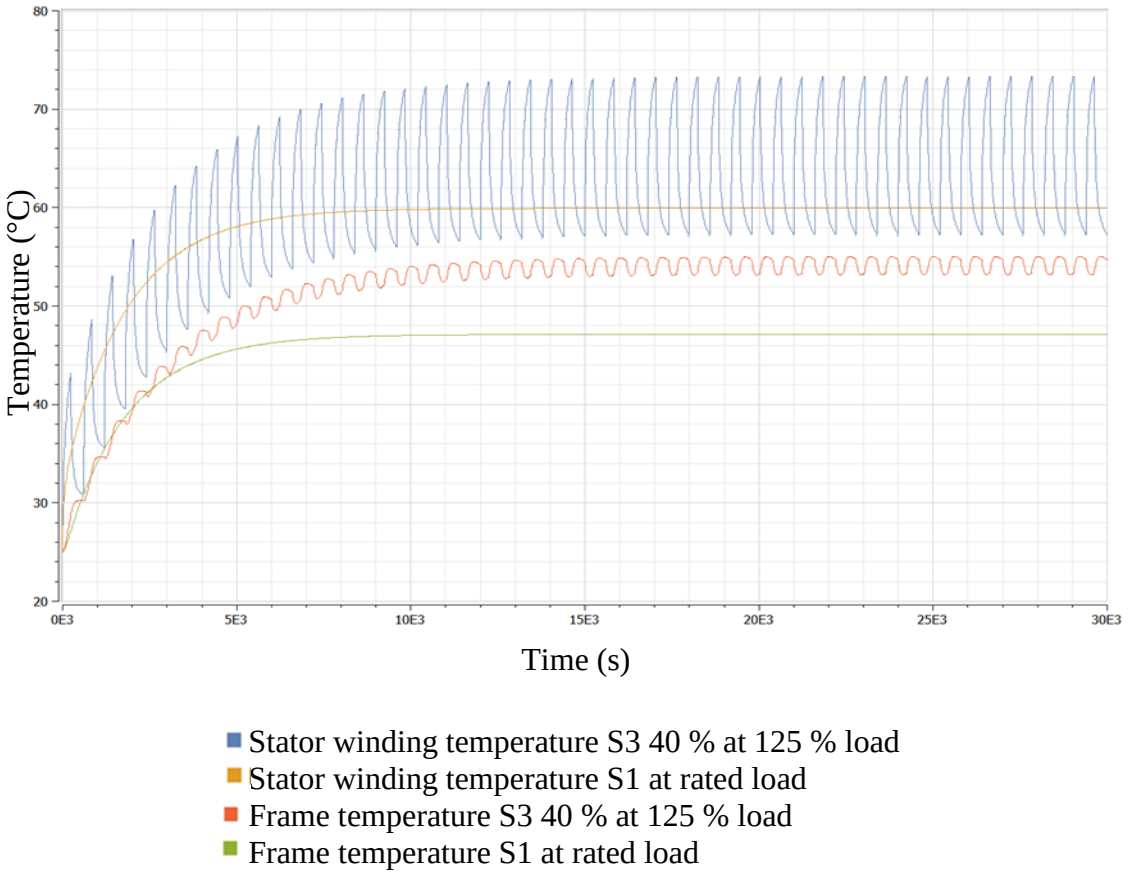

Figure 23. Intermittent duty cycle S3 40 % at 125 % load is simulated in SM and compared to the simulated steady state temperatures.

The simulated results for this S3 40 % duty cycle are not verified with measurements.The simulation suggests that the stator winding temperature would reach a higher value for the S3 40 % duty cycle at 125 % load than for the rated operating point.

For the same intermittent duty cycle, S3 40 % at 125 % load, these parameters were also plotted in SM: $R_{eca,}$ h_{ew} and Nu. The results are presented next.

The thermal resistance between the frame and the ambient is affected by the standstill periods and when plotting R_{eca} in SystemModeler it looks like in Figure 24.

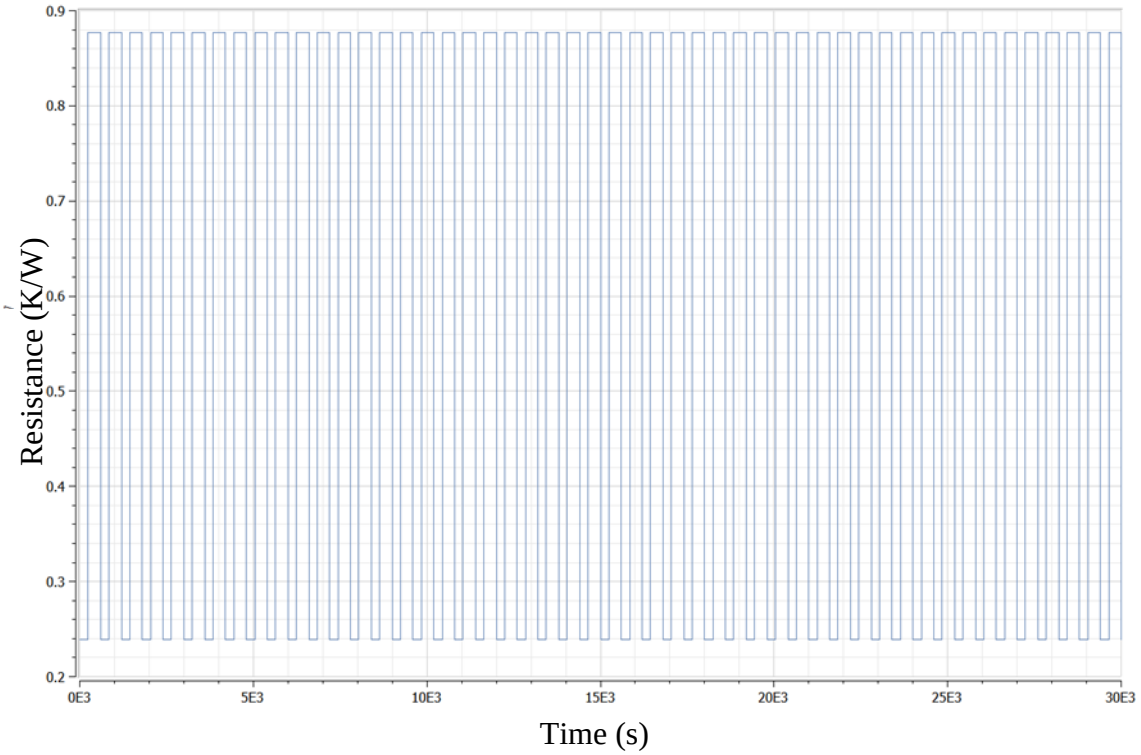

Figure 24. The thermal resistance R_{eca} and how it is varying for the S3 40 % duty cycle at 125 % load.

R_{eca} is much higher for the standstill periods when only natural convection and radiation are present, they are estimated with an empirical dependency.

In the end space region, the heat transfer coefficient h_{ew} is also affected by the stationary periods. Figure 25 shows how h_{ew} is varying.

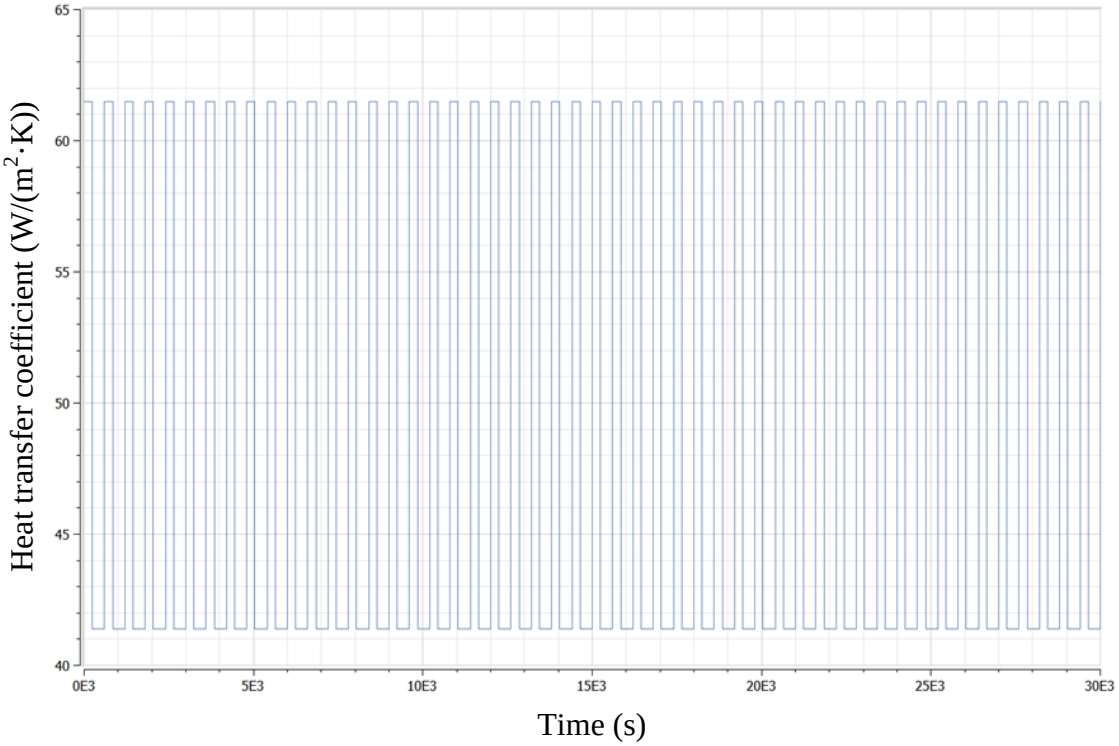

Figure 25. The heat transfer coefficient h_{ew} and how it is varying for the S3 40 % duty cycle at 125 % load.

When the motor is stationary, h_{ew} is only by natural convection and radiation and when the motor is rotating h_{ew} depends on the inner air velocity.

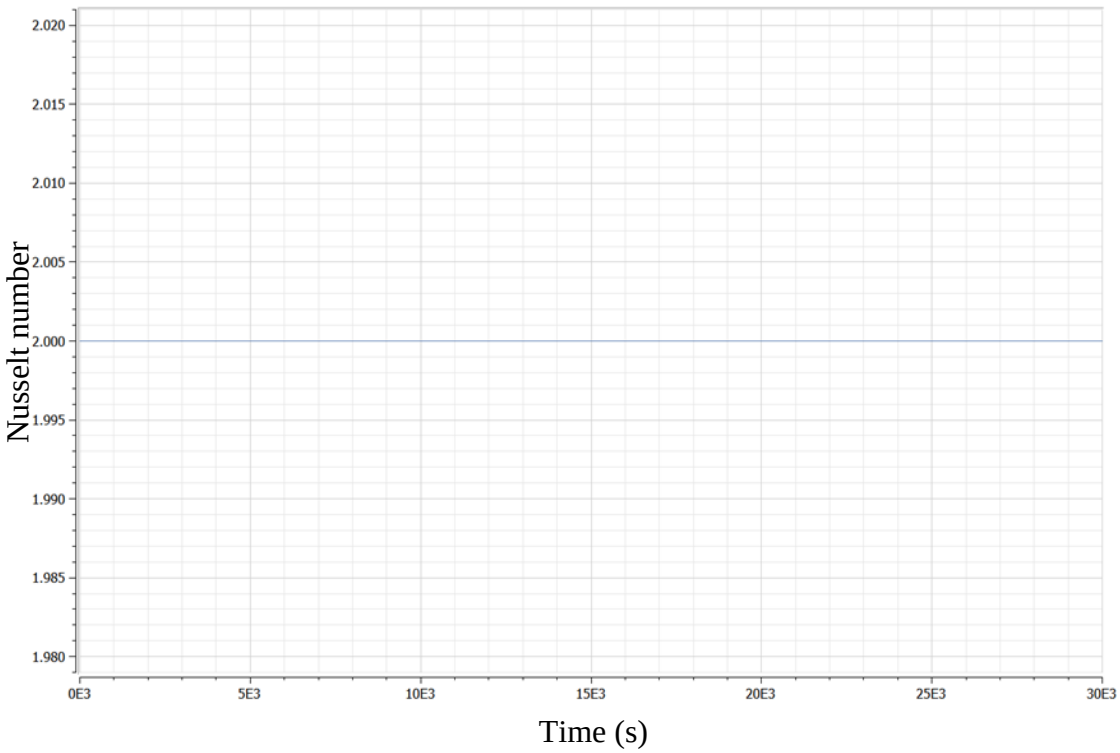

Figure 26. The Nusselt number *Nu* in the air gap for the S3 40 % duty cycle at 125 % load.

The air flow in the air gap is laminar for this motor, the Nusselt number is 2 when the motor is rotating and stationary which indicates that heat transfer is only by conduction for both cases.

For this motor, the equivalent thermal conductivity k_{cuir} was calculated to be 0.27 W/(m·K), which would according to some other relationships be a too high value.

5.4.2 IEC frame size 180

Information about this motor is presented in Table 16. First two different simulations for rated output steady state with test results are carried out in order to see how the model performs for this motor. Then an intermittent duty cycle is simulated.

Table 16. Information about M3BP 180 MLB 4. (ABB 2015b)

M3BP 180 MLB 4	**Rated values**
Nominal voltage (V)	400
Rated power (kW)	22
Connection	D
Speed (rpm)	1481
Frequency (Hz)	50
Nominal current (A)	41.4
Efficiency (100%) (%)	93.3
Power factor	0.82
Duty	S1

The tested steady-state thermal behavior of this motor is presented in Table 17.

Table 17. Tested temperature rises for M3BP 180 MLB 4. (ABB 2015b)

M3BP 180 MLB 4	**Temperature rise (K) at rated load with ambient temperature 25°C**	**Measurement method**	**Temperature in the motor part (°C)**
Stator winding	59	Resistance	84
Frame	30	Thermocouples	55
Bearing D-end	36	Thermocouples	61
Rotor	74	Thermometer	99

When simulating this motor for steady-state, the results presented in Table 18 are obtained. The simulation was started from ambient temperature. Figure 27 visualizes the comparison of stator winding and frame temperatures for test report and simulated with SM.

Table 18. Tested values compared to simulated values for M3BP 180 MLB 4.

M3BP 180 MLB 4	**Test report temperature (°C)**	**SystemModeler temperature (°C) calibrated l_{ig} (=0.027 mm)**	**SystemModeler temperature (°C) calibrated l_{ig} (=0.071 mm) and R_{eca}**
Stator winding average	84	84	84
Frame	55	59.9	55.3
Bearing D-end	61	-	-
Rotor	99	127	129

As can be seen, the rotor temperature will be too high for all motors except really small frame sizes. This can be explained by the fact that the rotor is modelled in a very inaccurate way and there should be more rotor nodes. The rotor temperature is however not so important for squirrel cage motors and the most important temperature is the winding temperature. The measured rotor temperature may in addition deviate by several degrees depending on the measurement location.

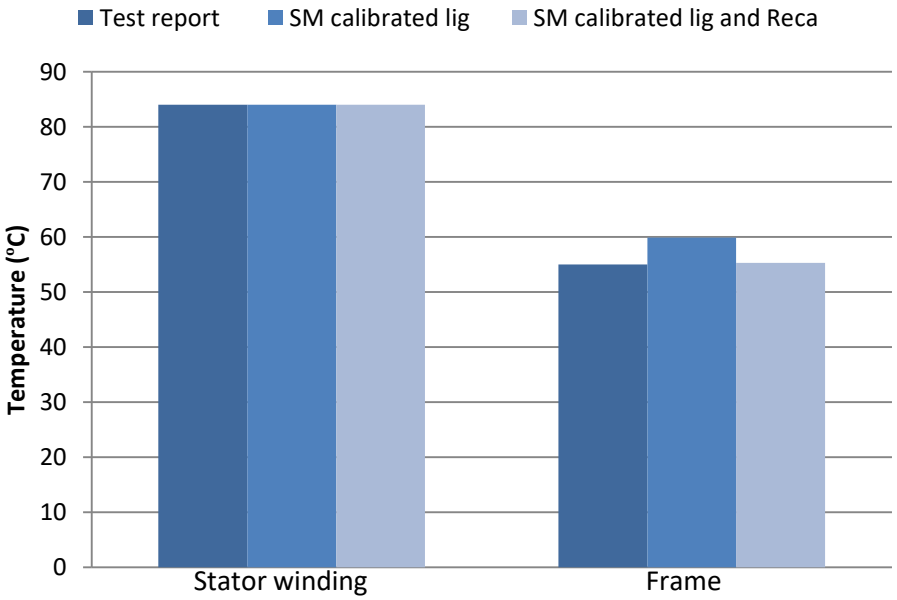

Figure 27. The stator winding and frame temperatures from test report and simulations compared for steady-state.

When only l_{ig} was adjusted and R_{eca} was calculated by giving the frame temperature rise from the test report, the stator winding obtained a temperature equal to the tested stator winding temperature. The frame temperature was slightly high. When R_{eca} was adjusted in order for the simulated frame temperature to match the tested frame temperature, consistent temperatures for both the stator winding and frame could be obtained.

After this motor was calibrated for steady state, a S3 15 % duty cycle was simulated. In this duty cycle the motor was running at 145 % load for 1.5 minutes and then kept at standstill for 8.5 minutes. This cycle was then repeated.

For 145 % overload (31.9 kW) Adept gave the loss values presented in Table 19.

Table 19. Losses for 145 % overload (31.9 kW) for M3BP 180 MLB 4. Losses are calculated by Adept.

Loss component	**Loss value (W)**
P_{Cus}	1237
P_{Cur}	693
P_{Fe}	326
P_{mech}	40
P_{add}	486

Figure 28 presents the simulation results when the S3 15 % duty cycle at 145 % load was simulated.

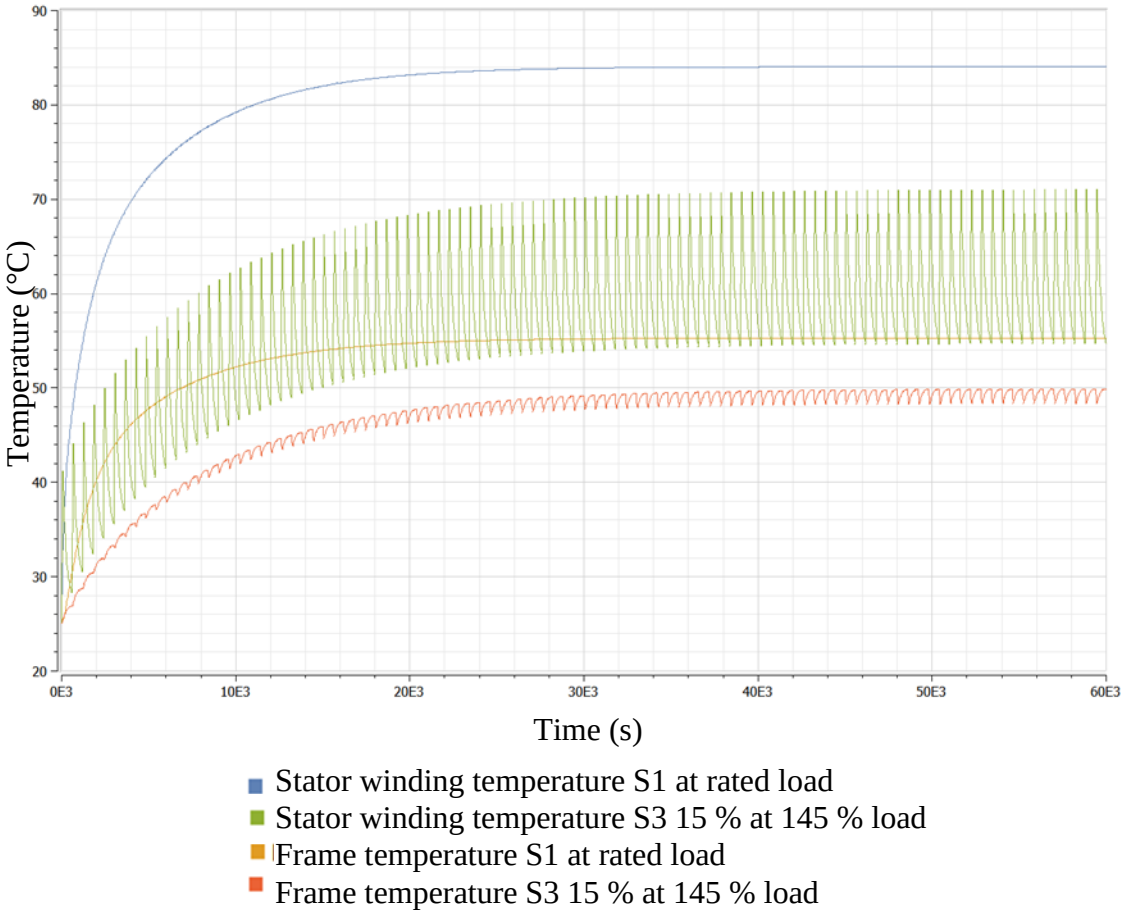

Figure 28. S3 15 % duty cycle at 145 % load simulated and compared to steady-state simulation results.

The simulated results for this S3 15 % duty cycle at 145 % load are not verified with measurements. The simulation suggests that the stator winding temperature would be significantly lower for the S3 15 % duty cycle at 145 % load than for the rated operation point.

For the same intermittent duty cycle, S3 15 % at 145 % load, these parameters were also plotted in SM: $R_{eca,}$ h_{ew} and Nu. The results are presented next.

The thermal resistance between the frame and the ambient is affected by the standstill periods and when plotting R_{eca} in SystemModeler it looks like in Figure 29.

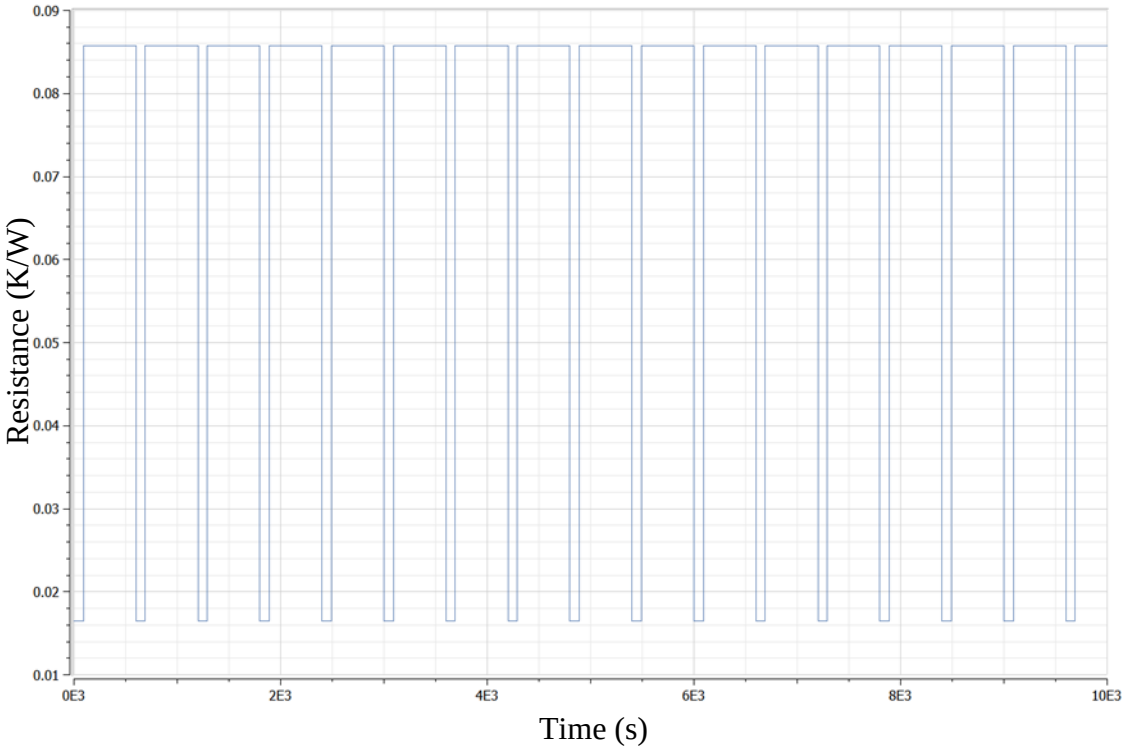

Figure 29. The thermal resistance R_{eca} and how it is varying for the S3 15 % duty cycle at 145 % load.

R_{eca} is much higher for the standstill periods when only natural convection and radiation are present, they are estimated with an empirical dependency.

In the end space region, the heat transfer coefficient h_{ew} is also affected by the stationary periods. Figure 30 shows how h_{ew} is varying.

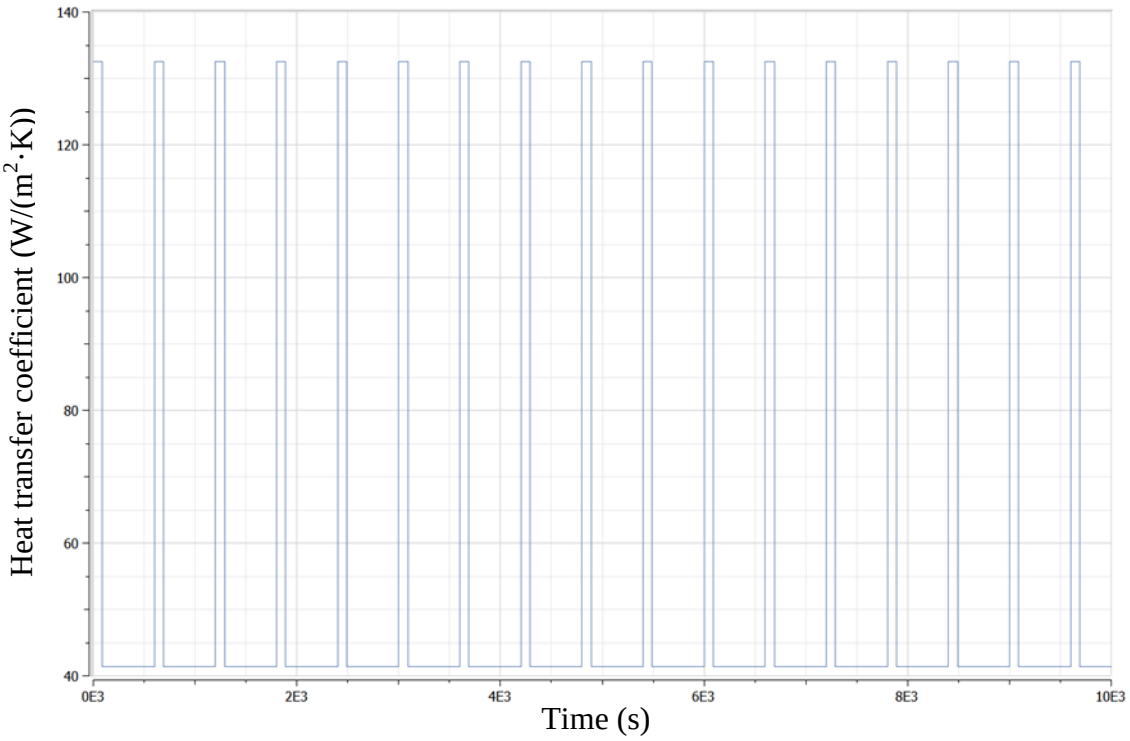

Figure 30. The heat transfer coefficient h_{ew} and how it is varying for the S3 15 % duty cycle at 145 % load.

When the motor is stationary, h_{ew} is only by natural convection and radiation and when the motor is rotating h_{ew} depends on the inner air velocity.

Figure 31 present the *Nu* number in the air gap.

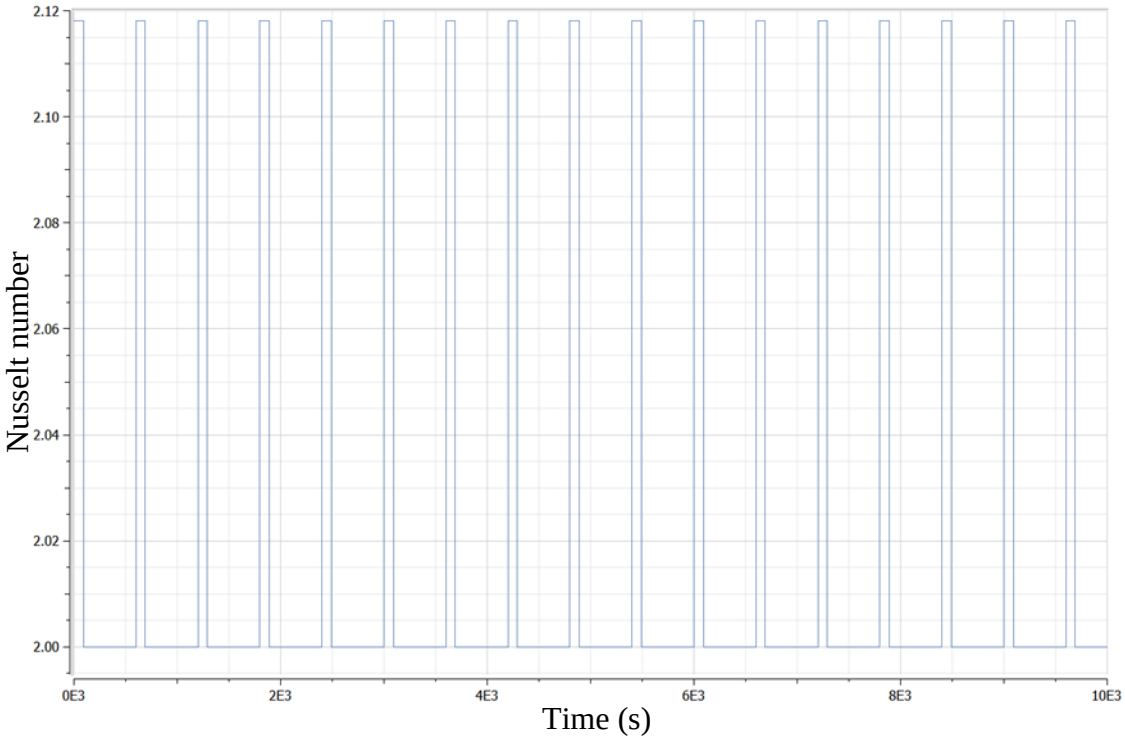

Figure 31. The Nusselt number *Nu* in the air gap for the S3 15 % duty cycle at 145 % load.

The air flow in the air gap is turbulent when the motor is rotating according to the Nusselt number. The turbulent flow enhances the heat transfer. When the motor is stationary the Nusselt number is 2 which corresponds to that the heat transfer is by conduction.

For this motor, the equivalent thermal conductivity k_{cuir} was calculated to be 0.0698 W/(m·K).

5.4.3 IEC frame size 355

Information about this motor is presented in Table 20. First two different simulations for rated output steady state with test results are carried out in order to see how the model performs for this motor. Then an intermittent duty cycle is simulated.

Table 20. Information about M3BP 355 SMB 2. (ABB 2016c)

M3BP 355 SMB 2	**Rated values**
Nominal voltage (V)	400
Rated power (kW)	315
Connection	D
Speed (rpm)	2980
Frequency (Hz)	50
Nominal current (A)	529.4
Efficiency (100%) (%)	96.2
Power factor	0.89
Duty	S1

The tested steady-state thermal behavior of this motor is presented in Table 21.

Table 21. Tested temperature rises for M3BP 355 SMB 2. (ABB 2016c)

M3BP 355 SMB 2	**Temperature rise (K) at rated load with ambient temperature 25°C**	**Measurement method**	**Temperature in the motor part (°C)**
Stator winding	66.7	Resistance	91.7
Frame	31.4	Thermometer	56.4
Bearing D-end	49.9	Thermometer	74.9
Rotor	-	-	-

When simulating this motor for steady state, the results presented in Table 22 are obtained. The simulation was started from ambient temperature. Figure 32 visualizes the comparison of stator winding and frame temperatures for test report and simulated with SM.

Table 22. Tested values compared to simulated values for M3BP 355 SMB 2.

M3BP 355 SMB 2	**Test report temperature (°C)**	**SystemModeler temperature (°C) calibrated l_{ig} (=0.01 mm)**	**SystemModeler temperature (°C) calibrated lig (=0.078 mm) and Reca**
Stator winding average	91.7	95.3	91.7
Frame	56.4	65.5	56.8
Bearing D-end	74.9	-	-

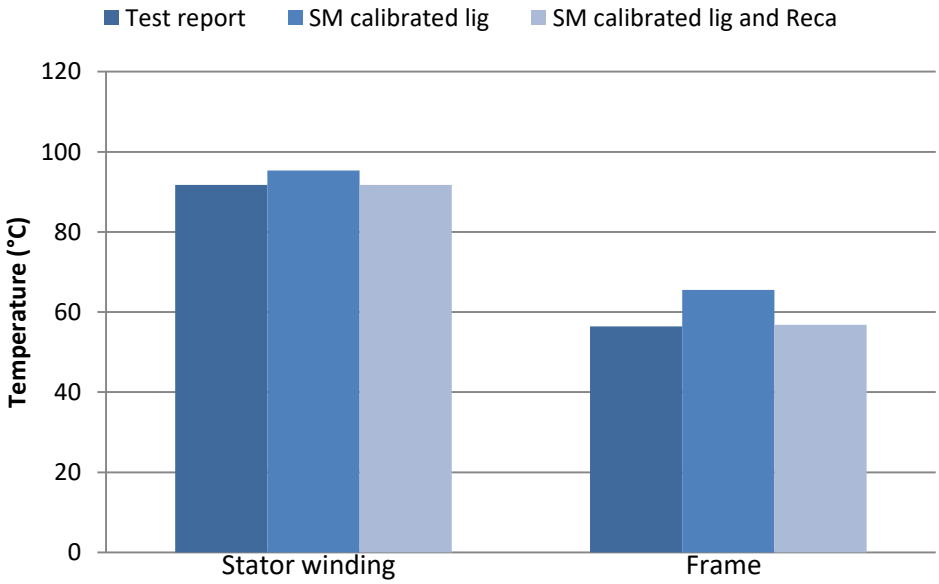

Figure 32. The stator winding and frame temperatures from test report and simulations compared for steady-state.

When only l_{ig} was adjusted and R_{eca} was calculated by giving the frame temperature rise from the test report, the simulated stator winding was 3.6 °C higher than the tested stator winding temperature. The frame temperature was higher. When R_{eca} was adjusted in order for the simulated frame temperature to match the tested frame temperature, consistent temperatures for both the stator winding and frame could be obtained.

After this motor was calibrated for steady state, a S3 60 % duty cycle was simulated. In this duty cycle the motor was running at 110 % load for 6 minutes and then kept at standstill for 4 minutes. This cycle was then repeated.

For 110 % overload (346.5 kW) Adept gave the loss values presented in Table 23.

Table 23. Losses for 110 % overload (346.5 kW) for M3BP 355 SMB 2. Losses are calculated by Adept.

Loss component	**Loss value (W)**
P_{Cus}	2655
P_{Cur}	2539
P_{Fe}	2690
P_{mech}	3000
P_{add}	2873

The simulation results for the S3 60 % duty cycle at 110 % load are presented in Figure 33.

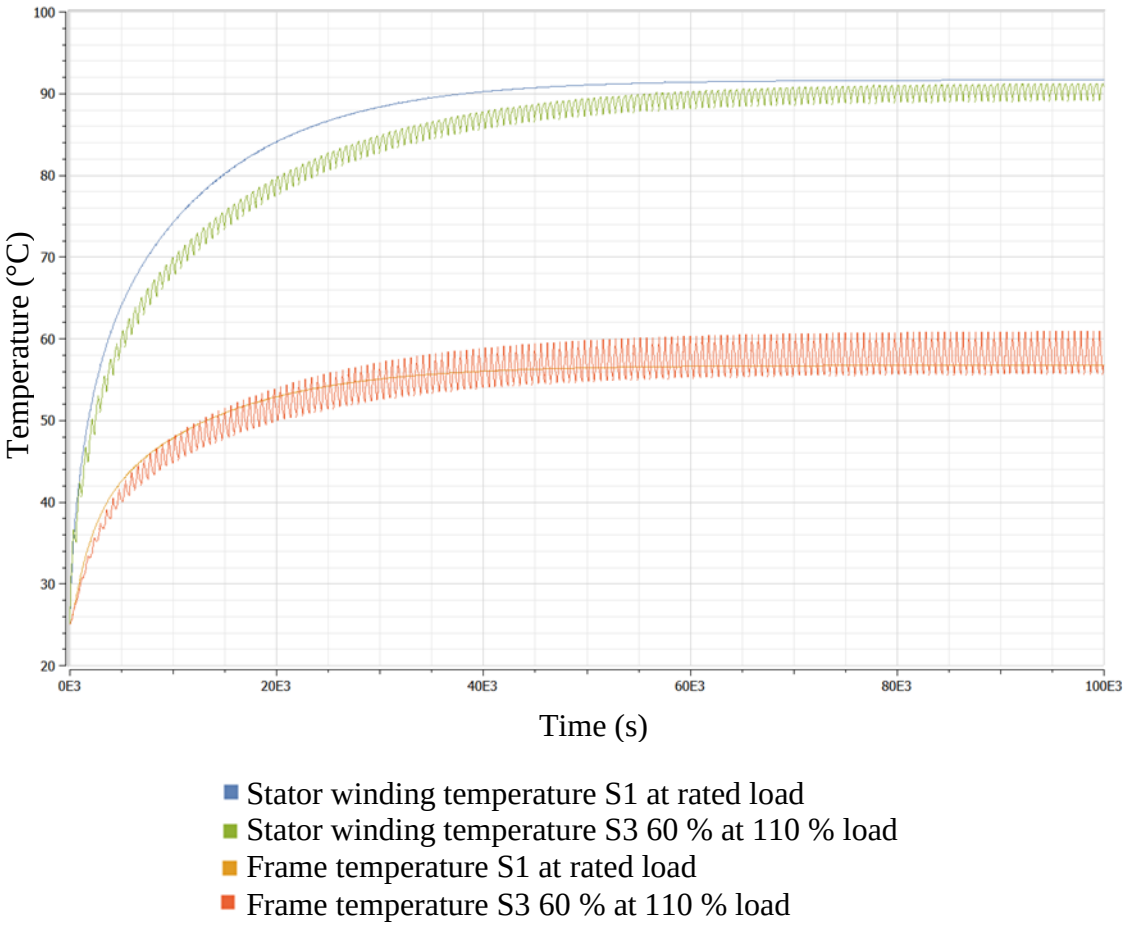

Figure 33. Intermittent duty cycle S3 60 % at 110 % load is simulated in SM and compared to the simulated steady state temperatures.

The simulated results for this S3 60% duty cycle are not verified with measurements. The simulation suggests that the stator winding temperature for the S3 60 % at 110 % load would be approximately the same as for the rated operating point.

For the same intermittent duty cycle, S3 60 % at 110 % load, these parameters were also plotted in SM: $R_{eca,}$ h_{ew} and Nu. The results are presented next.

The thermal resistance between the frame and the ambient is affected by the standstill periods and when plotting R_{eca} in SystemModeler it looks like in Figure 34.

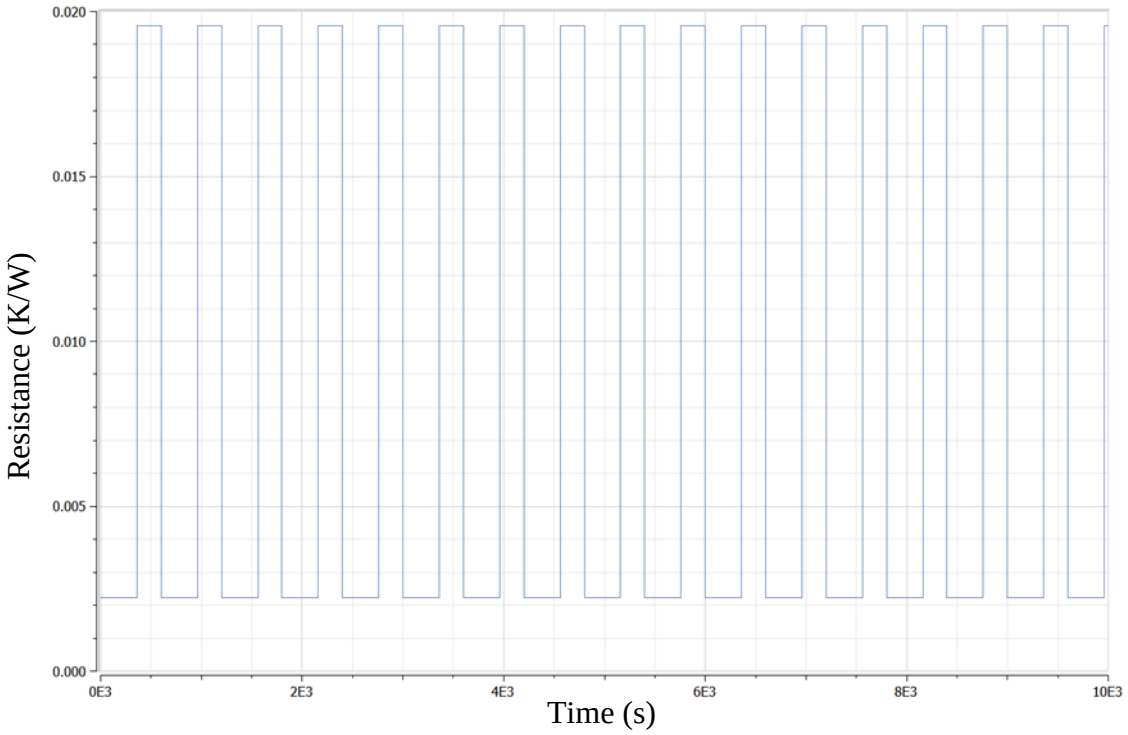

Figure 34. The thermal resistance R_{eca} and how it is varying for the S3 60 % duty cycle at 110 % load.

R_{eca} is much higher for the standstill periods when only natural convection and radiation are present, they are estimated with an empirical dependency.

In the end space region, the heat transfer coefficient h_{ew} is also affected by the stationary periods. Figure 35 shows how h_{ew} is varying.

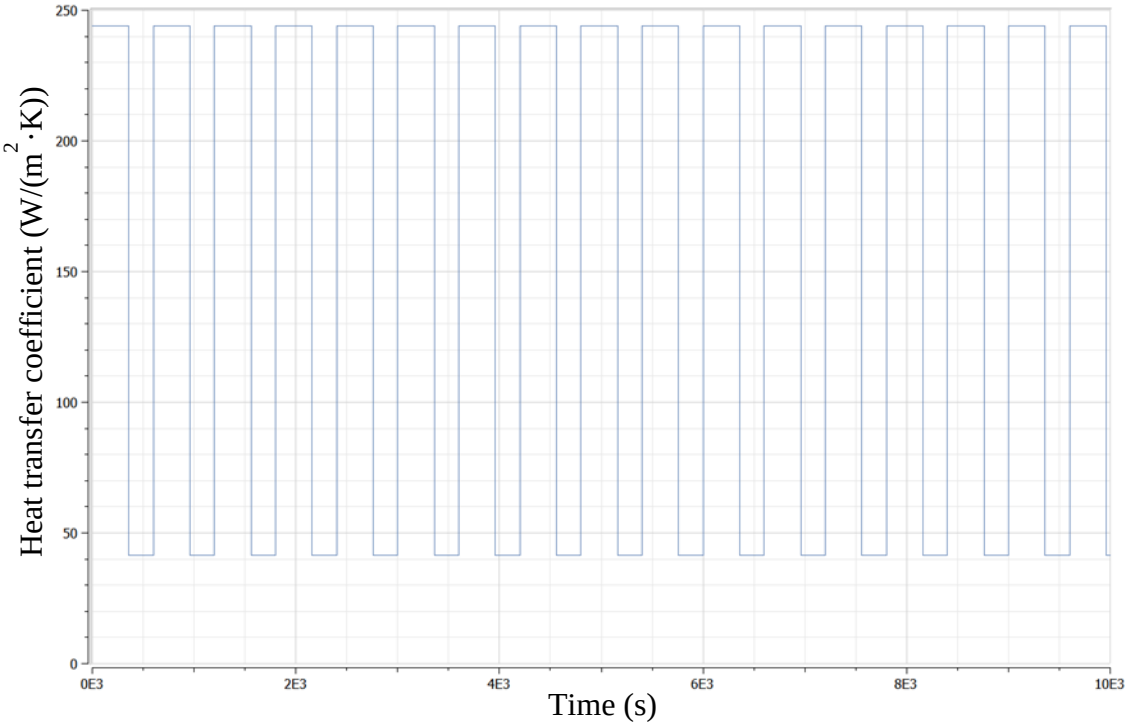

Figure 35. The heat transfer coefficient h_{ew} and how it is varying for the S3 60 % duty cycle at 110 % load.

For this motor, h_{ew} has a significantly higher value when the motor is rotating compared to standstill periods. However, the correlation for h_{ew} should be investigated further, especially for motors of this frame size and with a rotor pheriperal speed of 50.6 m/s which is the case for this motor. In the developed model, the correlation for h_{ew} when the rotor pheriperal speed exceeds 40 m/s is $41.4 + 4 \cdot v_p$ but it might still give h_{ew} an incorrect value.

Figure 36 present the *Nu* number in the air gap.

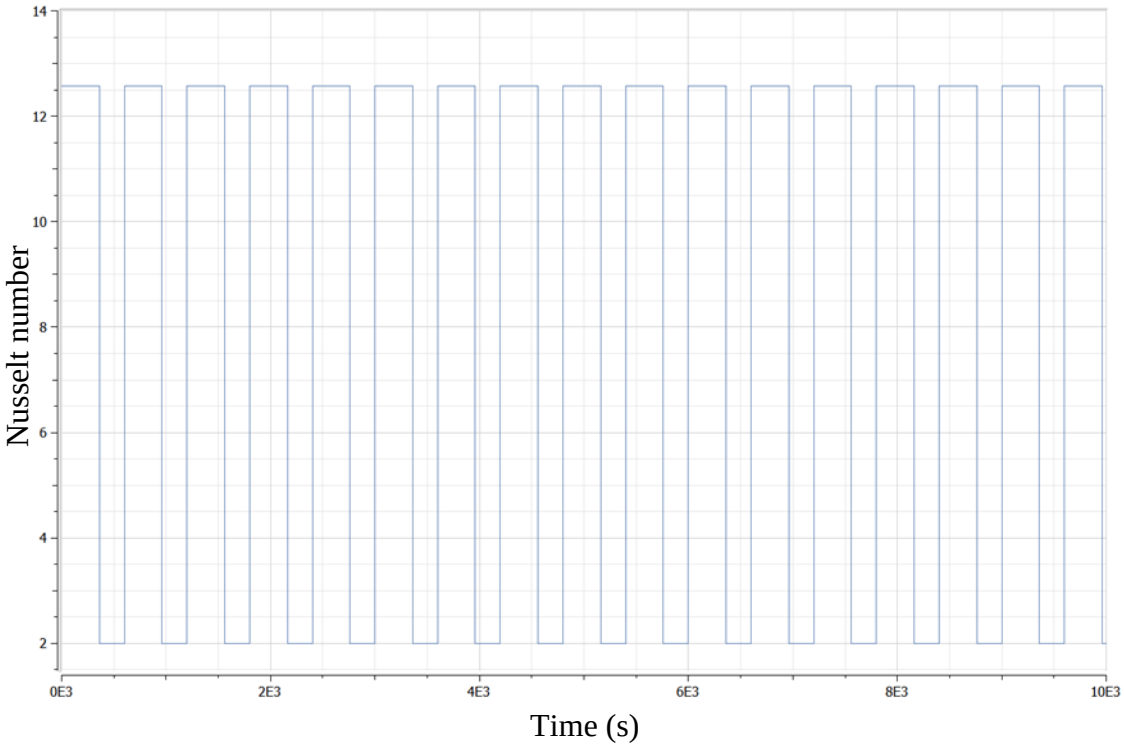

Figure 36. The Nusselt number *Nu* for the air gap and how it is varying for the S3 60 % duty cycle at 110 % load.

The air flow in the air gap is turbulent when the motor is rotating according to the Nusselt number. The turbulent flow enhances the heat transfer. When the motor is stationary the Nusselt number is 2 which corresponds to that the heat transfer is by conduction.

For this motor, the equivalent thermal conductivity k_{cuir} was calculated to be 0.0365 W/(m·K).

5.4.4 Water cooled motor of IEC frame size 500

The same thermal model can be used for a water cooled squirrel cage induction motor. In this way it is easy to simulate also water cooled squirrel cage motors. The differences that have to be made are that the ambient temperature is now the water inlet temperature and the temperature rise is the temperature rise of the cooling water. In this way the

total thermal resistance between the frame and the ambient, R_{eca}, gets a lower value compared to the fan cooled motors. The convection heat transfer coefficient for the frame is thus significantly bigger than for TEFC motors and thus natural convection and radiation can be neglected. The water cooling channels are located only on the stator frame and not on the end-shields and therefore natural convection and possibly radiation are present on the end-shields but their effects should be negligible for water cooled motors. If there are standstill periods, it is assumed that the waterflow is at the same rate as for a rotating motor.

The water cooling effect could also be modelled with Fluid Flow components from the Modelica Standard Library, but if there are test results for the water temperature rise and the total amount of losses, the total thermal resistance can be calculated in the same way as for the standard squirrel cage motors.

Table 24 presents measured temperature values for the water cooled motor M3LP 500 LC 4. First two different simulations for rated output steady state with test results are carried out in order to see how the model performs for this motor. Then an intermittent duty cycle is simulated.

Table 24. Measured temperature values for M3LP 500 LC 4. (ABB 2016b: 2)

M3LP 500 LC 4	**Measurement method**	**Temperatures for tested motor (°C)**
Stator winding phase U	Pt100	88.4
Stator winding phase V	Pt100	88.3
Stator winding phase W	Pt100	78.2
Stator winding average	Resistance	80.7
Water in	-	25.9
Water out	-	34.1
Bearing D-end	Pt100	45.1
Ambient temperature	-	25.3

When simulating this motor for steady-state, the results presented in Table 25 are obtained. The simulation was started from ambient temperature.

Table 25. Tested values compared to simulated values for M3LP 500 LC 4.

M3LP 500 LC 4	**Tested temperature (°C)**	**SystemModeler temperature (°C) calibrated l_{ig} (=0.07 mm)**	**SystemModeler temperature (°C) calibrated l_{ig} (=0.08 mm) and R_{eca}**
Stator winding average	80.7	80.5	80
Stator winding phase U	88.4	-	-
Stator winding phase V	88.3	-	-
Stator winding phase W	78.2	-	-
Water out	34.1	35.6	34.2

When only l_{ig} was adjusted and R_{eca} was calculated by giving the water temperature rise from the test report, the simulated stator winding temperature was too low compared to the measured Pt100 stator winding temperatures. The simulated stator winding average

temperature was however in accordance with measured stator winding average temperature. The water outlet temperature was 1.5 °C too high. When R_{eca} was adjusted in order for the simulated water temperature to match the measured water temperature, the stator winding temperature decreased slightly and is still lower than the Pt100 measured values but in accordance with measured average stator winding temperature.

After this motor was calibrated for steady state, a S3 60 % duty cycle was simulated. In this duty cycle the motor was running at 125 % load for 6 minutes and then kept at standstill for 4 minutes. This cycle was then repeated.

The water also store heat for water cooled squirrel cage motors. If the water mass is big, the water may store a significant amount of heat due to the high specific heat capacity of water (4190 J/(kg·°C)). However, when simulating this motor with a water mass of 50 kg, its effects were very small compared to a simulation without 50 kg water.

For 125 % load (1750 kW), the loss values presented in Table 26 was taken from test results.

Table 26. Losses for 125 % load. Loss values are taken from an internal test report. (ABB 2016b: 6)

Loss component	**Loss value (W)**
P_{Cus}	8879
P_{Cur}	7204
P_{Fe}	8231
P_{mech}	4947
P_{add}	7432

The simulation results for the S3 60 % duty cycle at 125 % load are presented in Figure 37.

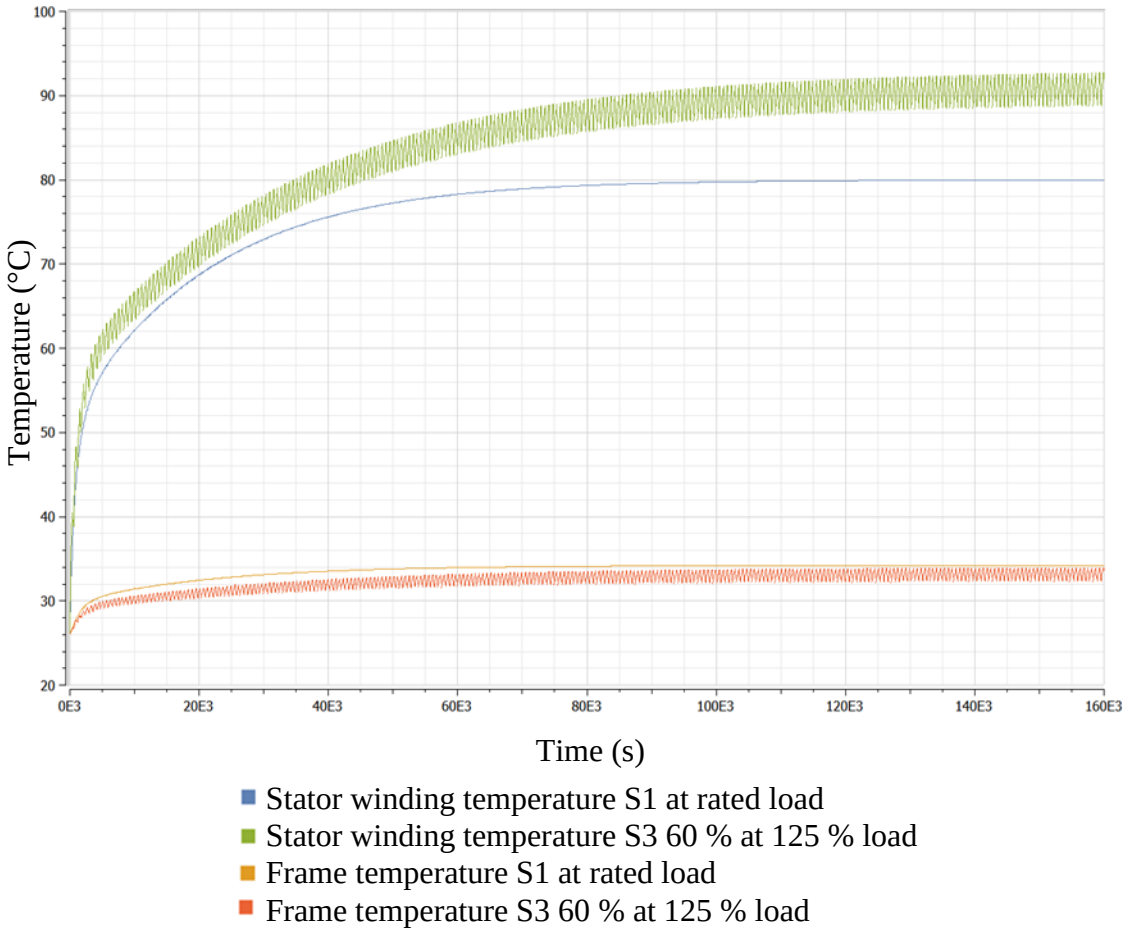

Figure 37. Intermittent duty cycle S3 60 % at 125 % load is simulated in SM and compared to the simulated steady state temperatures.

The simulated results for this S3 60% duty cycle are not verified with measurements. The simulation suggests that the stator winding temperature for the S3 60 % at 125 % load would be higher than the temperature for the rated operating point.

For the same intermittent duty cycle, S3 60 % at 125 % load, these parameters were also plotted in SM: $R_{eca,}$ h_{ew} and Nu. The results are presented next.

The thermal resistance between the frame and the ambient is not affected by the stand-still periods for this water cooled motor and when plotting R_{eca} in SystemModeler it looks like in Figure 38.

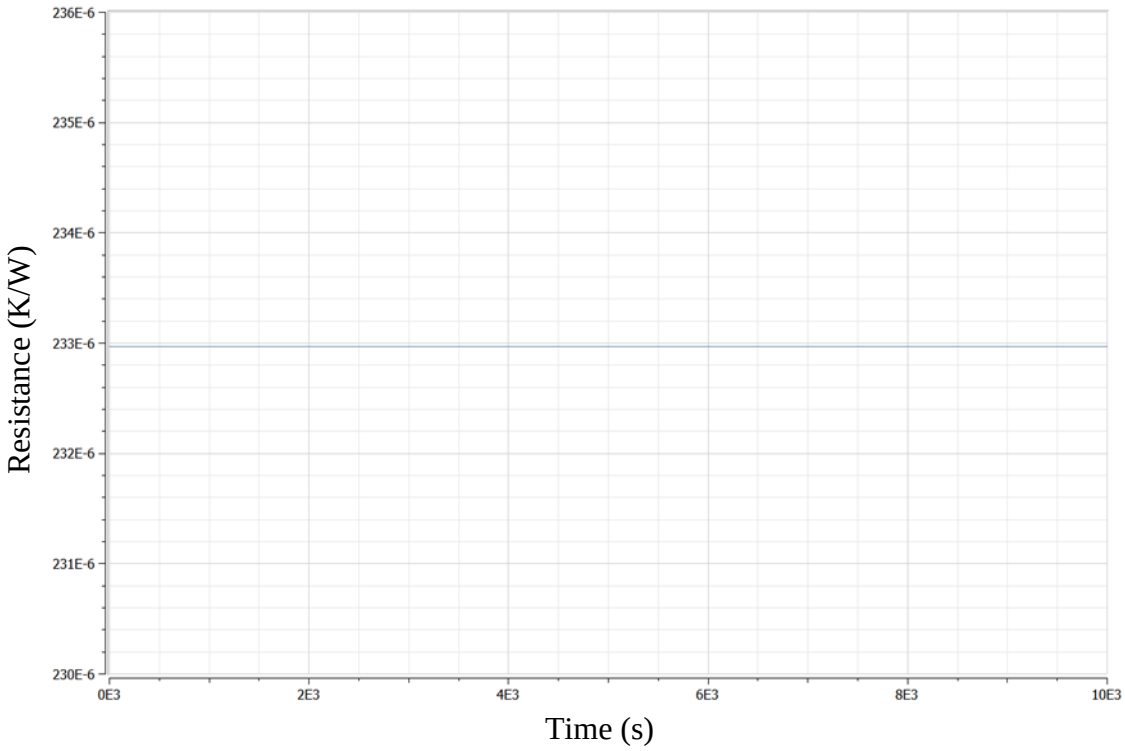

Figure 38. The thermal resistance R_{eca} for the water cooled motor, its value is kept constant for the intermittent duty cycle S3 60 % at 125 % load.

The value for the thermal resistance R_{eca} for a water cooled motor is affected by the water flow in the stator frame. For a water cooled motor, the flow is constant and hence the high heat transfer rate is retained also for standstill periods.

In the end space region, the heat transfer coefficient h_{ew} is affected by the stationary periods. Figure 39 shows how h_{ew} is varying.

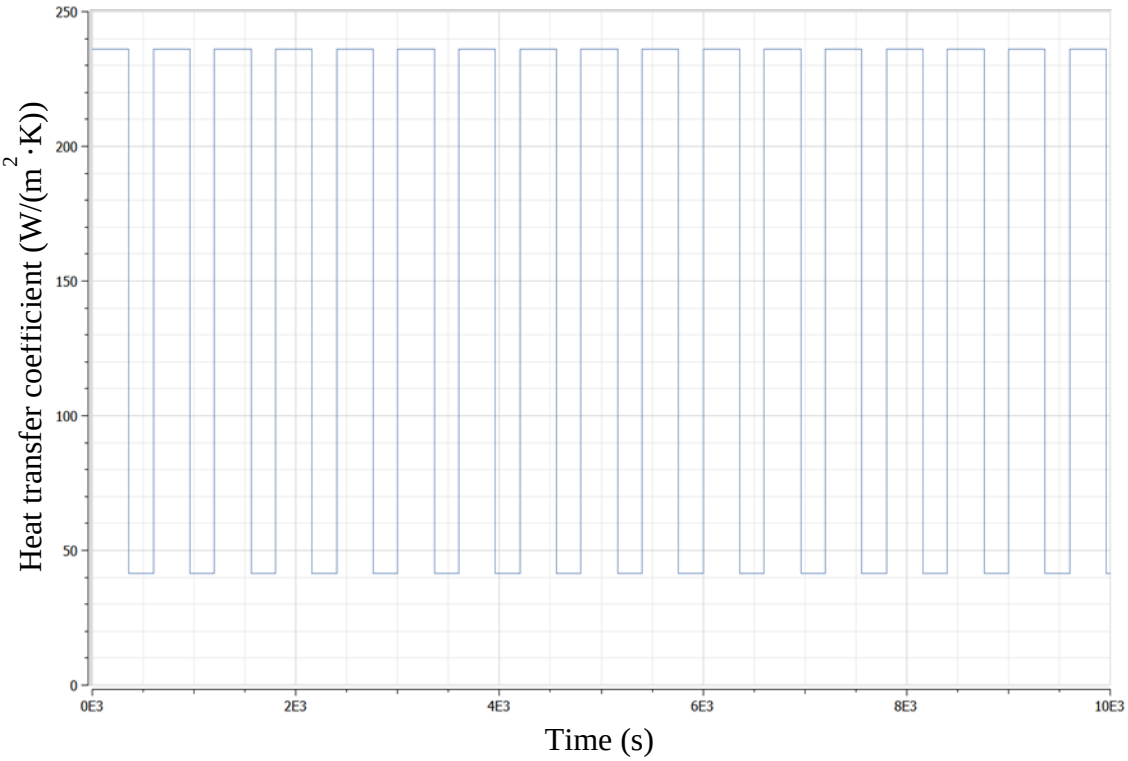

Figure 39. The heat transfer coefficient h_{ew} and how it is varying for the S3 60 % duty cycle at 125 % load for the water cooled motor.

This water cooled motor is also a large motor and h_{ew} has a significantly higher value when the motor is rotating compared to standstill periods. Empirical dependecies for h_{ew} should be investigated further for motors of this frame size and high rotor pheriperal speeds. This motor has a rotor pheriperal speed of 48.6 m/s which is significantly higher than the investigasted rotor pheriperal speed range studied in the articles referred to in Section 4.3.7.

Figure 40 presents the *Nu* number in the air gap.

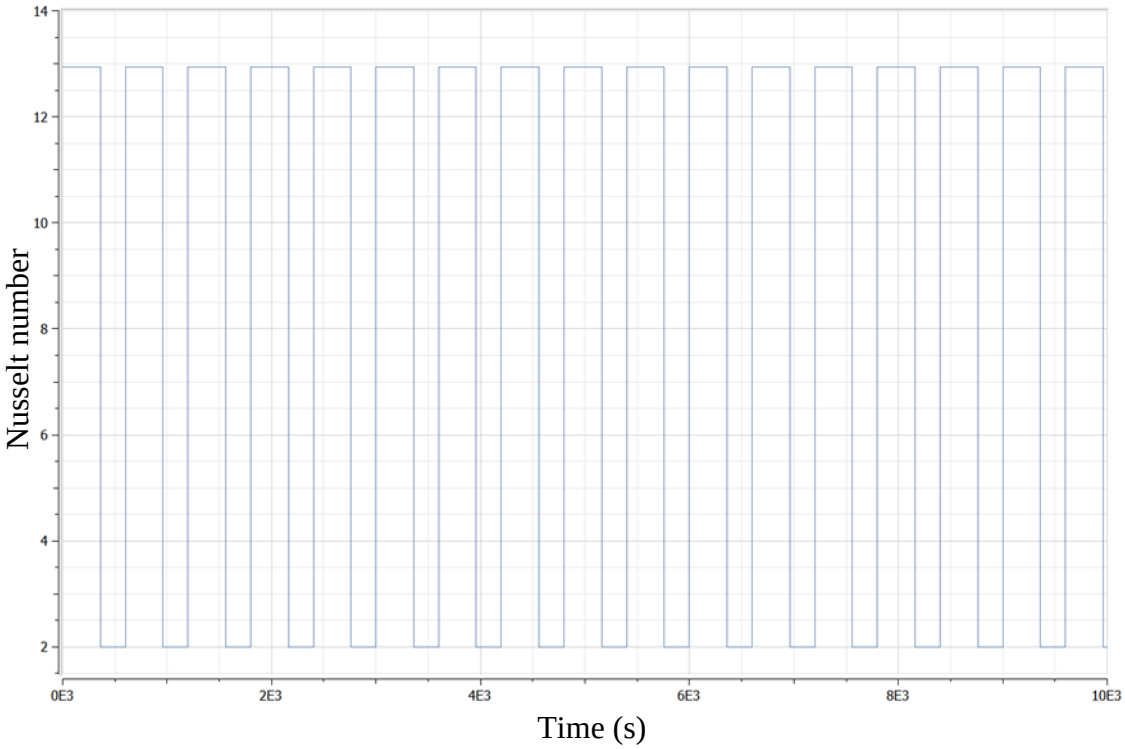

Figure 40. The Nusselt number *Nu* in the air gap and how it is varying for the S3 60 % duty cycle at 125 % load.

When the water cooled motor is rotating, the air flow in the air gap is turbulent according to the *Nu* number. When the water cooled motor is stationary, the heat transfer in the air gap is by conduction which corresponds to a *Nu* number of 2.

For this motor, the equivalent thermal conductivity k_{cuir} was calculated to be 0.022 W/(m·K) with the chosen dependency. According to another correlation, this value is too low and it should be closer to 0.07 W/(m·K) for this motor. If the value of k_{cuir} is set to 0.07 W/(m·K), it would affect the stator winding temperature for this motor, the stator winding temperature would be higher: 87.7 °C compared to 80 °C for k_{cuir} = 0.022W/(m·K). The frame temperature would practically be unaffected. This motor has rated output power 1400 kW and the chosen k_{cuir} dependency was discovered when induction motors up to 1000 kW were tested.

5.4.5 Sensitivity analysis

For a thermal model, it might be important to identify the most sensitive parameters in order to estimate them with special accuracy. There are many methods for sensitivity analysis but in this thesis a simple approach has been adopted; one parameter is modified at the time and the results are compared to the results for the original parameter value. The results are the temperatures for different motor parts. For the sensitivity analysis, the winding temperature is chosen because it is the most critical temperature in a squirrel cage motor. The sensitivity analysis is performed for steady-state temperature results with calibrated l_{ig} and R_{eca}.

The winding temperature percentage variation when varying different parameters is given in Tables 27, 28 and 29. In Table 27 the different parameters are increased with 20 %.

Table 27. Sensitivity analysis results.

Parameter	Parameter modification (%)	Winding temperature variation (%)			
		0.18 kW	**22 kW**	**315 kW**	**1500 kW**
R_{eca}	20	8.3	8.6	8.0	2.3
$R_{ia,ec}$	20	0.3	2.6	5.2	7.1
R_{sy1}	20	0.0	0.2	0.5	0.5
R_{sy2}	20	0.0	0.4	0.7	0.9
R_{st}	20	1.0	0.6	0.9	1.8
$R_{cu,ir}$	20	0.3	0.8	-1.5	-2.0
$R_{ew,ia}$	20	0.2	1.2	1.5	2.8
$R_{s,ag}$	20	0	0.2	1.3	1.1
$R_{r,ag}$	20	0	0.2	1.3	1.1
R_{sig}	20	1.7	1.9	1.4	1.9
R_{shf}	20	0.2	0.2	0.8	0.7
R_{r}	20	0.0	0.1	-0.1	-0.4
P_{Cus}	20	9.2	8.8	5.2	6.4
P_{Cur}	20	3.0	3.8	9.4	7.5
P_{Fe}	20	0.5	2.3	2.2	1.6
P_{mech}	20	0.0	0.2	2.2	2.5
P_{add}	20	0.2	2.3	2.4	1.1
h_{ag}	20	0	-0.2	-2.0	-1.8
h_{ew}	20	-1.0	-3.5	-6.0	-8.6
k_{ir}	20	-1.3	-0.8	-2.0	-2.9

Table continues

Table 27 continues

k_{cuir}	20	-0.5	-0.6	3.1	1.8
l_{sb}	20	-0.8	-1.2	2.7	3.5
A_{ew}	20	-0.5	-1.0	-1.4	-2.4
A_{ec}	20	-0.7	-2.4	-4.6	-6.3
S_{slot}	20	3.5	2.5	0.7	2
KCU1	20	-1.5	-2.3	4.5	5.1

The end winding heat transfer coefficient is challenging to estimate without numerical analysis or measurements. Therefore, it is alarming that an increase of 20 % of h_{ew} affects the stator winding temperatures by -6.0 % and -8.6 % for the two large motors of frame sizes 355 and 500 respectively. The stator slot cross sectional area S_{slot} also seems to have impacts on the stator winding temperature and therefore it should be considered to use the ASLOT1 parameter in Adept which gives a more exact value for the stator slot cross sectional area. However, this parameter was not yet used because the parameter ASLOT1 is not shown among the other easy to get parameters so in order to facilitate the parameter searching process, HSN1 and BSO1 were used instead. The S_{slot} differences between the estimated HSN1·BSO1 value and ASLOT1 value were compared for the four presented motors and the percentage differences were 2.5 %, 13.2 %, 3.2 % and 11.4 % for the four motors in ascending frame size order. In the sensitivity results the increase of S_{slot} was 20 % which is higher. If using ASLOT1 instead, it is a very easy modification in the developed model.

The equivalent interface gap between stator lamination and stator frame is a critical parameter which always needs calibration. Table 28 presents how it affects the stator winding temperatures for the four simulated motors when its lower and upper values are used in SystemModeler.

Table 28. The effects of the equivalent interface gap, l_{ig}, on the stator winding temperatures.

Equivalent interface gap l_{ig} (mm)	**Winding temperature (°C)**			
	0.18 kW	**22 kW**	**315 kW**	**1500 kW**
0.01	55.3	76.4	85.2	72.9
0.08	64.4	85	91.8	80

The stator winding temperature range that can be achieved when changing l_{ig} is quite broad for all four motors.

The amount of mechanical losses is important to estimate, especially for motors with higher rated output powers. Table 29 shows how the mechanical factor, P_{mech_factor} affects the stator winding temperatures for the four simulated motors.

Table 29. The effects of the mechanical factor, P_{mech_factor} on the stator winding temperatures.

P_{mech_factor}	**Winding temperature (°C)**			
	0.18 kW	**22 kW**	**315 kW**	**1500 kW**
0.25	59.9	84	89.0	73.6
0.75	60	84.1	94.3	77.8
1	60	84.2	96.9	80

As it is shown in Table 29, P_{mech_factor} has no significant impact on the two smaller motors since their amount of mechanical losses is small compared to the total losses. For the two bigger motors, the value of P_{mech_factor} has significant impacts. For TEFC motors, the fan losses are a significant part of the mechanical losses. Water cooled motors do not have fans and it is assumed that all of the mechanical losses contribute to the heating, hence the mechanical factor, P_{mech_factor} is equal to 1.

6 CONCLUSIONS AND DISCUSSION

The purpose with this thesis was to investigate if Wolfram SystemModeler can be utilized when estimating the thermal behavior for three phase squirrel cage motors of intermittent duty types. It is of highest importance that the stator winding temperature does not exceed its limit value and therefore the stator winding temperature was the critical temperature in this thesis. The study began from steady-state temperatures which are documented in test reports for every motor type; in this way it was possible to see how the model performed thermal calculations compared to measured temperature values. With the presented model, the results for steady-state temperatures were good. However, due the many complex thermal phenomena, there were two parameters which were calibrated for every motor type. It is recommended to calibrate the model with help of steady-state test results for every motor type before performing any transient state simulations. When calibrating the model, the user will also notice how accurate the steady-state temperatures are compared to measured values and can therefore make conclusions about the accuracy for transient simulations.

The needed calibration and temperature errors can be explained by the fact that the developed thermal model and the used empirical dependencies are not tailor made to suit a certain motor or motor type, instead they are adapted to suit a wide range of motors. It can however be noticed that especially the end winding heat transfer coefficient h_{ew} should be more accurately studied or at least there should be recommendations for how it can be adjusted; for example a frame size and end-space dependency. However, with the model calibration, sufficiently good results could be achieved for 14 of 15 tested standard squirrel cage motors, (after calibration of l_{ig} and R_{eca}). Since the steady-state temperatures are within the 10 % accuracy range for the majority of simulated motors, it can be concluded that the model can be used for estimating the thermal behavior for motors of continuous duty types. Simulated results for intermittent duty types are not verified but most likely the intermittent simulations can at least be used as guidelines. Transient state simulations can also be used for comparisons. If having for example two different scenarios for a motor, a short time S2 duty cycle, and then the question is if the stator winding is heated less when the motor operates at 145 % load for 60 minutes or

when the motor operates at 125 % load for 90 minutes. The temperature values may be false but it can still be seen in percentage how the temperatures are increasing or decreasing.

It seems that the developed dynamic thermal model also can be utilized for water cooled squirrel cage motors. The only difference when simulating water cooled squirrel cage IMs compared to TEFC squirrel cage IMs is that the ambient temperature is the water inlet temperature and $T_{\text{rise\_frame}}$ is the temperature rise of the cooling water, which can also be calibrated for water cooled motors. However, the thermal model should be tested for several different water cooled squirrel cage motor types in order to assure its reliability for water cooled motors.

When using the developed model for simulating standard squirrel cage motors with test reports, the model is used as the flowchart in Figure 41 describes.

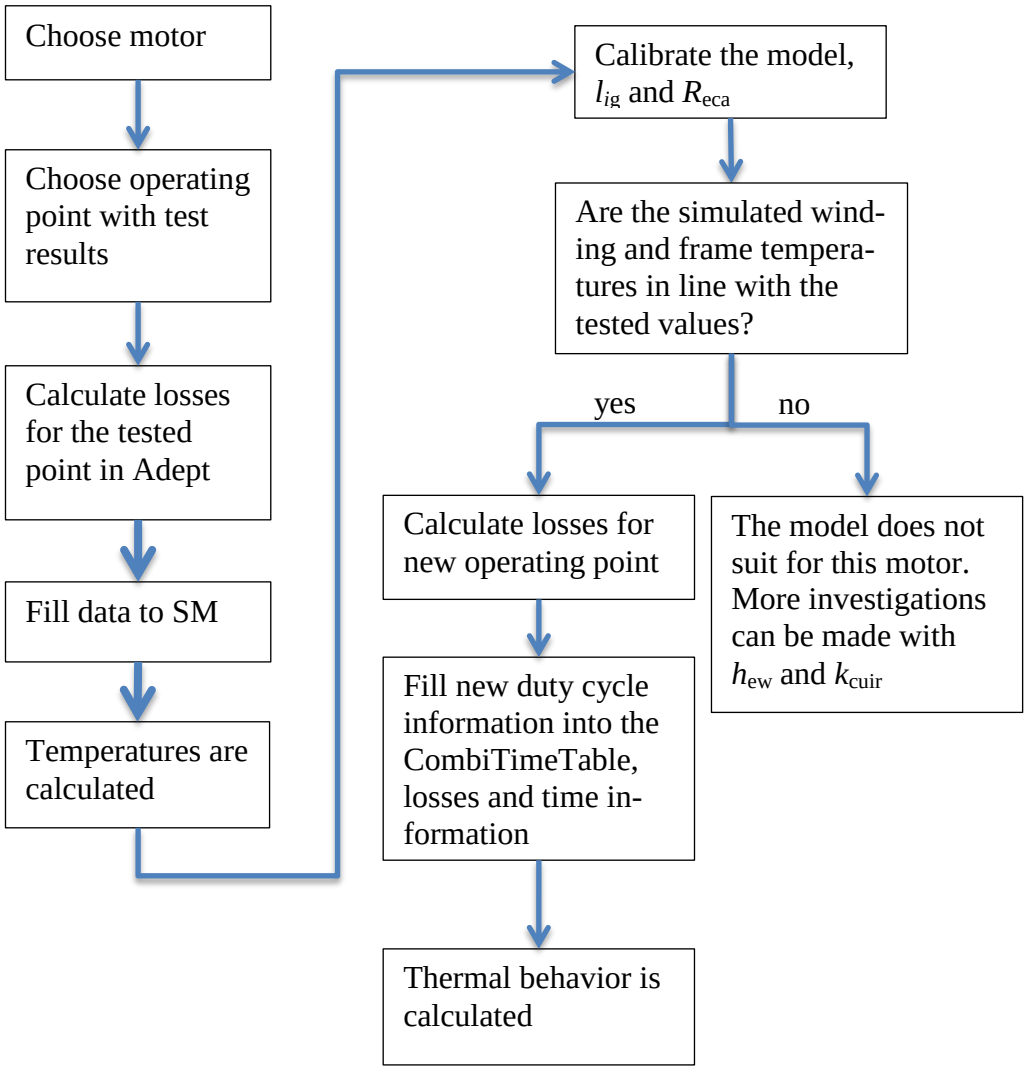

Figure 41. Flowchart describing the process when using the developed thermal model.

During the development of the presented thermal model, several different empirical dependencies for the convection heat transfer and other critical parameters were investigated and tested. Some different thermal networks were also tested. For example, a thermal network with a few more thermal resistances and as a consequence, also a few more parameters, was tested. When different modifications of the presented thermal model were tested, it was sometimes observed that for some motor types, different modified thermal models performed well while for other motor types they performed satisfactorily. For the chosen final thermal model, 14 of 15 standard squirrel cage motors were simulated within the 10 % accuracy range for average stator winding temperature.

However, with considerably more testing and comparing, the thermal model could be optimized further. For example, some empirical dependencies are best suited for a certain motor geometry or size and with help of extensive testing there could be different correlations for different motor types. Especially the estimation of h_{ew} and the use of different empirical dependencies for h_{ew} depending on frame size and end-space geometry could improve the thermal model.

There are squirrel cage motors that will perform satisfactorily with the developed model. Satisfactory temperature results are most likely due to the critical parameters in the thermal model. The critical parameters are:

- Equivalent thermal resistance between external frame and ambient
- Equivalent thermal conductivity between stator winding and lamination
- Equivalent thermal resistance between end winding and end-caps, and
- Interface gap between stator lamination and external frame.

The critical parameters should be measured or numerically simulated for every motor but since that is not possible for a simple to use with sufficient accuracy model, different ways to bypass measurements and numerical simulations were studied. With help of test reports it is possible to estimate the equivalent thermal resistance between external frame and ambient, which would otherwise be a large source of errors. The frame temperature for a given operating point is available in test reports and then the equivalent thermal resistance for frame to ambient can be calibrated to match the tested frame temperature. The interface gap between stator lamination and external frame is according to studies typically between 0.01–0.08 mm and with help of test reports and the stator winding temperature, this value is calibrated.

The two more demanding critical parameters are then the equivalent thermal conductivity between stator winding and lamination and the equivalent thermal resistance between end winding and end-caps. For the equivalent thermal conductivity between stator winding and lamination, there are different correlations available but the different correlations suggest a little bit different values, even if the variation between suggested values is small in magnitude, it may be big in percent and it will also cause non-negligible

variations in the stator winding temperature. However, the chosen dependency seems to work well for the majority of simulated motors. The equivalent thermal resistance between end winding and end-cap is a major uncertainty factor in the model. It seems like the chosen empirical dependency works reasonably for the majority of squirrel cage motors but it is also proven in different studies that this equivalent thermal resistance should be measured or numerically simulated due to the big variations in possible values which additionally affect the stator winding temperature quite significantly. The possible errors due to end-space dependencies become particularly noticeable for motors of bigger frame sizes since the rotor pheriperal speed is often high for these motors.

With SystemModeler, it is possible to easily modify existing programs; the developed tool could be modified in order to analyze a wider range of electrical motors. Improvements can also be made. There are enormous possibilities to develope the model further by using for example more if and when statements in order to simulate different motor types and sizes in more accurate ways. Development and improvement ideas of the developed analytical dynamic thermal model thought of during the writing of this thesis are:

- It could be possible to choose between more cooling methods, e.g: forced air cooling with shaft mounted fan or with auxiliary fan, cooled by natural convection and radiation only, water cooled
- It could be possible to choose between DOL and VSD if the problems associated with VSD are investigated firstly
- It would be possible to test the reliability of already existing empirical rotational speed dependencies for FC-operated TEFC motors
- The equivalent thermal conductivity between stator winding and lamination, k_{cuir}, could be investigated further especially for ABB's motors in order to find a consistent dependency
- Numerical methods could be used to simulate the convection heat transfer coefficients from the end windings to the end space inner air and from inner air to the end caps especially for larger motors with big rotor pheriperal speeds

- A comparison between simulated temperatures and test results for intermittent operation could be made for at least a few motors in order to see if simulated transient behavior is also in line with measurements
- With some modifications in the thermal model, for example, a more detailed modelled rotor, it could be possible to choose motor type, e.g.; squirrel cage induction motor, permanent magnet motor, synchronous reluctance motor, and
- Different environments could be investigated, for example how motors in high temperature environments could be simulated, e.g. how the importance of radiation changes as well as thermal expansion problems, but also motors operating in an environment below 0 °C.

7 SUMMARY

The purpose of this thesis was to investigate if Wolfram SystemModeler could be used for analyzing standard three phase squirrel cage motors thermally. Steady-state temperatures are already tested for every motor type at rated load, but if different intermittent duty cycles are run instead, the thermal behavior is not known. The target was to develope an analytical dynamic thermal model with which different duty cycles can be tested in order to estimate the thermal behavior.

In the theory sections of this thesis, there was a chapter about the squirrel cage motor; squirrel cage motor losses, insulation classes, duty class types, temperature measurement methods and cooling methods Then the theory behind this thesis contains a chapter about heat transfer in general and applied to electric motors. The theory behind the developed analytical dynamic thermal model was reviewed in detail. This is beneficial if the thermal model is modified, since it is easier to make modifications if the theory behind is fully clarified.

The proposed analytical thermal model is a reasonable compromise between network complexity and accuracy of the temperature results. The model however contains some critical parameters that may be sources of simulation errors. Due to this fact, it is important to simulate an operating point with test results before simulating operating points without measured temperature values. When simulating a point with measured temperatures, calibration is performed in accordance with test results. With this method, good results were achieved for steady-state simulations for the majority of simulated motors. With this method, the user also notices if a specific motor is not suitable for the model.

The developed thermal model could further be developed in many ways. It can be developed in order to be able to simulate a wider range of motors for different applications. Improvements can also be made in order to increase the accuracy for the critical parameters.

REFERENCES

ABB (2011). *Low voltage water cooled motors.* Additional manual. 28 p.

ABB (2014). *Low voltage motors*. Motor guide. Third edition. ISBN 952-91-0728-5. ABB Oy. 126 p.

ABB (2015a). *Test report – M3BP 71 ME 6*. Test report. Available from the internet: <https://library.e.abb.com/public/358c5bbbea1f4fd9a38242fc9544411e/M3BP%2071ME%206%20400VY%2050Hz%200.18kW.pdf>

ABB (2015b). *Test report – M3BP 180 MLB 4*. Test report. Available from the internet: <https://library.e.abb.com/public/9709d6c741d54b62b730c7b0682b839d/M3BP%20180MLB%204.pdf>

ABB (2016a). *Water cooled motors*. [Cited 25.9.2016]. Available from the internet: <http://new.abb.com/motors-generators/iec-low-voltage-motors/special-application-motors/water-cooled-motors>

ABB (2016b). *Test report – M3LP 500 LC 4*. ABB internal test report. Unpublished. 20 p.

ABB (2016c). *Test report – M3BP 355 SMB 2*. Test report. Available from the internet: <https://library.e.abb.com/public/ff1784ae93924da99752b64715c515e5/M3BP%20355SMB%202L%20400V%2050Hz%20315kW.pdf>

Bansal, Rajeev (2006). *Fundamentals of engineering electromagnetics*. ISBN: 0-8493-7360-3. Taylor & Francis Group. 400 p.

Buyukdegirmenci Veysel T, Krein Philip T (2013). *Machine Characterization for Short-Term or Instantaneous Torque Capabilities: An Approach Based on Transient Thermal Response*. IEEE, University of Illinois, Department of Electrical and Computer Engineering, p. 801–808.

Benamrouche N, Bouheraoua M, Haddad S (2006). *A Thermal Model for a TEFC Induction Motor – Development and Sensitivity Analysis*. Electric Power Components and Systems, 34. Taylor & Francis, p. 259–269.

Bergman Theodore L., Lavine Adrienne S., Incropera Frank P., Dewitt David P. (2011). *Fundamentals of Heat and Mass Transfer*. Seventh edition. ISBN 978-0470-50197-9. Hoboken: Wiley. 1048 p.

Boglietti Aldo, Cavagnino Andrea, Lazzari Mario, Pastorelli Michele (2003). *A Simplified Thermal Model for Variable-Speed Self-Cooled Industrial Induction Motor*. IEEE Transactions on Industry Applications, vol. 39, no. 4, July/August 2003, p. 945–952.

Boglietti A., Cavagnino A, Staton D.A., Popescu M., Cossar C., McGilp M.I. (2009b). *End Space Heat Transfer Coefficient Determination for Different Induction Motor Enclosure Types*. IEEE Transactions on Industry Applications, July 2009, p. 1–8.

Boglietti Aldo, Carpaneto Enrico, Cossale Marco, Vaschetto Silvio (2016). *Stator-Winding Thermal Models for Short-Time Thermal Transients: Definition and Validation*. IEEE Transactions on industrial electronics, vol. 63, no. 5, p. 2713–2721.

Boglietti Aldo, Cavagnino Andrea (2007). *Analysis of the Endwinding Cooling Effects in TEFC Induction Motors*. IEEE Transactions on Industry Applications, vol. 43, no. 5, p. 1214–1222.

Boglietti Aldo, Cavagnino Andrea, Parvis Marco, Vallan Alberto (2006). *Evaluation of Radiation Thermal Resistances in Industrial Motors*. IEEE Transactions on Industry Applications, vol. 42, no. 3, p. 688–693.

Boglietti Aldo, Cavagnino Andrea, Staton David (2008). *Determination of Critical Parameters in Electrical Machine Thermal Models*. IEEE Transactions on Industry Applications vol. 44, no. 4, p. 1150–1159.

Boglietti Aldo, Cavagnino Andrea, Staton David, Shanel Martin, Mueller Markus, Mejuto Carlos (2009a). *Evolution and Modern Approaches for Thermal Analysis of Electrical Machines*. IEEE Transactions on Industrial Electronics, vol. 56, no. 3, p. 871–882.

Cengel, Yunus A. (2003). *Heat transfer – a practical approach*. Second edition. ISBN 0-07-245893-3. The McGraw-Hill Companies, New York. 932 p.

Dajaku G., Gerling D. (2006). *An Improved Lumped Parameter Thermal Model for Electrical Machines*. Institute for Electrical Drives, University of Federal Defense Munich. 6 p.

Hachicha M.R., Ghariani M., Neji R. (2011). *Thermal model for induction machine*. 8th International Multi-Conference on Systems, Signals & Devices. National School of Engineers of Sfax Tunisia, p. 1–5.

Hettegger Martin, Streibl Bernhard, Bíró Oszkár, Neudorfer Harald (2010). *Characterizing the heat transfer on the end – windings of an electrical machine for transient simulations*. IEEE Mediterranean Electrotechnical Conference, p. 581–586.

Hettegger Martin, Streibl Bernhard, Bíró Oszkár, Neudorfer Harald (2012). *Measurements and Simulations of the Convective Heat Transfer Coefficients on the End Windings of an Electrical Machine*. IEEE Transactions on Industrial Electronics, vol. 59, no. 5, p.2299–2308.

Jääskeläinen Mikko (2009). *Determination of coefficients of thermal convection in a high – speed electrical machine*. Master thesis. Helsinki University of Technology. Espoo, Finland. 55 p.

Kylander Gunnar (1995). *Thermal modelling of small cage induction motors*. Doctoral dissertation. Chalmers University of Technology. Göteborg, Sweden. ISBN 91-7197-061-4. 113 p.

Mäkelä Mikko, Soininen Lauri, Tuomola Seppo, Öistämö Juhani, Kulmala Marko (2010). Tekniikan kaavasto. Ninth edition. ISBN 978-952-5491-48-7. Kariston Kirjapaino Oy, Hämeenlinna. 205 p.

Mellor P.H., Roberts D., Turner D.R. (1991). *Lumped parameter thermal model for electrical machines of TEFC design*. IEEE Proceedings-B, vol. 138, No. 5, p. 205–218.

Modelica Association (2014). *Modelica® - A Unified Object-Oriented Language for Systems Modeling, Language Specification.*Version 3.3, Revision 1. 295 p.

Otter Martin, Elmqvist Hilding (2001). *Modelica Language, Libraries, Tools, Workshop and EU – Project RealSim*. German Aerospace Center, Ober pfaffen hofen, Germany and Dynasim AB, Lund, Sweden. 8 p.

Pechanek Roman, Kindl Vladimir, Skala Bohumil (2015). *Transient Thermal Analysis of Small Squirrel Cage Motor Through Coupled FEA*. MM Science Journal. March 2015, p. 560–563.

Puranen Jussi (2006). *Induction motor versus permanent magnet synchronous motor in motion control applications: a comparative study*. Doctoral dissertation. Lappeenranta University of Technology. Lappeenranta. ISBN 952-214-297-2 (PDF). 147 p.

Pyrhönen Juha, Tapani Jokinen, Valéria Hrabovková (2014). *Design of Rotating Electrical Machines*. Second edition. ISBN 978-1-118-58157-5. Chichester: Wiley. 584 p.

Staton Dave, Boglietti Aldo, Cavagnino Andrea (2005). *Solving the More Difficult Aspects of Electric Motor Thermal Analysis in Small and Medium Size Industrial Induction Motors*. IEEE Transactions on Energy Conversion, vol. 20, no. 3, p. 620–628.

University of Helsinki (2007). *Mittaustekniikan perusteet / luento 10: Antureita*. Electronics research laboratory. Available from the internet: <http://electronics.physics.helsinki.fi/wp-content/uploads/2011/02/Luento10_2007_anturit.pdf >

Valenzuela M. Aníbal, Tapia Juan A., Rooks James A. (2004). *Thermal Evaluation of TEFC Induction Motors Operating on Frequency-Controlled Variable-Speed Drives*. IEEE Transactions on Industry Applications, vol. 40, no. 2, p. 692–698.

Wolfram (2016). *How SystemModeler Compares*. [Cited 12.1.2016]. Available from the internet: <http://www.wolfram.com/system-modeler/features/modeling-tools-comparison/>

Wolfram Research, Inc (2012). *Wolfram SystemModeler, User guide*. Wolfram, Additive, Soft- & Hardware für technik & wissenschaft. 194 p.